UNIVERSITY OF CALIFORNIA SAN DIEGO

Interaction Studies of the Chemokine Interleukin-8 with the G Protein-Coupled Receptor CXCR1 by Nuclear Magnetic Resonance Spectroscopy

A dissertation submitted in partial satisfaction of the requirements for the degree

Doctor of Philosophy

in

Chemistry

by

Sabrina Berkamp

Committee in charge:

Professor Stanley J. Opella, Chair
Professor Timothy S. Baker
Professor Marilyn G. Farquhar
Professor Patricia Jennings
Professor Robert Pomeroy

2018

The Dissertation of Sabrina Berkamp is approved, and it is acceptable in quality and form for publication on microfilm and electronically:

_____

_____

_____

_____

_____

Chair

University of California San Diego

2018

DEDICATION

To my mother, Yvonne Blaauw, my sister, Larissa Berkamp,

and my boyfriend, Mehmet Koç

who provided a lot of support and encouragement of the years.

EPIGRAPH

It's the questions we can't answer that teach us the most. They teach us how to think. If you give a man an answer, all he gains is a little fact. But give him a question and he'll look for his own answers.

- Patrick Rothfuss

TABLE OF CONTENTS

LIST OF ABBREVIATIONS

^{1}H	Proton
^{13}C	Carbon - 13
^{15}N	Nitrogen – 15
AMS	Ammonium sulfate
1TM-CXCR1	The first transmembrane domain of CXCR1, corresponding to residues 1-72
COPD	Chronic Obstructive Pulmonary Disease
CP	Cross-polarization
CP-MOIST	Cross-polarization with mismatch-optimized IS transfer
CSA	Chemical shift anisotropy
CSI	Chemical shift index
CXCL8	C-X-C chemokine ligand 8
CXCR1	C-X-C chemokine receptor type 1
Da	Dalton
DHPC	1,2-diheptanoyl-sn-glycero-3-phosphocholine
DMPC	1,2-dimyristoyl-sn-glycero-3-phosphocholine
DNA	Deoxyribonucleic acid
DOPC	1,2-dioleoyl-sn-glycero-3-phosphocholine
DPC	Dodecylphosphocholine

GPCR	G Protein-Coupled Receptor
Hepes	4-(2-hydroxyethyl)-1-piperazineethanesulfonic acid
HQA	2-amino-3-(8-hydroxyquinolin-3-yl)propanoic acid dihydrochloride
HSQC	Heteronuclear single quantum coherence
IL-8	Interleukin-8
INEPT	Insensitive Nuclei Enhanced by Polarization Transfer
IPAP	In-phase/anti-phase
IPTG	Isopropyl-β-thiogalactoside
ITC	Isothermal Titration Calorimetry
KSI	Ketosteroid isomerase
LB	Luria-Bertani
LP	Linear prediction
MAS	Magic-angle-spinning
MSP1	Membrane Scaffold Protein 1
ND-CXCR1	The N-terminal domain of CXCR1, corresponding to residues 1-38
NMR	Nuclear Magnetic Resonance
NOE	Nuclear Overhauser effect
NT-CXCR1	CXCR1, lacking the N-terminal domain , corresponding to residues 39-350
OS	Oriented sample

PBS	Phosphate-buffered saline
PDB	Protein data bank
PDSD	Proton-driven spin diffusion
PISEMA	Polarization Inversion Spin Exchange at the Magic Angle
PMSF	Phenylmethane sulfonyl fluoride
PRE	Paramagnetic relaxation enhancement
RDC	Residual dipolar coupling
RMSD	Root mean squared deviation
RF	Radiofrequency
SDS	Sodium dodecyl sulfate
SDS-PAGE	Sodium dodecyl sulfate-polyacrylamide gel electrophoresis
S/N	Signal-to-noise
SLF	Separated-local-field
SPINAL-16	Small phase incremental alternation, with 16 steps
t1	Incremented time interval in a two-dimensional experiment
t2	Signal acquisition interval in a two-dimensional experiment
TFE	2,2,2-Trifluoroethanol
TM	Transmembrane
Tris	*Tris*(hydroxymethyl)aminomethane

LIST OF FIGURES

LIST OF TABLES

ACKNOWLEDGEMENTS

First and foremost, I would like to thank my thesis advisor, Professor Stanley Opella for giving me the opportunity to research in his laboratory. My thesis work would not have been possible without his encouragement to do the best research I can, in one of the best membrane protein NMR labs in the world. He has taught me a great deal, not only about NMR spectroscopy, but also about presenting your work in a clear and concise manner both in writing and in presentations. I would also like to thank the other members of my thesis committee, Professor Patricia Jennings, Professor Timothy Baker, Professor Robert Pomeroy and Professor Marilyn Farquhar, for their guidance and support in the discussion of my project and other scientific questions.

I would like to thank all the current and former members of “team GPCR”; Dr. Sang Ho Park, Jasmina Radoicic, Dr. Anna de Angelis, Dr. Ratan Rai, Dr. Bibhuti Das and Zheng Long. Together, we have worked hard to study a very challenging protein system and we’ve made great progress! Every step of the way, they have helped and guided me, both in the wetlab as well as with the spectroscopy. I can’t even begin to list how much of their protein, samples, protocols, buffers, spectra and NMR time I have used to conduct my research. I also really appreciate the many discussions and conversations we’ve had on all things GPCR, IL-8 and NMR. Another special thanks to Professor Francesca Marassi and her lab members, especially Dr. Ye Tian, and Dr. Samit Dutta, at the Sanford Burnham Prebys Medical Discovery Institute. They have been an

amazing help with most of the computational aspects of my project, not only the IL-8 structure calculation, but also help with XPLOR-NIH and trying to match my experimental oriented sample solid-state NMR data to my protein structure, but also with general help and guidance on NMR spectroscopy and my project. Also, a special acknowledgement to all my former office and PhD program mates; Dr. Hua Zhang, Dr. George Lu, Dr. Eugene Lin, Dr. Ye Tian, Dr. Lindsay Dawson, Megan Chu and Vivian Wang. All have been a great help in developing my research skills, discussing results, helping me process NMR data, listening to my problems regarding experiments that did not work as expected, and helping me troubleshoot protein expression and purification protocols on a daily basis. I would also like to thank Dr. Albert Wu, Dr. Xuemei Huang, Dr. Anthony Mrse and Dr. Chris Grant for all the help with the NMR instruments, help with the pulse sequences, probes and your patience while teaching me everything I know about NMR spectroscopy. Next, my former undergraduate student, Mitchell Zhao, has been a tremendous help, started a great project on his own and is a hard-working and gifted researcher. Thank you to all former lab members of the Opella lab: Dr. Gabriel Cook, Dr. Anna Pavlova, Dr. Dongtao Cui, Dr. Andreea Balaceanu, Dr. Yan Wang, Yanwen Mai, Dr. Hank Nothnagel, Dr. Ilya Litvak and Dr. Mike Kaiser for your help and support, both in the lab and outside of it. I would also like to thank Dr. Andrej Bobkov at the Sanford Burnham Prebys Medical Discovery Institute for all the help with my ITC experiments. Last, but not least, I would like to thank Elena Vitoshka, our former administrative assistant, for all of her help

with all the various administrative tasks that come with doing research, but also for all of her tireless support and encouragement in and out the lab.

I would also like to thank my undergraduate research advisor, Professor Marc Baldus, my master thesis supervisor, Dr. Klaartje Houben and my master research advisor, Professor Emmanuel Wiertz, for all their help, guidance and words of encouragement and opening the door to my scientific career in structural biology.

Chapter 2, in full, is a reprint of the material as it appears in the Journal of Biomolecular NMR (2017) 69:111–121. Berkamp, S., Park, S.H., De Angelis, A. A., Marassi, F. M. and Opella, S. J. The dissertation author was the primary author of this paper.

Chapter 3, in full, is a reprint of the material as it appears in the Biophysical Journal (2017) 113, 2695–2705. Park, S.H., Berkamp, S., Radoicic, J. De Angelis, A. A., and Opella, S. J. The dissertation author was the secondary author of this paper.

Chapter 4 is currently being prepared for submission for the publication of the material, Rai, R. K, de Angelis, A.A., Berkamp, S., Park, S.H. and Opella, S.J. The dissertation author was the tertiary author of this material.

Chapter 5 is currently being prepared for submission for the publication of the material, Berkamp, S., Radoicic, J., Tian, Y, Park, S.H. and Opella, S.J. The dissertation author was the primary author of this material.

Chapter 6, in full, is a reprint of the material as it appears in Biochemistry, (2011), 50, 8983–8985. Park, S.H., Berkamp, S., Cook, G. A., Chan, M. K., Viadiu, H. and Opella, S. J. The dissertation author was the secondary author of this paper.

VITA

2009 Bachelor of Science, Utrecht University, the Netherlands

2011 Master of Science, Utrecht University, the Netherlands

2018 Doctor of Philosophy, University of California San Diego

PUBLICATIONS

Interaction of Monomeric Interleukin-8 with CXCR1 Mapped by Proton-detected Fast MAS Solid-state NMR. Park S.H., Berkamp S., Radoicic J., De Angelis A.A., Opella S.J. , Biophysical Journal (2017) Dec 19;113(12):2695-2705

Structure of Monomeric Interleukin-8 and Its Interaction with the N-terminal Binding Site-I of CXCR1 by solution NMR spectroscopy. Berkamp, S., Park, S.H., De Angelis, A.A., Marassi, F.M., Opella, S.J. J Biomol NMR (2017) Nov;69(3):111-121

Paramagnetic relaxation enhancement of membrane proteins by incorporation of the metal-chelating unnatural amino acid 2-amino-3-(8-hydroxyquinolin-3-yl)propanoic acid (HQA). Park S.H., Wang V.S., Radoicic J., De Angelis A.A.,

Berkamp S., Opella S.J. J Biomol NMR. (2015) Apr;61(3-4):185-196

Nanodiscs versus macrodiscs for NMR of membrane proteins,

Park S.H., Berkamp S., Cook G.A., Chan M.K., Viadiu H., Opella S.J.,

Biochemistry. (2011) Oct 25;50(42):8983-8985

ABSTRACT OF THE DISSERTATION

Interaction Studies of the Chemokine Interleukin-8 with the G Protein-Coupled Receptor CXCR1 by Nuclear Magnetic Resonance Spectroscopy

by

Sabrina Berkamp

Doctor of Philosophy in Chemistry

University of California San Diego, 2018

Professor Stanley J. Opella, Chair

The chemokine Interleukin-8 is a major mediator in inflammation. It interacts with the G Protein-Coupled Receptor CXCR1, which is expressed on neutrophils and other cells. Activation of CXCR1 leads to the neutrophils traveling to the site of infection and degranulation. The molecular mechanism between IL-8 – CXCR1 binding and receptor activation is not well understood. IL-8 contacts the two main interaction sites on CXCR1; one located on the flexible N-terminal

domain (Binding Site-I) and the other on extracellular loop 2 and 3 (Binding Site-II). Solution and solid-state NMR spectroscopy have been used to better understand the IL-8 – CXCR1 complex. The solution NMR structure of monomeric IL-8 was solved and its interaction with constructs only composed of Binding Site-I studied. The presence of a membrane or the first transmembrane helix was found not to affect the interaction of IL-8. Proton-detected fast MAS solid-state NMR spectroscopy was used to map the interaction between IL-8 and Binding Site-II and as well as the wildtype CXCR1 receptor. Around 11 residues in IL-8 were immobilized upon contact with Binding Site-II, however almost all residues of IL-8 were immobilized upon contact with both Binding Site-I and Binding Site-II. Interestingly, IL-8 does not undergo a major conformational change upon binding to CXCR1. MAS solid-state NMR spectroscopy was used to study the interaction site and the change in dynamics in 1TM-CXCR1(1-72) upon IL-8 binding. Part of the flexible N-terminal domain was immobilized upon interaction with IL-8, but no tilt angle changes in the transmembrane helix were found. Oriented sample solid-state NMR spectroscopy was used to study the orientation of IL-8 bound to CXCR1. The receptor was reconstituted in uniaxially aligned bicelles and orientation dependent parameters were measured in IL-8. Additionally, a new membrane mimetic, called macrodisc, was developed based on the nanodisc. By changing the ratio of belt protein to lipid, larger discs were created that could be aligned in a magnetic field and used for oriented sample solid-state NMR spectroscopy.

CHAPTER 1 GENERAL INTRODUCTION

1.1 Introduction into protein structures and protein-protein interactions

Besides having a primary structure and a secondary structure, almost all proteins have a tertiary structure. Having an atomic resolution understanding of this tertiary structure helps us understand how proteins function, how they interact with each other and as an ultimate goal to help us design better pharmaceuticals to inhibit or enhance their function. Several techniques can be used to study protein structures: X-ray crystallography, electron microscopy, X-ray and light scattering, and nuclear magnetic resonance (NMR) spectroscopy. Each of these techniques has its limitations and strengths. X-ray crystallography, for instance, requires high-quality crystals, which are not always compatible with membrane proteins or with proteins that have disordered domains. While solution NMR spectroscopy can be used to study membrane proteins and proteins with many dynamical regions, it has an upper size limit of approximately 40kDa. Depending on the research question at hand, one technique may be more suitable than another.

In structural biology, membrane proteins pose a particular challenge. They only constitute about 2% of total protein structures solved and deposited in the Protein Data Bank (PDB) despite the fact that about 30% of all genes encode a membrane protein and over 60% of all drugs target a membrane protein. The lack

of membrane protein structures is mainly due to the fact that they are more challenging to express, purify and reconstitute due to their need of a proper membrane mimetic. Membrane mimetics are generally composed of detergents, small molecules, phospholipids or combinations of them. Examples of the most commonly used membrane mimetics are: lipid cubic phase [1], micelles, bicelles [2], liposomes, nanodiscs [3], amphipols [4] and SMALPs [5]. Lipid composition, membrane thickness, membrane curvature, pH and fluidity can all affect protein function and structure so they need to be selected with care [6].

Most proteins are not static; they undergo small and large motions; sidechains move around and jump between different rotamers, protein loops can be disordered and even entire protein domains can undergo conformational changes. These motions can be on the order of Ångstroms to nanometers and can take place on different time scales, from nanoseconds to hours. Protein motion is important to study and understand as it stands at the basis of, among others, enzyme function, transport across membranes and protein – protein interactions. In X-ray crystallography and electron microscopy the only evidence of protein dynamics is often a lack of density in the structure, NMR spectroscopy, however, is uniquely qualified to study and quantify protein motions on many timescales.

Many proteins function by interacting with other proteins, DNA, RNA or small molecules. The study of protein complexes has its own challenges due to the need to quantify the stoichiometry and binding affinity, study the conformational changes in the individual subunits, to determine the binding site location and to determine the distance between the different units of the complex. Several techniques are available to study protein-protein interactions, each with its own specificity and sensitivity. Examples are; phage display, Förster resonance energy transfer (FRET), immune-precipitation, H-D exchange mass spectrometry, NMR spectroscopy and isothermal titration calorimetry (ITC). ITC is one of the most commonly used techniques to not only obtain the binding constant but also the stoichiometry and enthalpy of binding for protein-protein-, or protein-small molecule complexes. It works by quantifying the change in temperature upon addition of a ligand into a solution of the protein. Distance information in a protein-protein complex can be obtained by using a paramagnetic tag in NMR spectroscopy or EPR spectroscopy, or by quantifying the energy transfer in two chromophores using FRET, for instance. Structures of large protein – protein complexes can be solved by X-ray crystallography, single-particle cryo-EM and by NMR spectroscopy.

1.2 The use of NMR spectroscopy to study protein structure and protein-protein interactions

1.2.1 Solution NMR spectroscopy

Several different nuclei prevalent in biomolecules are used to determine a structure using NMR spectroscopy; ^{1}H, ^{15}N ^{13}C, ^{17}O and ^{31}P. The chemical shift of the different nuclei depends on the electronic environment they are in and can therefore be used to solve protein structures, assess protein dynamics and study protein – protein interactions. NMR spectroscopy can be divided into two related, but complimentary techniques; solution NMR and solid-state NMR. Solution NMR spectroscopy, unlike solid-state NMR, has an upper size limit of samples that can be studied of about 40kDa. This is due to the fact that the rapid isotropic tumbling of the molecule averages out some anisotropic spin interactions that negatively affect spectra. As the protein increases in size, the correlation time decreases, which in turn leads to broadening of peaks, until they can longer be resolved.

This upper size limit is especially problematic for the study of membrane proteins, because they require a membrane to adopt a native conformation. Most commonly, membrane proteins are reconstituted in small detergent micelles, nanodiscs or bicelles that can still undergo rapid tumbling. The presence of detergents can perturb membrane protein structures; so several membrane environments may need to be screened to ensure a native-like structure of the membrane protein [6].

To determine a protein structure from chemical shifts several NMR experiments need to be performed. The protein is typically ^{15}N and ^{13}C isotopically labeled, but could also contain ^{2}H, or be selectively labeled at certain amino acids of interest. Each resonance peak needs to be assigned to a single site in the protein. This is generally achieved via a series of triple resonance experiments that correlate resonances to each other through chemical bonds or through space. The protein backbone resonances are typically assigned using a so-called backbone walk, using HNCA, HNCACB, HNCO and HNCOCA experiments, while the sidechain resonances are assigned using CC(Co)NH, HCC(Co)NH or TOCSY-type experiments. Each amino acid has a characteristic chemical shift that depends on the electronic and chemical environment in which it resides; residues in an α-helix or β-sheet deviate in a predictable way from those in a random coil. This so-called chemical shift index (CSI) can be used as a dihedral restraint in a protein structure calculation [7]. Residual Dipolar Couplings (RDC) can be used as an angular restraint in the protein structure calculation. The size of the dipolar coupling between two spins depends on the distance between the two atoms, but also the angle the bond vector makes to the magnetic field. In solution NMR, proteins tumble rapidly, which averages out the dipolar coupling. By using an alignment media, such as a polyacrylamide gel [8], bacteriophage [9], bicelles [10], or DNA nanotubes [11], the protein can be weakly aligned, the dipolar couplings are only partially averaged out and the relative angles of all the

amino acids to the magnetic field can be calculated. The nuclear Overhauser effect (NOE) can be used to obtain distance information in a protein. In NOESY experiments the magnetization is not transferred through chemical bonds, but through space. The intensity of the crosspeaks can be converted to inter-atomic distances since the intensity is proportional to $1/r^6$, with r representing the distance between the two nuclei. Long-range distance information can be obtained using paramagnetic relaxation enhancement (PRE). A paramagnetic probe is placed in the protein; the unpaired electron in the probe broadens out all resonances that are within 25-30Å. Finally, a computer program such as CYANA [12] or Xplor-NIH is used to calculate a structure from the dihedral angles, angular, and distance restraints using an energy minimization function in conjunction with theoretical values for bond lengths, bond angles and potential energy values.

Besides protein structures, NMR spectroscopy can also be used to study protein – protein interactions. Because the chemical shift is so sensitive to the environment, it can be used to probe which residues of a protein are involved in the interaction surface. One protein in the protein complex is generally isotopically labeled, an unlabeled binding partner is slowly titrated into the sample and the changes in the chemical shifts of the labeled protein are recorded. These chemical shift perturbations can then be plotted against the residue number to analyze the binding site. NOE and PRE can be used to obtain distance

information between the binding partners. In the NOESY experiment both intramolecular as well as intermolecular crosspeaks can be assigned to specific residues. Long-range distance information between two proteins can be obtained using PRE; the paramagnetic probe is placed in one protein and the induced line broadening is observed in its binding partner.

1.2.2 Solid State NMR Spectroscopy

Solid-state NMR can be divided in two related methods; oriented sample solid-state NMR and magic angle spinning (MAS) solid-state NMR. In both techniques, samples that have restricted motion are used, varying from single crystals, powders, amyloid fibrils to membrane proteins in lipid environments. Orientation-dependent interactions in these samples are not averaged out and generally lead to broad lines. However, solid-state NMR spectroscopy allows membrane proteins to be studied in a native environment, such as in liposomes and phospholipid bilayers, because it lacks an upper size limit [13].

When using oriented sample solid-state NMR to study membrane proteins, the protein is embedded in a membrane, which is then uniaxially aligned. This can be achieved in two ways: by immobilization on glass plates, or by using the natural tendency of bicelles to align in a magnetic field. In the most commonly performed experiments, the Separated Local Field-type experiments [14] PISEMA [15] and SAMMY [16, 17], the orientation dependent ^{1}H-^{15}N dipolar coupling and

^{15}N Chemical Shift Anisotropy (CSA) are measured. Signal assignment is less straightforward in oriented sample solid-state NMR than solution NMR. It is generally attempted using selectively labeled samples, using the PISA-wheel [18], spin exchange experiments [19] or through correlation of resonances obtained with solution or MAS solid-state NMR [20].

In Magic-Angle Spinning (MAS) solid-state NMR, the sample is not uniaxially aligned, but is instead spun rapidly around an angle 54.7° relative to the magnetic field. At this angle, the lines become narrower and the anisotropic dipolar couplings and anisotropic chemical shifts are averaged out, while the isotropic chemical shift is retained. Many techniques similar to solution NMR are used, including assignment experiments and PRE. Distance restraints can be obtained in experiments similar to NOE; but based on spin diffusion. The heteronuclear and homonuclear dipolar couplings, as well as chemical shift anisotropy, can be reintroduced with specialized pulse sequences. Recent developments have allowed for a spinning speed up to 111kHz, at which even the ^{1}H-^{1}H dipolar couplings are removed, allowing the direct detection of proton resonances.

1.3 Introduction to chemokines and Interleukin-8

To date, almost 50 different chemokines have been described in mammals [21]. Many are considered to be pro-inflammatory and constitute the chemotactic

gradients responsible for directing neutrophil, macrophage and lymphocyte migration. Chemokine-mediated activation results from the interactions of chemokines with their G Protein-Coupled Receptors (GPCRs), which are involved in a myriad of cellular processes ranging from depolarization of neurons, cell growth and immune response. A complex signaling network results from monomeric, dimeric, and tetrameric chemokines being able to bind several different GPCRs and individual GPCRs being able to bind several different chemokines [22, 23]. Heterodimeric chemokines [24, 25] as well as heterodimeric GPCRs [26-28] have been identified, and may modulate the biological activity of the individual proteins. The molecular basis for chemokine-GPCR interactions is not fully understood, despite extensive studies [29-36]. An example of one of the best-studied chemokines is CXCL8 (Interleukin-8 (IL-8)), which has high affinity for the receptors CXCR1 and CXCR2. The binding of IL-8 to CXCR1 and the subsequent activation of signaling cascades are involved in neutrophil chemotaxis and activation, angiogenesis and wound healing [37-40]. The central role of IL-8 in the immune system means that its misregulation contributes to many diseases, including cancer, COPD and various immune diseases [41, 42].

Chemokines are divided into four classes [43, 44], with IL-8 being part of the CXC class, based on the presence of a motif composed of two cysteines separated by one amino acid. Many chemokines have similar three-dimensional structures. This so-called chemokine fold consists of a disordered N-terminus, the

N-loop, one turn of a 3_{10}-helix, three β-strands connected by the so-called 30s loop, the so-called 40s loop and the so-called 50s loop, and a C-terminal α-helix. The structure of IL-8 has been determined by NMR spectroscopy and X-ray crystallography under a variety of conditions and with different mutations [45-50].

Most chemokines can dimerize with the dimerization interface formed by the first β-sheet and the C-terminal α-helix. It is likely that IL-8 is a monomer under physiological conditions [51], but both the monomer and dimer can bind CXCR1 and CXCR2. Monomeric and dimeric IL-8 have been shown to have different recruitment profiles, with IL-8 dimers being retained longer and showing less activation of neutrophils [52-54]. Furthermore, CXCR1 has higher affinity for the IL-8 monomer than dimer, while the opposite is true for CXCR2 [55-57]. Therefore, the monomer/dimer equilibrium of IL-8 appears to be important for regulation.

1.4 Introduction to G Protein-Coupled Receptors and the chemokine receptor CXCR1

It is estimated that 40% of all drugs currently on the market target a G Protein – Coupled Receptor (GPCR) [58]. The entire family of GPCRs exhibits an incredible amount of variety, not only in the type of ligands that can be bound, but also their connection to a myriad of signaling pathways and cellular processes. Their overall fold, however, is very similar; all GPCRs have seven transmembrane

spanning helices, a flexible extracellular N-terminus that varies in length between different receptors, and an intracellular C-terminus. Most ligands and agonists studied to date interact with the N-terminus, the extracellular loops or the extracellular side of the helical bundle. After the initial interaction, a conformational change takes place, which includes a change in the tilt angle of some of the transmembrane helices, after which an intracellular heterotrimeric G-protein bound to the C-terminus initiates one or more of the associated signaling cascades. The heterotrimeric G-protein consists of α, β and γ subunits, see figure 1. Upon activation, GDP is exchanged for GTP on the Gα subunit, which diffuses away from the G$\beta\gamma$ dimer [59]. Four different classes of Gα proteins have been identified that all activate different signaling cascades; Gαi inhibits adenylyl cyclase and the production of intracellular cAMP, Gαq activates phospholipase C, Gαs stimulates adenylyl cyclase and cAMP, and Gα12/13, activates monomeric GTPases belonging to the Rho family of proteins [60]. Inactivation of the GPCR and signaling cascades is regulated via different proteins: RGS proteins, Regulator of G protein Signaling, have GTPase activity and return the Gα proteins back to their inactive GDP-bound state. The β-arrestin family of proteins has dual functions; they bind the C-terminus of a GPCR and recruit clathrin to help internalize the receptor, and they also recruit G Protein Receptor Kinases (GRK), which phosphorylates the GPCR and displace the G Proteins from the receptor [61, 62]. The GPCR activation process is not very well understood on a molecular level and is likely to vary from receptor to receptor. Several motifs are conserved

among GPCRs that are likely important for its function; the D-R-Y motif in TM3 is thought to be involved in receptor activation, because mutations in this motif result in a constitutively active receptor [29]. The C-W-x-P motif in TM6 is thought to act as a rotameric switch in the activation process [63]. And the N-P-x-x-Y motif in TM7 is likely involved in relaying the activation signal to the G-protein [64]. Despite knowing about the different motifs and their apparent function, the exact molecular mechanism of ligand binding, receptor activation, and G-protein signaling is not fully understood. Thus far, almost forty GPCR structures have been determined, in both active as well as inactive conformations. A total of six chemokine receptors structures were solved, one example is the solid-state NMR structure of CXCR1.

The chemokine receptors CXCR1 and CXCR2 are expressed on the surface of several cells that are part of the immune system; neutrophils, NK cells, dendritic cells, T cells and mast cells. CXCR1 and CXCR2 have 77% sequence identity, with most of the differences clustered in the N- and C-termini. CXCR1 is only able to interact with chemokines IL-8 and GCP-2, whereas CXCR2 is more promiscuous and can interact with seven chemokines; CXCL1, CXCL2, CXCL3, CXCL5, CXCL6, CXCL7 and IL-8 [65-67]. CXCR1 and CXCR2 are both involved in neutrophil chemotaxis but are thought to play different roles, see figure 1. They both interact with $G\alpha i$, decrease cAMP levels, stimulate $(PI)^3$ hydrolysis and increase intracellular Ca^{2+}, however, only CXCR1 activates phospholipase D and

initiates a respiratory burst [68-70]. Additionally, CXCR2 is desensitized and internalized faster than CXCR1 [71].

Our lab solved the structure of the chemokine receptor CXCR1. The receptor was reconstituted in DMPC bilayers and solved using rotationally aligned solid-state NMR spectroscopy [13, 72, 73]. The overall fold is very similar to that of CXCR4, another chemokine receptor solved earlier using X-ray crystallography [74]. Both structures were found to have kinks in the transmembrane helices, all in similar locations. The largest differences occur close to the C-terminus: helix 7 in CXCR1 is slightly longer, extending a couple residues beyond the conserved N-P-x-x-Y sequence, and CXCR1 has an 8^{th} helix located in the mobile C-terminus that aligns along the membrane surface.

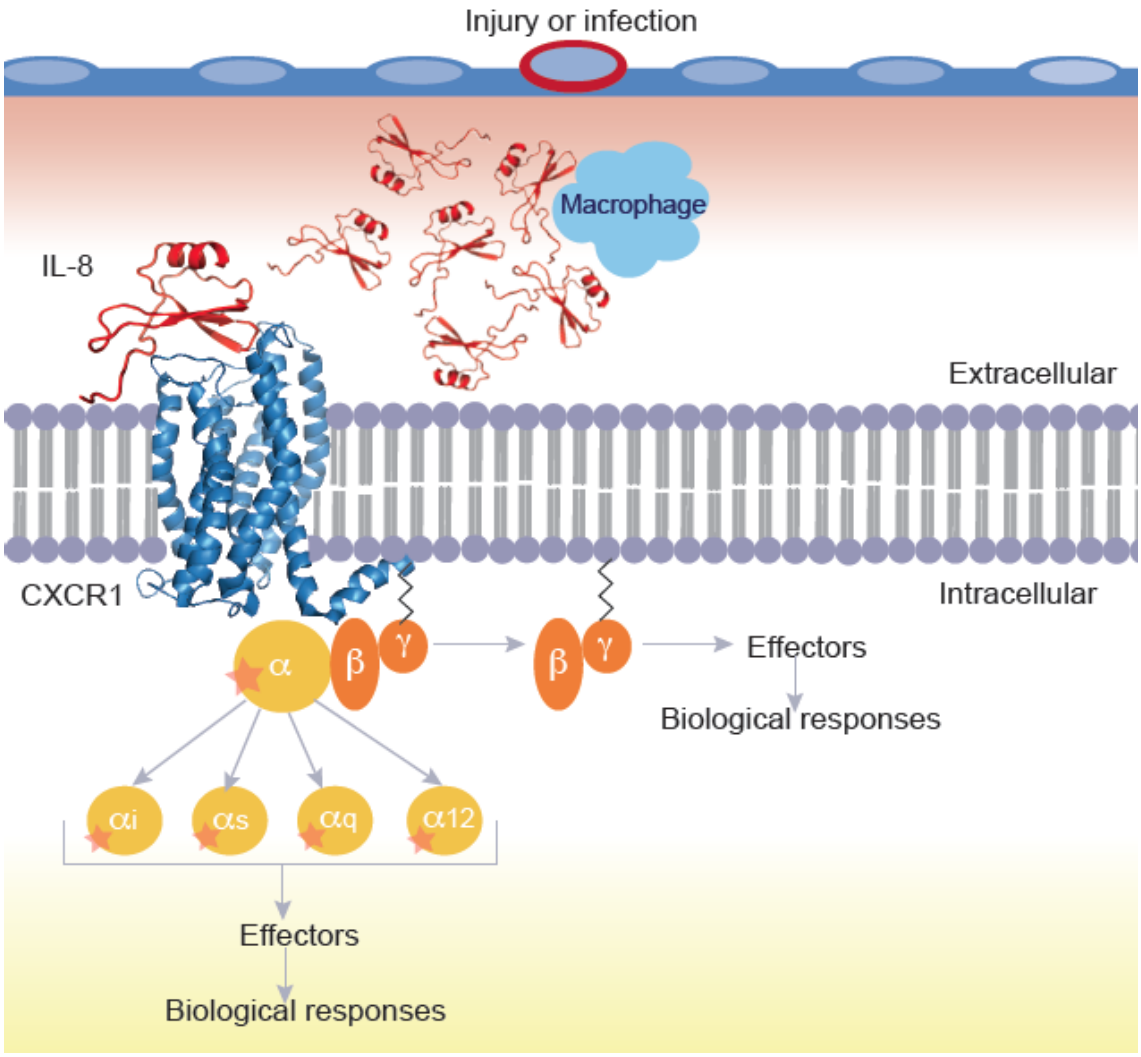

Figure 1.1 Schematic diagram depicting the interaction between IL-8 and CXCR1

The interaction between chemokine IL-8 and receptor CXCR1 is only partially understood. Mutational and biophysical data suggest that there are two main interaction sites on CXCR1: Site-I composed of the flexible 38-residue N-terminus, and Site-II, composed of extracellular loops 2 and 3. Site-I is likely involved in the selection of the ligand. This area has the highest sequence diversity among GPCRs; CXCR1 and CXCR2 have only 33% sequence identity in

this region. Exchanging site-I between CXCR1 and CXCR2 alters their binding specificity [31, 75-77]. Several residues in Site-II are thought to be less important for the interaction with IL-8, but crucial for receptor activation. The triple mutant R199H/R203H/D265H, for instance has high affinity for IL-8 binding but no receptor activation is observed [78].

CHAPTER 2: STRUCTURE OF MONOMERIC INTERLEUKIN-8 AND ITS INTERACTIONS WITH THE N-TERMINAL BINDING SITE-I OF CXCR1 BY SOLUTION NMR SPECTROSCOPY

2.1 Summary

The structure of monomeric human chemokine IL-8 (residues 1-66) was determined in aqueous solution by NMR spectroscopy. The structure of the monomer is similar to that of the full-length protein (residues 1–72), which is a dimer, with the main differences being the location of the N-loop (residues 10–22) relative to the α-helix and the position of the side chain of phenylalanine 65 near the truncated dimerization interface (residues 67–72). NMR was used to analyze the interactions of monomeric IL-8 (1–66) with ND-CXCR1 (residues 1-38), a soluble polypeptide corresponding to the N-terminal portion of the ligand binding site (Binding Site-I) of the chemokine receptor CXCR1 in aqueous solution, and with 1TM-CXCR1 (residues 1-72), a membrane-associated polypeptide that includes the same N-terminal portion of the binding site, the first trans-membrane helix, and the first intracellular loop of the receptor in nanodiscs. The presence of neither the first transmembrane helix of the receptor nor the lipid bilayer significantly affected the interactions of IL-8 with Binding Site-I of CXCR1.

2.2 Introduction

Chemokines are signaling proteins secreted by cells in response to infection or injury. They direct leukocytes, which contain chemokine receptors in their membranes, to the affected cells by providing a concentration gradient for chemotaxis, and activate them for killing the infectious agent through phagocytosis and other mechanisms [40]. Chemokines participate in many diseases, including cancer, and various immune disorders [79]. Humans have about fifty chemokines that interact with twenty-three different G protein-coupled receptors (GPCRs) [21]; the complexity of the system is witnessed by the ability of individual chemokines to interact with multiple receptors, and for individual receptors to interact with multiple chemokines.

Chemokines are small globular proteins typically containing less than one hundred residues. They are divided into four classes [43], although members in different classes have limited sequence homology, the polypeptides share common features of secondary and tertiary structure. In particular, they have one or two disulfide linkages that stabilize the protein fold, and whose disposition in the sequence provides a classification system. The N-terminal residues are flexible; starting with the first cysteine residue, the protein is structured, with the long N-loop terminated by one turn of a 3_{10}-helix, which is followed by three β-strands connected by short loops, and a C-terminal α-helix. Interleukin-8 is a member of the CXC class of chemokines, some of which have a highly conserved glutamate - leucine - arginine (ELR) sequence motif that is crucial for biological

activity [80]. The commonality of structural features suggests that findings about the structure, dynamics, and interactions of an individual chemokine are likely to apply to a broad array of chemokine – receptor structures and functions.

Interleukin-8 (IL-8, CXCL8) was the first chemokine to be discovered [81]. It has 72 residues in its most common form and is a homodimer at high concentrations, although it is a monomer at low concentrations and interacts with its receptor in this form [55-57]. The structure of the wild-type IL-8 dimer was first determined by solution NMR and X-ray crystallography [45, 47]. Subsequently, its structure has been characterized under a range of conditions and with a number of mutations [48-50].

Relatively minor amino acid sequence changes enable the preparation of IL-8 samples that exist as stable monomers or dimers in solution. Non-dissociating IL-8 dimers result from the introduction of a disulfide bond across the dimerization interface [56]. IL-8 monomers have been produced in several ways; by replacing Leu 25 at the dimerization interface with the unnatural amino acid N-methyl leucine, by mutating residues Leu 25, Val 27 and Glu 29 to disrupt the hydrogen bonding network that stabilizes the dimeric form [82, 83], and by removing the last 6 residues of the protein to disrupt the dimerization interface [84, 85], which is the monomeric form used here. The structures of each subunit of dimeric wild type IL-8 and of the monomeric IL-8 containing N-methyl leucine

are similar, with some differences in the position of the first β–sheet and the helical structure of residues 67-72 [47, 50].

CXCR1 and CXCR2 were the first chemokine receptors to be discovered and have high sequence homology [44, 86]. Of the forty GPCR structures that have been determined, six are chemokine receptors, including CXCR1 [72], CXCR4 [74, 87], CCR2 [88], CCR9 [89], CCR5 [90] and the viral receptor US28 [91]. CXCR4 and US28 were co-crystallized with viral chemokines to obtain structural information about the complex [87], however, there are currently no structures available of IL-8 bound to a chemokine receptor. The available experimental data suggest that IL-8 interacts with two main binding sites that may be spatially contiguous on CXCR1. Binding Site-I is located within the extracellular 38-residue N-terminal region of the receptor. Binding Site-II includes Arg119, Arg203 in extracellular loop 2, and Asp265 in extracellular loop 3, among other residues [31, 78, 92, 93]; a synthetic peptide derived from these two extracellular loops connected by a linker was shown to bind IL-8 with a K_D of 0.5mM [94].

There is evidence that wild-type IL-8(1-72) interacts with CXCR1 as a monomer under physiological conditions [51, 84]. Monomeric IL-8(1-66) has been shown to have the same potency in neutrophil chemotaxis and Ca^{2+} mobilization assays [84, 85, 95].

The residues in Binding Site-I of chemokine receptors display high sequence diversity, and are likely responsible for the binding specificity of chemokines. Indeed, the sequences of CXCR1 and CXCR2 vary the most in this region, and swapping N-terminal residues between the two receptors alters their binding specificity [31, 77]. The flexible N-terminal region appears to be a defining characteristic of chemokine receptors, and this has motivated the study of these residues in soluble peptides separate from the rest of the receptor. The affinity of IL-8 for various N-terminal peptides derived from CXCR1 is in the low micromolar range. The first atomic resolution insights came from NMR studies of IL-8 bound to a 21-residue peptide whose sequence corresponds to residues 9 - 29 of CXCR1 [96]. By itself, the peptide does not have a well-defined structure, but it becomes more ordered upon binding IL-8. Several specific residues clustered in the center of the peptide, including Pro21, Pro22, Asp24, Glu25, Asp26 and Pro29, were found to be involved in binding IL-8. More recently, we have shown [97] that additional residues near the N-terminus of CXCR1, including Asn16, Thr18 and Gly19, undergo large chemical shift perturbations upon interaction with IL-8. Moreover, Rajagopalan and Rajarathnam (2004) have shown that IL-8 can bind CXCR1 N-terminal peptides of different lengths, with affinities that are increased by the presence of micelles, suggesting that lipids may influence the interactions of IL-8 with CXCR1. There is evidence that a Trp residue in a 34-mer peptide derived from the CXCR1 N-terminus interacts with DOPC lipid bilayers [98]. Additionally, we have shown that the N-terminus of CXCR1 interacts with the

membrane surface in the absence of IL-8, but dissociates from the membrane in the presence of IL-8 [97].

IL-8 residues responsible for functions of CXCR1 have been identified. Although the characteristic ELR residues (Glu4, Leu5 and Arg6) have been shown to be essential for CXCR1 activation they are not involved in IL-8 binding to N-terminal peptides [84, 99, 100]. The main binding sites on IL-8 have been mapped to the N-loop (residues 12-18) and the 40s loop and third β–sheet (residues 44-51) and include both charged and hydrophobic residues [55, 57, 95-97, 101-103]. Residues Tyr13, Lys15 and Phe21 of the N-loop appear to confer specificity for individual receptors [104]. Furthermore, it has been shown that IL-8 does not undergo a major conformational change upon interaction with the peptide corresponding to the N-terminus of CXCR1 [96]. There is also evidence that IL-8 dimers dissociate upon binding the N-terminal residues of CXCR1, and that there are some minor differences between a covalent IL-8 dimer binding and that of an obligatory IL-8 monomer [54, 55, 57, 102].

Despite extensive studies [105] much remains to be learned about the molecular basis of chemokine-receptor interactions. Here we present the structure of monomeric IL-8(1–66) obtained by deleting the C-terminal residues 67-72, which contribute to the dimerization interface. We also describe binding studies of monomeric IL-8(1-66) with polypeptides corresponding to the N-terminal residues of CXCR1, ND-CXCR1(1-38) and 1TM-CXCR1(1-72), which includes the first

transmembrane helix of CXCR1 in addition to the flexible N-terminal domain.

2.3 Materials and Methods

2.3.1 Protein Expression and Purification

The gene for human IL-8(1-66) was cloned and expressed as described previously [106]. Cell lysis was achieved by sonication in lysis buffer (20mM Tris, 500mM NaCl, 20 mM imidazole, pH=7.4) in the presence of phenylmethane sulfonyl fluoride (MP Biomedicals) and lysozyme. Cell debris was removed by centrifugation, and the supernatant was incubated for one hour on a Nickel-NTA column (Qiagen, Ni-NTA Superflow). The beads were washed with wash buffer 1 (20mM Tris, 300mM NaCl, 30 mM imidazole, pH=7.4) and wash buffer 2 (20mM Tris, 150mM NaCl, 30 mM imidazole, pH=7.4) before being eluted in 20mM Tris, 150mM NaCl with a gradient of 150-300 mM imidazole. The eluate was cleaved using factor Xa (New England BioLabs Inc) and purified by reverse-phase high-performance liquid chromatography on a C18 column (Waters DeltaPak 15mm, 300Å) using an acetonitrile gradient. The purified protein was stored as a lyophilized powder at -20°C. The polypeptide ND-CXCR1(1-38) containing the C30S mutation to enhance its stability was expressed and purified as described previously [107, 108]. The gene for the polypeptide 1TM-CXCR1(1-72) including the C30S mutation and a C-terminal 5x His tag was also expressed and purified

as described previously [107, 109]. 1TM-CXCR1(1-72) from the final HPLC purification was lyophilized and stored at -20°C.

2.3.2 Nanodisc Preparation

Nanodiscs were made with MSP1D1DH5 protein and 1,2-dimyristoyl-sn-glycero-3-phosphocholine (DMPC) [3]. MSP1D1DH5 was expressed and purified as described previously [110]. The optimal molar ratio of 1TM-CXCR1: MSP1D1DH5: DMPC was found to be 0.1 : 1 : 43.3 by gel filtration chromatography screening. This ratio ensures that one nanodisc containing 1TM-CXCR1(1-72) is formed for every four nanodiscs that do not contain this polypeptide, which minimizes protein aggregation and oligomerization. Purified 1TM-CXCR1(1-72) and DMPC (Avanti Lipids) were solubilized in solutions of 0.5% and 1% SDS, respectively, and mixed. MSP1D1DH5 in 20mM Hepes buffer was then added, and all three components incubated for 1 hour with agitation. The detergent was slowly removed overnight by incubation with BioBeads SM-2 (Biorad). The absence of SDS was confirmed by testing with a colorimetric SDS-detection kit (G-Biosciences). Nanodiscs containing 1TM-CXCR1(1-72) were separated from empty nanodiscs by Ni-NTA chromatography exploiting the His-tag on the C-terminus of 1TM-CXCR1; the mixture was allowed to bind and the empty nanodiscs removed using a wash buffer (40mM Tris 300mM NaCl, pH=8). Nanodiscs containing 1TM-CXCR1(1-72) were eluted using elution buffer (20mM Tris, 150mM NaCl, 150mM Imidazole pH=8). Finally, the remaining impurities

were removed by size-exclusion chromatography (20mM Tris, 50 mM NaCl, pH=7.4, Amersham Biosciences, HiLoad 16/60 Superdex 200).

2.3.3 NMR spectroscopy

Uniformly ^{13}C, ^{15}N-labeled IL-8(1-66) was dissolved in 20mM Hepes pH=7.3 containing 10% D_2O. The NMR experiments were performed on a 600 MHz Bruker AVANCE spectrometer equipped with a 5-mm triple-resonance cryoprobe (^{1}H, ^{13}C, and ^{15}N) and *z*-axis pulsed gradient and on a Varian VS 800 MHz spectrometer equipped with a XYZ-gradient triple resonance cryoprobe (^{1}H, ^{13}C, and ^{15}N). Triple-resonance HNCA, HNCO and HNCACB assignment experiments were performed on uniformly ^{13}C, ^{15}N labeled IL-8 (1-66) at 40°C. The side-chain assignments were made with HCC(CO)NH, CC(CO)NH, CbHd and CbHe experiments. Distance restraints were obtained using ^{15}N-edited NOESY–HSQC (mixing time, 200 ms) and ^{13}C-edited NOESY–HSQC (mixing time, 120 ms and 80 ms) experiments. Heteronuclear ^{1}H–^{15}N NOEs were measured by comparing signal intensities obtained with and without ^{1}H saturation during a relaxation delay of 6 seconds at 40°C and 15°C . Hydrogen bond restraints were obtained from a two-dimensional ^{1}H-^{15}N HSQC spectrum of uniformly ^{15}N labeled IL-8(1-66) in 90% D_2O. The experiment was started following a one-hour incubation period. Residual dipolar couplings (RDCs) were measured with HSQC in-phase and anti-phase (IPAP) experiments on IL-8(1-66) in a solution of empty nanodiscs in the presence and absence of 13.5 mg/ml

Y21M fd phage and 70mM NaCl . The Y21M fd phage was produced using a previously described protocol. All NMR experiments were processed using NMRPipe and analyzed using SPARKY. The Chemical Shift Index was determined using TALOS. Chemical Shift Perturbations were calculated using the following equation: $CSP = \sqrt{\Delta H^2 + (\Delta N/5)^2}$

2.3.4 Structure Calculations

All calculations were performed with Xplor-NIH [111], using the EEFx energy function with the topology and parameter files protein_eefx2.top and protein_eefx2.par, and the statistical potential torsionDBPot to restrain dihedral angles. Experimental NMR restraints were implemented with the potentials: NOEPot, for distances derived from NOEs and hydrogen bonds; CDIH for dihedral angles; and RDCPot for RDCs. RDCs were used for cross-validation and not imposed as restraints. Each calculation was initiated from a fully extended polypeptide strand. Simulated annealing calculations were performed as described previously [112], using two protocols, the first to fold a total of 100 initial structures, and the second to refine the 10 folded structures with lowest energy. A total of 100 structures were refined, and the 10 structures with lowest energy were selected for the final ensemble. The coordinates were deposited in the protein data bank (PDB: 5WDZ) and the BMRB (ID: 30316).

2.3.5 Isothermal Titration Calorimetry (ITC)

The ITC experiments were performed at 23°C using a MicroCal iTC200 instrument (GE healthcare Life Sciences) in 20 mM Tris, 50 mM NaCl, pH 7.4 buffers. The concentrations of ND-CXCR1(1-38) in the cell were 65 mM and 50 mM, and that of 1TM-CXCR1(1-72) reconstituted in nanodiscs was 100 mM. IL-8 containing solutions present in the syringe had concentrations of 760 mM, 600 mM and 985 mM. Experiments consisted of 19 injections of 2 mL aliquots separated by 150 seconds.

2.4 Results

2.4.1 Solution NMR structure of monomeric IL-8

As shown in Figure 2.1A, both dimeric [47] and monomeric [50] forms of IL-8 yield well-resolved solution NMR spectra. Although many resonances have similar chemical shifts in both spectra, large differences are observed for selected signals, as marked in the Figure. The largest shifts are from the residues Ile10, Lys15, Lys20, Lys23, Val27, Ser30, Asp52, Val 61, Glu63, Lys64 and Phe65. These residues are located in the N-loop, the first β–strand, and the C-terminal α–helix, and the differences can be readily accounted for by the effects of truncation of six residues (67–72) at the C-terminus. For example, in the structure of the IL-8(1-72) dimer (PDB id: 1IL8), the side chains of Val27 and Ser30 in one

of the monomers contact residues in the first β-strand and the α-helix of the other monomer, respectively.

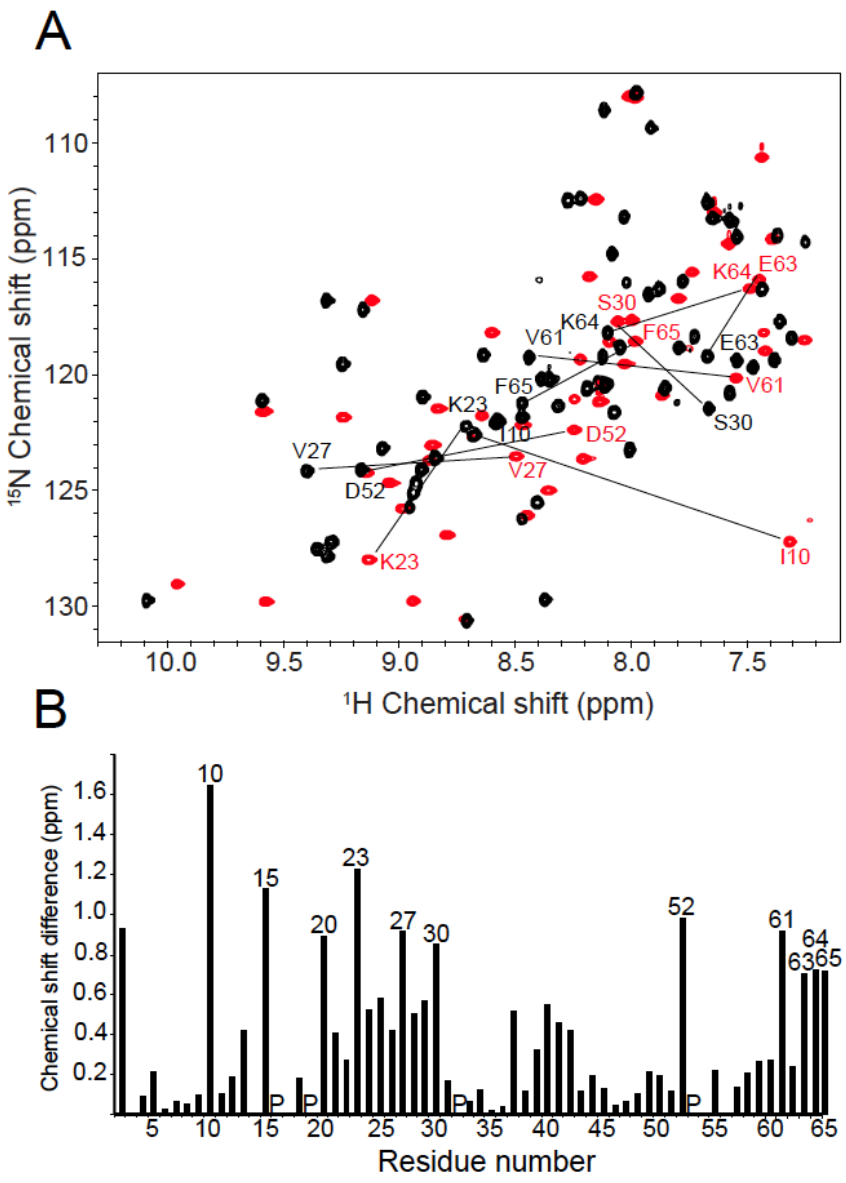

Figure 2.1 Differences between monomeric and dimeric IL-8 (A) Two-dimensional ^{1}H/^{15}N HSQC spectra of uniformly ^{15}N labeled dimeric and monomeric IL-8 obtained under identical conditions in 20 mM HEPES buffer at pH 7.3 and temperature of 313 K. The spectra of dimeric full-length IL-8 (1-72) (in black) and of monomeric IL-8 (1-66) (in red) are superimposed with selected amide backbone resonances marked by their sequential assignments. (B) Bar graph of the weighted chemical shift differences observed between the resonances of dimeric IL-8 (1-72) and monomeric IL-8 (1-66) as a function of residue number; the resonances with the largest differences are marked by their sequential assignments

Samples of uniformly ^{13}C, ^{15}N labeled monomeric IL-8(1-66) enabled a variety of triple-resonance NMR experiments to be used to assign backbone and side chain resonances, to measure chemical shift index (CSI), residual dipolar coupling (RDC), and amide hydrogen exchange parameters as structural restraints, and to measure heteronuclear $^{1}H/^{15}N$ nuclear Overhauser enhancements (NOEs) as indicators of local dynamics. These data are summarized in Figure 2.2 and Table 2.1

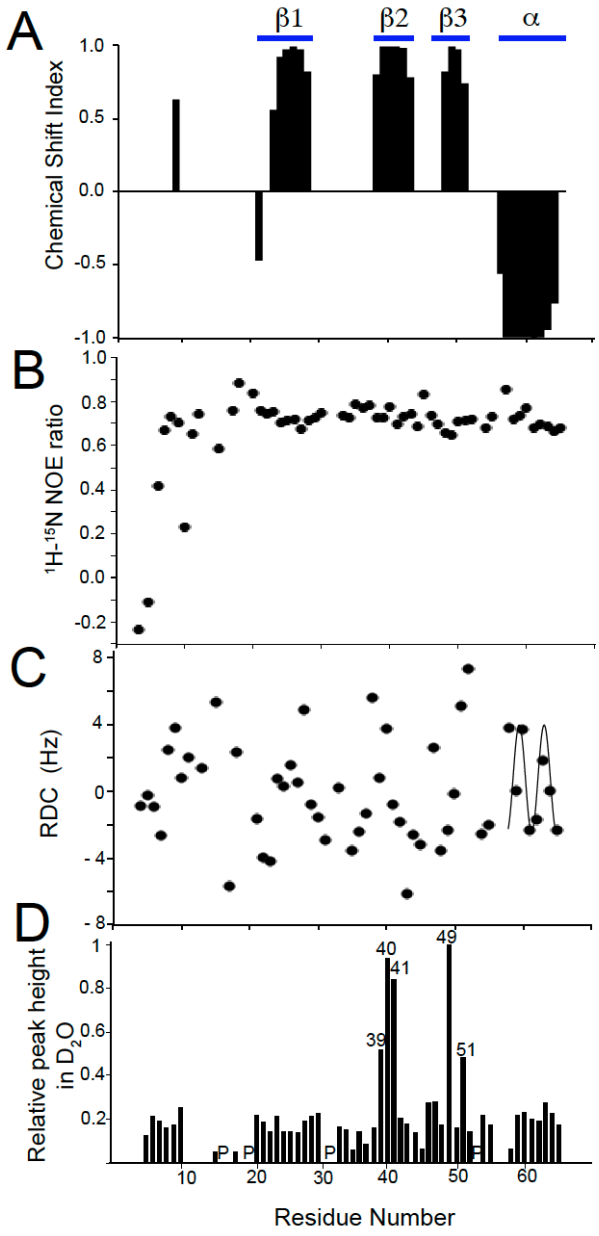

Figure 2.2. Plots of experimental data measured on monomeric IL-8(1-66) in solution as a function of residue number. (A) Chemical Shift Index. (B) ^{1}H/^{15}N heteronuclear NOE. (C) Residual Dipolar Couplings used to cross-validate the solution NMR structure of monomeric IL-8 (1-66). The helical region of the protein displays a characteristic Dipolar Wave pattern. (D) Resonance intensities after incubation of IL-8(1-66) in D_2O for 1 hour. Peak height was measured for all peaks in a ^{1}H/^{15}N HSQC spectrum and normalized to the peak height of residue Leu49. The locations of proline residues are indicated with a 'P'

Table 2.1. Restraint table to calculate the structure of monomeric IL-8 (1-66)

NMR distance and dihedral constraints	
Number of unambiguous NOEs	417
short-range	204
medium-range	159
long-range	54
Hydrogen bond restraints	22
Dihedral angle restraints (TALOS)	107
Structure statistics	
Molprobity analysis	
molprobity score	1.76
clashscore	8.39
poor rotamer (%)	2.90
ramachandran favored (%)	99.68
ramachandran outliers (%)	0.00
Pairwise backbone RMSD (residues 7-65)	0.97 Å
Heavy-atom RMSD (residues 7-65)	1.83 Å

The four types of NMR data displayed in Figure 2.1 are aligned according to residue number. The major regions of secondary structure are delimited at the top of the Figure. Analysis of the CSI plot in Figure 2.1A is consistent with the locations of the secondary structure elements established in previous studies of IL-8 [45, 47-50]. Notably, monomeric IL-8(1-66) has three β-strands in the middle of the sequence and an α-helix located at the C-terminus. Although the C-terminus of the 72-residue full-length protein is shortened by six residues, the remaining helical residues (57-66) maintain a stable secondary structure as

evidenced by the heteronuclear NOE values for these residues (Figure 2.2B) and the ability to fit a Dipolar Wave to the RDCs for these residues (Figure 2.2C).

Signals could not be observed for either residue 66, the C-terminal residue, or residue 1, the N-terminal residue, most likely due to local dynamics interfering with the NMR experiments. Signals from all of the other residues could be observed, even though the N-terminal residues of IL-8(1-66) show evidence of minimal structure and substantial local dynamics. Signals from residues 2-6 have negative $^{1}H/^{15}N$ heteronuclear NOEs (Figure 2.2B) indicative of local motions, and the residues closest to the N-terminus have near-zero values for their $^{1}H/^{15}N$ RDCs (Figure 2.2C) and only six observable long-range ^{1}H-^{1}H homonuclear NOEs, all of which connect this region to residues 32 and 33 in the 30s loop (residues 29-37). Notably, the three conserved residues (4–6) of the ELR motif essential for activity show evidence of local motions. These results are consistent with those of previous solution NMR and X-ray crystallography studies of IL-8 where the positions of residues 1-6 could not be well defined [45, 47, 50, 113].

The data in Figure 2.2B show that residues 7 - 65 have $^{1}H/^{15}N$ heteronuclear NOE values of about 0.8, which indicates that, except for the N-terminal region, IL-8(1-66) has a stable backbone structure consistent with a well-folded protein. Using fd bacteriophage as the alignment medium, the measured $^{1}H/^{15}N$ RDCs plotted in Figure 2.2C have values between 6.6 Hz and -6.2 Hz. As mentioned above, the RDCs for residues 58-65 were well fit to a Dipolar Wave

with a periodicity of 3.6 [114], which provide strong additional evidence that the C-terminal residues form a stable α-helix until the last residue of monomeric IL-8(1-66), despite the removal of the final six residues from the full-length wild-type protein. Hydrogen bonding restraints for structural analysis were obtained by measuring the loss of amide H-N resonance intensities in $^{1}H/^{15}N$ HSQC spectra of IL-8(1-66) following its transfer from H_2O to D_2O solution, see Figure 2.3.

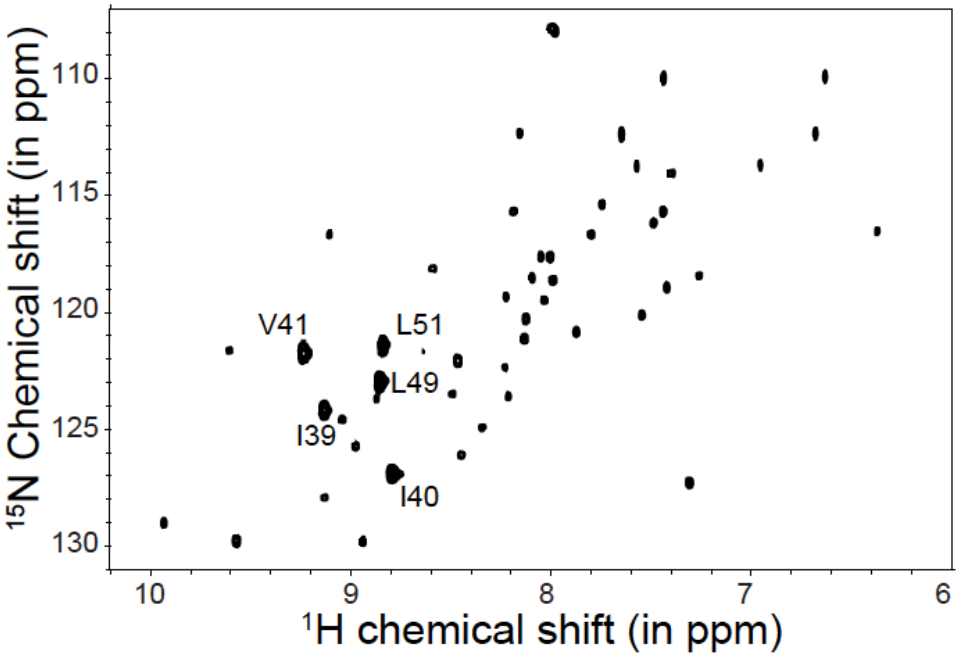

Figure. 2.3 ^{1}H-^{15}N HSQC spectrum of monomeric IL-8(1-66) after 1 hour incubation in D_2O. The five most intense resonances are marked with their residue numbers

These results are summarized in the plot of relative signal intensities as a function of residue number in Figure 2.2D. Five particularly intense resonances are observed in spectra obtained after several hours of incubation in D_2O, indicating the presence of stable hydrogen bonds in a number of residues located

near the middles of the second and third β–strands; weaker but still observable signals from sites throughout the protein are present in the spectrum.

We determined the structure of monomeric IL-8(1-66) in solution using NMR restraints summarized in Table 2.1 and methods described in the Experimental Section. As anticipated from the data in Figure 2.2, the structure of IL-8(1-66) is well defined for residues 6-65, which contains three anti-parallel β–strands and the C-terminal α-helix, with a pairwise RMSD of 0.97 Å. Including the flexible N-terminal residues, the structure of residues 1 - 66 has an overall pairwise RMSD of 1.6 Å. This is illustrated graphically by the superimposed 10 lowest energy structures in Figure 2.4A.

The overall structure of monomeric IL-8(1-66) (PDB 5WDZ) shown in red in Figure 2.4 is similar to that of each of the monomeric subunits of dimeric full-length IL-8(1-72) (PDB id: 1IL8) shown in blue. The principal differences in the structures are associated with the N-loop (residues 10-19) and the side chain of Phe65. In the previously determined structures of wild-type IL-8(1-72) and monomeric Leu25-NMe IL-8(1-72) (PDB id: 1IKL) the N-loop runs roughly parallel to the α-helix at a slight angle that places its N-terminal end further away from the α-helix than the C-terminal end (blue in Figure 2.4D). By contrast, in the structure of monomeric IL-8(1-66) the N-loop and the α-helix are almost parallel (red in Figure 2.4D). The C-terminal part of the N-loop in IL-8(1-66) shifts away from the α-helix by about 3 Å compared to full-length IL-8, regardless of whether the

protein is a monomer or a dimer. In the NMR structure of dimeric wild-type IL-8(1-72), the amide nitrogen atoms of Ser14 and Trp57, which are located in the N-terminal parts of the N-loop and the α-helix, respectively, are separated by 10.9 Å, and residues Lys20 and Phe65, which are in the C-terminal parts of the N-loop and α–helix, respectively, are separated by 7.5 Å. The same residues, Lys20 and Phe65, are separated by 10.52 Å and 10.46 Å, respectively, in the structure of monomeric IL-8(1-66). This is shown in Figure 2.4D. The difference in the relative position of the N-loop may be related to the change in position of the side chain of Phe65. In the structure of wild-type IL-8(1-72) the aromatic ring of Phe65 points away from the N-loop towards the dimerization interface; by contrast, in the structure of monomeric IL-8(1-66) the same side chain points towards the N-loop, in the space occupied by the N-loop in the other structures. This corresponds to a movement of 4.3 Å for the Cd2 atom, as illustrated in Figure 2.4E.

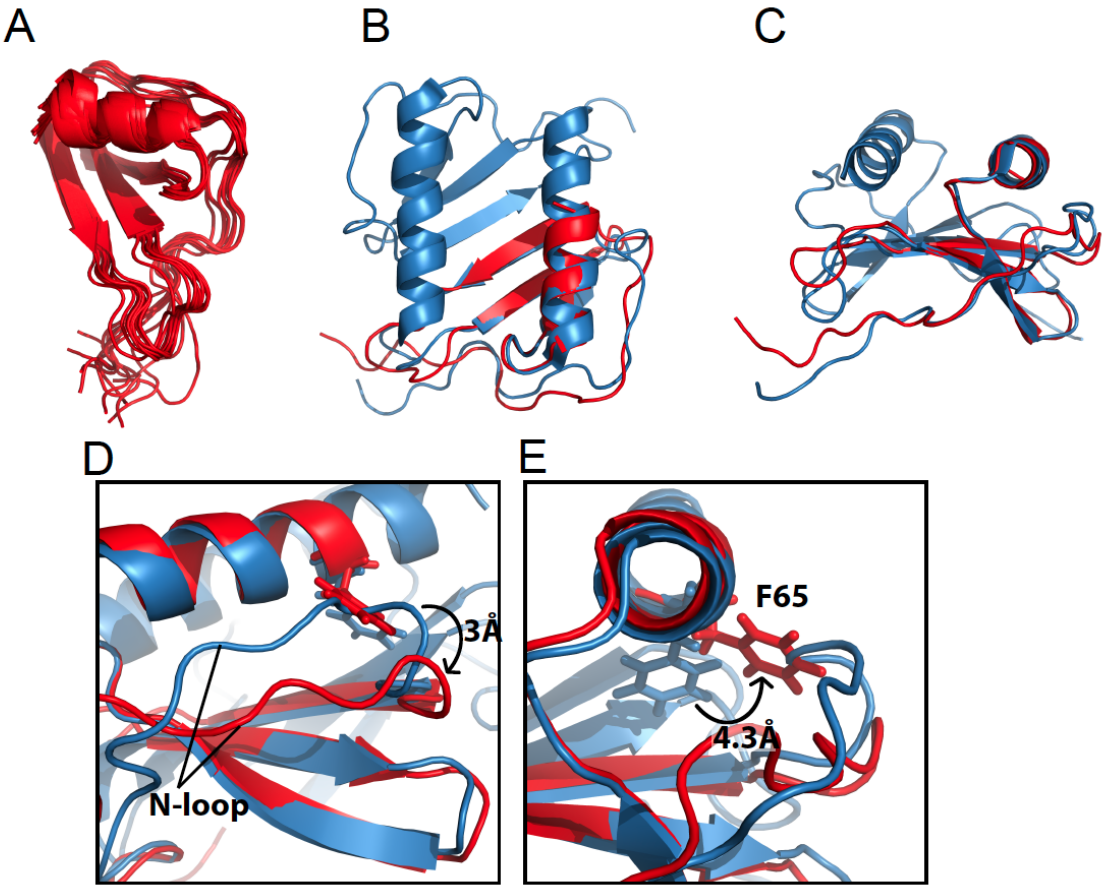

Figure 2.4 Solution NMR structure of monomeric IL-8 (1-66). (A) Overlay of the ten lowest energy structures of monomeric IL-8(1-66). (B) Structure of monomeric IL-8(1-66) in red overlayed with the solution NMR structure of full-length IL-8(1-72) in blue (PDB ID: 1IL8). (C) Same as in (B) only rotated 90°. (D) Expanded structural region of monomeric IL-8(1-66) in red and wild type IL-8 in blue. The change in position of the N-loop relative to the C-terminal helix between monomeric IL-8 and wild type IL-8 is shown. Differences in distances as measured between the amide nitrogen atoms of residues K20 and F65 (E) Expanded structural region of monomeric IL-8(1-66) in red and wild-type IL-8 in blue. The difference in position of the Cd atom of Phe65 between monomeric IL-8(1-66) and wild type IL-8(1-72) is shown.

2.4.2 Interaction of monomeric IL-8(1-66) with ND-CXCR1 and 1TM-CXCR1

To gain insight into how the chemokine IL-8 interacts with its receptor CXCR1 we expressed and purified polypeptides with sequences corresponding to residues 1-38 and 1-72 of CXCR1. There have been many studies of soluble

peptides similar to ND-CXCR1(1-38) because the N-terminal domain (ND) contains the part of the agonist binding site referred to as Binding Site-I [75-77, 93, 115]. The longer polypeptide 1TM-CXCR1(1-72) includes the complete N-terminal domain, the first transmembrane helix (1TM), and the first intracellular loop of CXCR1. This polypeptide is not soluble in aqueous solution and requires the presence of detergents or lipids for solubilization. The transmembrane helix ensures the proximity of Binding Site-I to the surface of the lipid bilayer when the polypeptide 1TM-CXCR1(1-72) is in nanodiscs.

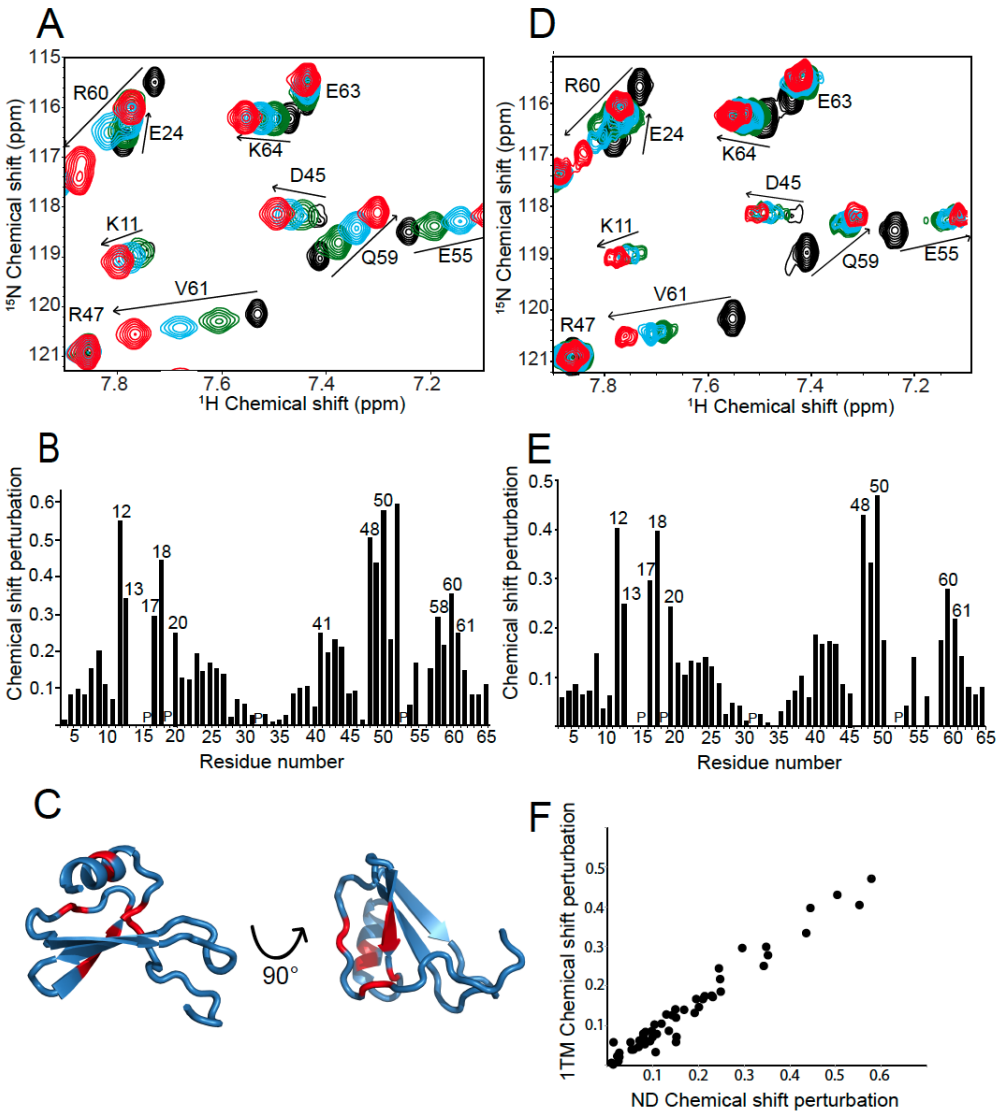

Figure 2.5 Characterization of IL-8 binding to 1TM-CXCR1 and ND-CXCR1 (A). Selected region of solution $^{1}H/^{15}N$ HSQC spectra of uniformly ^{15}N labeled monomeric IL-8(1-66) with increasing amounts of unlabeled ND-CXCR1(1-38) added. The colors represent the molar ratio ND-CXCR1:IL-8. Black is 0, green is 0.25, blue is 0.5, and red is 1. (B) Chemical Shift Perturbation plot of the data in (A). The locations of proline residues are indicated with a 'P' (C) Structure of monomeric IL-8(1-66) with red marking the residues with the largest chemical shift perturbation upon interaction with ND-CXCR1. (D). Selected region of a solution $^{1}H/^{15}N$ HSQC spectrum of uniformly ^{15}N labeled monomeric IL-8(1-66) with increasing amounts of unlabeled 1TM-CXCR1 reconstituted in nanodiscs. The same color representation of molar ratios as used in Panel A. (E) Chemical shift perturbation plot of the data in (D). (F) Scatter plot showing the correlation between the chemical shift perturbations of monomeric IL-8(1-66) bound to ND-CXCR1(1-38) and to 1TM-CXCR1(1-72). R^2 is 0.95.

The effects on residues of IL-8(1-66) by interaction with Binding Site-I of CXCR1 were determined using NMR titration experiments. Two-dimensional $^{1}H/^{15}N$ HSQC spectra were obtained from samples containing a fixed amount of uniformly ^{15}N labeled IL-8(1-66) and varying amounts of unlabeled ND-CXCR1(1-38) or 1TM-CXCR1(1-72). Signals from IL-8 residues that occupy a different chemical environment upon addition of a receptor-derived polypeptide, either due to direct interaction or a local change in conformation, undergo changes in their ^{1}H and/or ^{15}N chemical shift frequencies. The expanded spectral regions in Figure 2.5 compare the effects of IL-8(1-66) binding to ND-CXCR1(1-38) (panel A) and to 1TM-CXCR1(1-72) (panel D). The three main interaction regions of IL-8(1-66) can be discerned from the bar graphs of the chemical shift differences as a function of residue number in panels B and E. Signals from the N-loop (residues 10-19), the third β–strand (residues 47-51), and part of the C-terminal α–helix (residues 56-65) are affected by binding to the polypeptides containing Binding Site-I; in particular, the resonances from Thr12, Tyr13, Phe17, and His18 have the most strongly perturbed chemical shifts. No signal from Ser14 could be observed in any of the experiments, and the signal from Lys15 was broadened beyond detection upon interaction with both ND-CXCR1 and 1TM-CXCR1. No signal from residue 16 could be observed because proline lacks an amide N-H.

It has been proposed that residues in the N-loop confers receptor binding specificity [83]. Evidence of interactions with the N-terminal part of the receptor by residues in the third β–sheet and part of the α-helix has been detected in studies

of using similar constructs [57, 95-97, 102-104]. Both non-polar (Leu49, Val58, Val61) and charged (Glu48, Asp52, Arg60) residues of IL-8(1-66) are affected by binding to the polypeptides containing sequences from the N-terminal region of CXCR1. Chemical shift perturbations for Asp52 and Val58 could only be observed upon binding to ND-CXCR1, since the signals were broadened beyond detection upon interaction with 1TM-CXCR1 in nanodiscs.

The residues whose chemical shifts are affected by binding to the polypeptides containing the N-terminal domain of the receptor are marked by their residue numbers in Figure 2.5B and E. They are located in three distinct regions of the sequence and are colored red in the structure of IL-8(1-66) shown in Figure 2.5C where they are shown to be in close spatial proximity. Notably, signals from residues in the conserved ELR motif near the N-terminus and from the extreme C-terminus of the α-helix undergo only minor chemical shift perturbations upon binding.

Significantly, the chemical shift perturbation patterns for IL-8(1-66) binding to the polypeptides ND-CXCR1(1-38) and 1TM-CXCR1(1-72) are similar. The chemical shift perturbations resulting from binding to ND-CXCR1(1-38) are compared to those from binding to 1TM-CXCR1(1-72) in the scatter plot shown in Figure 2.5F. The linear correlation has an R^2 value of 0.95, and indicates that IL-8(1-66) binds similarly to the N-terminal domain of CXCR1 in the absence and presence of the first trans-membrane helix. Further, it suggests that the

interactions between IL-8(1-66) and Binding Site-I of the receptor are not influenced by the presence of a lipid bilayer.

To ensure that the absence of spectroscopic differences in IL-8(1-66) binding to ND-CXCR1(1-38) and 1TM-CXCR1(1-72) are not due to different binding affinities or to the nanodiscs themselves, isothermal titration calorimetry experiments were performed, see Figure 2.6

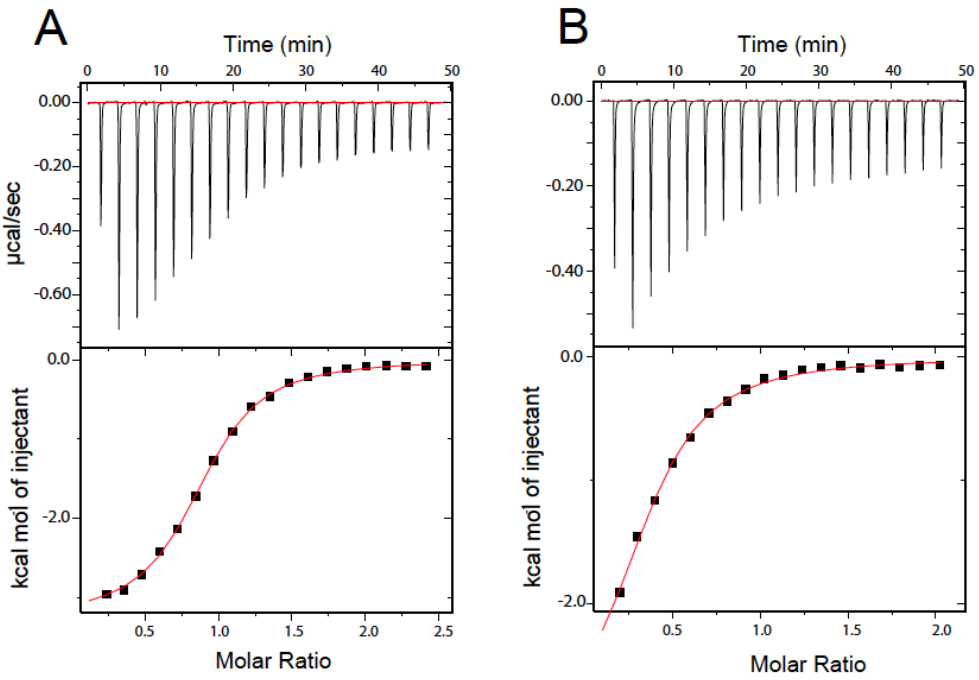

Figure. 2.6 Isothermal Titration Calorimetry experimental results. (A) ITC titration of monomeric IL-8 (1-66) and ND-CXCR1(1-38). N=0.869, K_D=3.5μM, DH=-3.2 kcal/mol and DS=14.1 cal/mol/deg (B) ITC titration of monomeric IL-8 (1-66) and 1TM-CXCR1 (1-72) reconstituted in MSP1D1DH5 nanodiscs N= 0.357, K_D=12.5μM, DH=-3.1 kcal/mol and DS=11.7 cal/mol/deg Top panel shows experimental data. Bottom panel shows integrated data fitted to extracted values of K_D, DH and DS, after subtraction of titrations of IL-8 in buffer and empty nanodiscs, respectively.

ND-CXCR1(1-38) and 1TM-CXCR1(1-72) reconstituted into nanodiscs were placed in the chamber and aliquots from a concentrated solution of IL-8(1-66) were added. The K_D for IL-8(1-66) binding to ND-CXCR1(1-38) was determined to be 3.5 μM, and that for IL-8 binding to 1TM-CXCR1(1-72) was 12.5 μM. These results suggest that IL-8(1-66) has a slightly weaker interaction with 1TM-CXCR1(1-72) than it does with ND-CXCR1(1-38). The enthalpy and entropy changes associated with binding were also comparable; DH=-3.2 kcal/mol and DS=14.1 cal/mol/deg for the interaction between IL-8(1-66) and ND-CXCR1 and DH=-3.1 kcal/mol and DS=11.7 cal/mol/deg for the interaction between IL-8(1-66) and 1TM-CXCR1(1-72) in nanodiscs. No interactions were observed in control experiments performed with IL-8(1-66) titrated into blank buffer solution and into empty nanodiscs. An additional control experiment was performed by titrating IL-8 into a solution containing both ND-CXCR1(1-38) and empty nanodiscs. The K_D for IL-8(1-66) binding to ND-CXCR1(1-38) in the presence of empty nanodiscs was determined to be 3.2 μM, very similar to the value found in the absence of nanodiscs, further demonstrating that the presence of a membrane does not affect the binding of IL-8(1-66) to Binding Site-I of CXCR1 (data not shown).

2.5 Discussion and conclusions

The chemokine IL-8 interacts with the chemokine receptor CXCR1. The structure of monomeric IL-8(1-66) is similar to that of full-length IL-8(1-72) in both monomeric and dimeric forms, which demonstrates that the truncation of six

residues at the C-terminus, necessary to form a stable monomeric species, does not have a significant effect on the overall fold of the chemokine. IL-8(1-66) binds to two polypeptides with sequences corresponding to the N-terminal region of the CXCR1 receptor. ND-CXCR1(1-38) includes Binding Site-I and is water soluble, while 1TM-CXCR1(1-72) includes Binding Site-I and the first hydrophobic trans-membrane helix of CXCR1 and requires the presence of lipids.

Docking and molecular dynamics studies between IL-8 and CXCR1 have been performed using the solid-state NMR structure of CXCR1 in lipid bilayers (PDB id: 2LNL) supplemented with NMR data on N-terminal domain derived peptides and homology studies to other GPCRs [72, 116, 117]. In the resulting model, charged residues in the N-loop of IL-8 interact with residues in the N-terminal domain of CXCR1 (Binding Site-I), and hydrophobic residues in IL-8 contact hydrophobic residues in the N-terminus of CXCR1, which results in a rotation of IL-8. Finally, electrostatic interactions attract the ELR motif in IL-8 to the extracellular loops of CXCR1, which constitute Binding Site-II, triggering a conformational change that activates the receptor. A very similar series of events is expected to take place in other chemokine receptors [105].

The residues of IL-8(1-66) involved in the interactions with Site I of CXCR1 were identified by chemical shift perturbations. Three main regions of IL-8(1-66) were shown to interact with ND-CXCR1(1-38), the N-loop, the third β–sheet, and the N-terminal part of the α-helix. This result agrees with previous studies

performed on wild-type IL-8 and similar soluble peptides with sequences derived from CXCR1 [54, 57, 95-97, 99, 101-104, 118, 119]. The studies of the interaction of IL-8 with soluble polypeptides containing Binding Site-I were extended by the preparation of a longer polypeptide that contains the N-terminal domain and the first trans-membrane helix of CXCR1. This insoluble polypeptide was reconstituted into nanodiscs, which provide a bilayer environment proximal to Binding Site-I. No significant differences were found in how IL-8(1-66) binds to the shorter construct ND-CXCR1(1-38) or the longer membrane –associated construct 1TM-CXCR1(1-72)..

These results indicate that the presence of the first trans-membrane helix does not affect the interaction of IL-8 with Binding Site-I in the N-terminal domain of CXCR1. Similar conclusions have been reached based on experiments where the N-terminal domain of the chemokine receptor CCR2 was fused to the trans-membrane segment of an unrelated receptor; chemokine binding was not affected, showing that the N-terminal portion of a chemokine receptor is both necessary and sufficient for chemokine-receptor interactions [120].

It has been hypothesized that another possible difference between studies on the peptide and ligand binding *in vivo* could be the presence of the lipid bilayer [106, 121]. However, we do not observe significantly different chemical shift perturbations between IL-8(1-66) binding to ND-CXCR1(1-38) in an aqueous environment and to 1TM-CXCR1(1-72) in nanodiscs. This suggests that it is

unlikely that the membrane influences the final conformation of ND-CXCR1 upon interaction with IL-8. However, the presence of the lipid bilayer may affect the conformation of the unbound N-terminal domain. Previously, we observed that ND-CXCR1 is immobilized in the presence of DMPC/DHPC bicelles, but appears to lose this interaction upon binding IL-8 [97, 98].

Activity and mutational studies have shown that residues Glu4, Leu5 and Arg6 are essential for receptor activation, but not for receptor interactions. The ELR motif is therefore thought to be important for the interaction with the second binding site associated with extracellular loops of CXCR1 and not involved in binding the N-terminal domain [84, 99-101]. This is supported by the lack of chemical shift perturbations for these residues upon interaction with both ND-CXCR1(1-38) and 1TM-CXCR1(1-72). Only small chemical shift perturbations are observed at the C-terminus. This is the location of the α-helix and the site of the truncation to make this construct of IL-8(1-66) monomeric, confirming experimental data obtained by others that the truncation of the most C-terminal 6 amino acids has no effect on CXCR1 binding or activation [84, 118, 122]. However, these residues are thought to be important for interaction with glycosaminoglycans [123, 124].

IL-8(1-66) is a stable monomer because of the truncation of the last 6 residues, which participate in the dimer interface. This structure is very similar to those of dimeric and monomeric full-length IL-8(1-72), with the exception of the

location of the N-loop relative to the α-helix and the side chain of phenylalanine 65. IL-8 binds to the residues in the N-terminal domain of CXCR1 that constitute Binding Site-I regardless of the presence of the first trans-membrane helix or a lipid membrane. This suggests that the presence of IL-8 the N-terminal domain of CXCR1 does not interact with the membrane. Thus, investigations of the interactions of IL-8 with Binding Site-II, located among the extracellular loops of CXCR1, are essential for understanding the how the agonist triggers the conformational changes and receptor activation in the membrane environment.

Chapter 2, in full, is a reprint of the material as it appears in the Journal of Biomolecular NMR (2017) 69:111–121. Berkamp, S., Park, S.H., De Angelis, A. A., Marassi, F. M. and Opella, S. J. The dissertation author was the primary author of this paper.

CHAPTER 3: INTERACTION OF MONOMERIC INTERLEUKIN-8 WITH CXCR1 MAPPED BY PROTON-DETECTED FAST MAS SOLID-STATE NMR

3.1 Abstract

The human chemokine interleukin-8 (IL-8; CXCL8) is a key mediator of innate immune and inflammatory responses. This small, soluble protein triggers a host of biological effects upon binding and activating CXCR1, a G protein-coupled receptor, located in the cell membrane of neutrophils. Here, we describe ^{1}H-detected magic angle spinning solid-state NMR studies of monomeric IL-8 (1-66) bound to full-length and truncated constructs of CXCR1 in phospholipid bilayers under physiological conditions. Cross-polarization experiments demonstrate that most backbone amide sites of IL-8 (1-66) are immobilized and that their chemical shifts are perturbed upon binding to CXCR1, demonstrating that the dynamics and environments of chemokine residues are affected by interactions with the chemokine receptor. Comparisons of spectra of IL-8 (1-66) bound to full-length CXCR1 (1-350) and to N-terminal truncated construct NT-CXCR1 (39-350) identify specific chemokine residues involved in interactions with binding sites associated with N-terminal residues (binding site-I) and extracellular loop and helical residues (binding site-II) of the receptor. Intermolecular paramagnetic relaxation enhancement broadening of IL-8 (1-66) signals results from interactions of the chemokine with CXCR1 (1-350) containing Mn^{2p} chelated to an unnatural amino acid assists in the characterization of the receptor-bound form of the

chemokine.

3.2 Introduction

More than 800 G protein-coupled receptors (GPCRs) are encoded in the human genome. These membrane proteins have seven transmembrane helices and each binds to one or multiple extracellular molecular signals, typically small molecules, but in some cases proteins. Their activation triggers many physiological processes through interactions with intracellular proteins. The structures, dynamics, and functions of GPCRs are of keen interest to both physiology and medicine, especially because they are receptors for a large fraction of the drugs in current use and provide fertile ground for the targeted development of new drugs [125]. Although there has been significant progress in recent years in the characterization of static structures of crystalline GPCRs at low temperatures [126-128], relatively little is known about their binding to, and activation by, naturally occurring agonists, especially proteins, under physiological conditions where both agonist and receptor dynamics are likely to play important roles. Here we examine the interactions between a chemokine agonist and its receptor in the near-native environment of hydrated phospholipid bilayers by NMR spectroscopy.

About 50 chemokines and 20 chemokine receptors constitute an important part of the innate immune system [21]. Not only do these proteins play key roles

in the defense against microbial infections, but they are also associated with responses to inflammatory diseases such as arthritis, asthma, and cancer [79]. The chemokine interleukin-8 (IL-8; CXCL8) binds to and activates the GPCR CXCR1 in the cell membranes of neutrophils, which then interact with G-proteins, arrestins, and other intracellular proteins to initiate biochemical responses of the cell. IL-8 and CXCR1 serve as a prototypical chemokine system because they are the first of their types to be discovered and are among the best characterized [81].

IL-8 is a small soluble protein with 72 residues. Its structure, determined by solution NMR spectroscopy [47] and x-ray crystallography [45], is characterized by having a flexible N-terminal segment containing a conserved Glu-Leu-Arg (ELR) motif just before the characteristic CXC arrangement of cysteine residues (X represents another type of amino acid) that participate in the two disulfide bonds that stabilize the tertiary fold of the three β-strands and single a-helical segment. Most CXC chemokines have between 70 and 130 residues with substantial variation of sequences. However, they share the characteristic three-dimensional chemokine fold first described for IL-8, which suggests that there may be commonality in how they interact with their receptors.

At the high concentrations used in NMR spectroscopy and x-ray crystallography, most chemokines form noncovalent dimers or larger oligomers. IL-8 has been shown to exist and function both as a monomer and dimer [51, 53, 83]. The monomer binds to the N-terminal domain of CXCR1 with higher affinity

than the dimer [54, 55, 57], and is believed to be the biologically active form of the protein. Modification, mutation, or truncation of residues at the dimer interface stabilizes the monomeric form of IL-8 [83, 95]. The structure of monomeric IL-8 (1-66), obtained by truncation of the last six C-terminal residues, using solution NMR is shown in Fig. 3.1 A [129]. Overall, the structure of monomeric IL-8 is very similar to that of each subunit in the wild-type IL-8 (1-72) dimer [50].

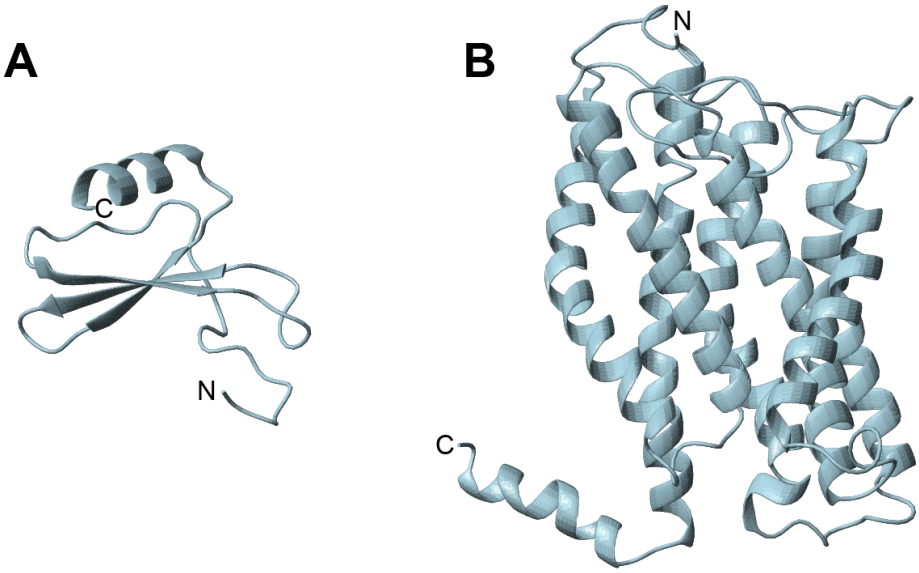

Figure 3.1 Structures of the chemokine IL-8 and its receptor CXCR1. (A) Structure of the monomeric chemokine IL-8 (1-66) in aqueous solution (PDB: 5WDZ). (B) Structure of the chemokine receptor CXCR1 (1-350) in phospholipid bilayers (PDB: 2LNL). Extracellular N-terminal and intracellular C-terminal residues of CXCR1 involved in ligand and G-protein interactions, respectively, are not included in the Figure because they are mobile on the timescales of the NMR experiments used to determine the structure of the receptor.

CXCR1 and CXCR2 were the first chemokine receptors to be identified and cloned [130], and were originally referred to as IL-8RA [86] and IL-8RB [44], respectively. They share 80% sequence identity. Most of the differences are in the N- and C-terminals, which bind chemokines and G-proteins, respectively. Both receptors have high affinity for IL-8, with a low nanomolar dissociation constant

[72, 122]. Finding that two similar but distinct receptors bind the same chemokine, and that CXCR1 almost exclusively binds to IL-8 whereas CXCR2 also binds to several other chemokines, provided an early indication of the complexity of the chemokine defense system. At present, the structures of six chemokine receptors have been reported: the crystal structures of CXCR4 [74, 87], CCR2 [88], CCR5 [90], CCR9 [89], and viral US28 [91], and our NMR structure of CXCR1 in lipid bilayers [72], which is shown in Fig. 3.1 B. Although none of the structures represent complexes of a receptor with one of its native chemokine agonists, the structures of receptors bound to viral chemokines provide information that is complementary to the many mutagenesis and binding studies of their interactions. There have been many solution NMR and other biophysical studies of IL-8 interacting with polypeptides whose sequences correspond to N-terminal residues of CXCR1 [55, 57, 95-97, 102, 103, 118]. The current model for chemokine-receptor interactions involves two binding sites on the receptor. Residues in both the N-terminal domain (binding site-I) and in one or more extracellular loops (binding site-II) of CXCR1 have been shown to interact with IL-8 [54, 84, 93, 97, 131].

Solid-state NMR spectroscopy enables studies of the structure and dynamics of membrane proteins in near-native phospholipid bilayer environments [132-135]. There are several examples where solid-state NMR methods have been used to characterize the structures of ligands bound to GPCRs [136-139] as

well as GPCRs themselves. Most prior studies of membrane proteins or their ligands have involved the direct detection of signals from labeled ^{13}C or ^{15}N sites; this continues to be a fruitful approach and we applied it in our earlier studies of CXCR1 [72, 97, 140]. However, dramatic improvements in sensitivity have been obtained by the implementation of ^{1}H-detected magic angle spinning (MAS) solid-state NMR methods [141, 142], especially when fast MAS is combined with perdeuteration of the samples [141, 143-146]. This approach is being applied to an increasing number of membrane proteins [109, 147-149].

Here, we describe the effects on IL-8 when it binds to CXCR1 in phospholipid bilayers using ^{1}H-detected MAS solid-state NMR. We prepared uniformly ^{2}H and ^{15}N labeled monomeric IL-8 (1-66) [129], and examined its interactions with unlabeled full-length CXCR1 (1-350), which contains both binding site-I and binding site-II, and an N-terminal truncated construct of CXCR1, NT-CXCR1 (39-350), which lacks binding site-I associated with the N-terminal region but retains binding site-II associated with the extracellular loops. Changes observed in spectra of IL-8 (1-66) upon binding CXCR1 (1-350) and NT-CXCR1 (39-350) identify chemokine residues involved in the interactions with CXCR1. In addition, we incorporated the metal-chelating unnatural amino acid 2-amino-3-(8-hydroxyquinolin-3-yl)propanoic acid dihydrochloride (HQA) into full-length CXCR1, expanding upon earlier work [109], to observe intermolecular paramagnetic relaxation enhancement (PRE) between IL-8 (1-66) and CXCR1 (1-

350). This provides additional information about the structures and spatial arrangement of the complexed proteins.

3.3 Materials And Methods

3.3.1 Incorporation of HQA

The unnatural amino acid HQA was purchased from BOC Sciences (http:// www.bocsci.com). The replacement of tryptophan by HQA at position 10 in the sequence of full-length CXCR1 (1-350) was performed as previously described for a different construct of CXCR1 [109]. The complete replacement of tryptophan by HQA was confirmed by NMR and fluorescence spectroscopies. Purification and refolding procedures of HQA-containing CXCR1 (W10HQA CXCR1) were identical to those applied to the wild-type protein [72].

3.3.2 Sample preparation

Monomeric IL-8 (1-66) containing residues of 1-66 of the wild-type human protein was expressed and purified using the protocol described previously [106]. Uniformly ^{2}H- and ^{15}N-labeled samples were obtained by growing bacteria in BioExpress cell growth media (U-^{2}H, 98%; U-^{15}N, 98%) and deuterium oxide (^{2}H, 99.9%) (Cambridge Isotope Laboratories, Tewksbury, MA; http://www.isotope.com). High deuteration levels (>90%) were verified by comparing the ^{1}H solution NMR spectrum of perdeuterated IL-8 (1-66) to that of

an unlabeled sample. The proteoliposome samples of 1,2-dimyristoyl-sn-glycero-3-phosphocholine lipid bilayers containing full-length CXCR1 (1-350) or N-terminal truncated construct NT-CXCR1 (39-350) were prepared as described previously [72, 108]. The lipid/protein molar ratio was 300:1.

3.3.3 NMR experiments

The solution NMR experiments were performed at 40 C on a Bruker 600 MHz spectrometer equipped with 5 mm triple-resonance cryoprobe with z-axis gradient. The concentration of monomeric IL-8 (1-66) was 50 mM in 20 mM HEPES buffer (pH 7.3). One-dimensional ^{15}N-edited ^{1}H NMR spectra of uniformly ^{15}N-labeled monomeric IL-8 (1-66) were obtained by signal-averaging 128 transients in the absence and presence of CXCR1-containing proteoliposomes at a molar ratio of 1:1.

The samples for solid-state NMR experiments contained 30–50 mg of uniformly ^{2}H- and ^{15}N-labeled IL-8 (1-66) in 3 mL of 20 mM HEPES buffer in 100% $^{1}H_2O$. Spectra were obtained in the absence and presence of various unlabeled CXCR1 constructs in liposomes at a receptor to IL-8 (1-66) molar ratio of 1:1. Samples were prepared by adding an appropriate amount of isotopically labeled IL-8 (1-66) in solution to proteoliposomes containing unlabeled CXCR1 constructs in 5 mL of 20 mM HEPES buffer (pH 7.3). The mixtures were incubated for 30 min at room temperature before ultracentrifugation for 20–40 h at

645,000 g at 15 C. Approximately 3 mL of fully hydrated proteoliposomes containing IL-8 (1-66) bound to the receptor was transferred into a 1.3 mm MAS rotor. For the PRE experiments, a 200-fold molar excess of $MnCl_2$ was added to the proteoliposome samples before ultracentrifugation.

Solid-state NMR experiments were performed at 900 MHz (21.2 Tesla) on a Bruker Avance III HD spectrometer equipped with a triple-resonance 1.3 mm MAS probe. The sample-spinning rate was controlled to 60 kHz (52 Hz). The probe temperature was maintained at 8°C using nitrogen cooling gas at 30°C and a flow rate of 1500 L/h; the actual sample temperature, as monitored by the resonance frequency of the water signal, was estimated to be 30°C due to frictional heating.

Two-dimensional ^{1}H-detected ^{1}H-^{15}N chemical shift correlation spectra were acquired using either a ^{1}H-^{15}N heteronuclear single quantum correlation (HSQC) pulse sequence via double insensitive nuclei enhanced by polarization transfers (INEPT) [150] with presaturation for water signal suppression, or via double cross-polarization (CP) transfers [141] with multiple intense solvent suppression intended for sensitive spectroscopic investigation of protonated proteins instantly [142]. ^{15}N globally optimized alternating phase rectangular pulse [151] decoupling with irradiation of 22.6 kHz was applied during ^{1}H signal acquisition. In these pulse sequences, the hard $\pi/2$ pulses had nutation

frequencies of 100 and 55.6 kHz for ^{1}H and ^{15}N, respectively. The delay t was set to 1/4 J (2.5 ms) for INEPT transfers. The contact time was 1 ms for the first CP transfer from ^{1}H to ^{15}N, and 0.4 ms for the second CP transfer from ^{15}N to ^{1}H. Two-dimensional INEPT correlation spectra were acquired using 64 complex time-domain points with a total acquisition time of 10 ms in the indirect ^{15}N chemical shift dimension, and 2048 complex time-domain points with a total acquisition time of 56.8 ms in the directly detected ^{1}H chemical shift dimension. Two-dimensional CP correlation spectra were acquired using 64 complex time-domain points with a total acquisition time of 10 ms in the indirect ^{15}N chemical shift dimension, and 1024 complex time-domain points with a total acquisition time of 11.3 ms in the directly detected ^{1}H chemical shift dimension. The relaxation delay for all experiments was 1.2 s. The NMR data were processed using TopSpin 3.5 (http://www.bruker.com) and the structures were visualized using PyMol (http://www.pymol.org).

3.4 Results

3.4.1 Immobilization of IL-8 bound to CXCR1 in phospholipid bilayers

Although IL-8 exists as a homodimer in solution [47], monomeric IL-8 has been shown to bind to CXCR1 with similar or higher affinity than the dimer [55, 57]. Truncation of the last six C-terminal residues results in a stable monomeric form of IL-8 (1-66) [84]. Studies of IL-8 (1-66) avoid potential complications due to dimer-to-monomer interconversion of either the free or bound forms of IL-8.

Binding of IL-8 (1-66) to full-length CXCR1 (1-350) is tight enough that IL-8 (1-66) can be found in the insoluble proteoliposome pellet along with CXCR1 (1-350) after ultracentrifugation (Fig. 3.2 A, lane 3). Similar results were obtained for IL-8 (1-66) binding to NT-CXCR1 (39-350), where the residues responsible for the receptor's N-terminal binding site are missing (data not shown). However, no IL-8 (1-66) was detected in the pellet obtained by ultracentrifugation of a sample of the protein suspended in the presence of empty liposomes. This indicates that IL-8 does not interact with or partition to phospholipids. Purified uniformly ^{15}N-labeled IL-8 (1-66) (Fig. 3.2 A, lane 2) in aqueous ($^{1}H_2O$) buffer yields a well-resolved ^{15}N-edited ^{1}H solution NMR spectrum of the amide region (Fig. 3.2 B), which is similar to that obtained from the wild-type dimeric IL-8 (1-72) [97, 129]. The binding of IL-8 (1-66) to CXCR1 (1-350) in phospholipid bilayers at a molar ratio of 1:1 (Fig. 3.2 A, lane 3) results in the broadening of all IL-8 (1-66) ^{1}H amide signals beyond detection by solution NMR (Fig. 3.2 C). This demonstrates that the global reorientation of IL-8 (1-66) is highly restricted by binding to CXCR1 embedded in phospholipid bilayers. Similar results were observed for the interaction of wild-type dimeric IL-8 (1-72) with the receptor under the same sample and spectroscopic conditions (data not shown). Notably, signals from those residues of wild-type dimeric IL-8 (1-72) not directly involved in the interaction with CXCR1 (1-350) could be observed in solution NMR spectra when the protein complexes are in rapidly reorienting isotropic bicelles, but not when they are in slowly and anisotropically reorienting lipid environments, such as magnetically aligned

bicelles or proteoliposomes [97]. The slow global reorientation of IL-8 complexed with CXCR1 in phospholipid bilayers severely compromises the application of solution NMR methods to these samples. However, it is possible to use solid-state NMR methods to investigate IL-8 bound to CXCR1 in phospholipid bilayers. Fig. 3.3 compares two-dimensional ^{1}H-^{15}N chemical shift correlation spectra of IL-8 (1-66) obtained under various experimental conditions. The use of uniformly ^{2}H- and ^{15}N-labeled IL-8 (1-66), where the perdeuteration facilitates the suppression of ^{1}H-^{1}H dipolar couplings, is essential to obtain these high-resolution MAS spectra.

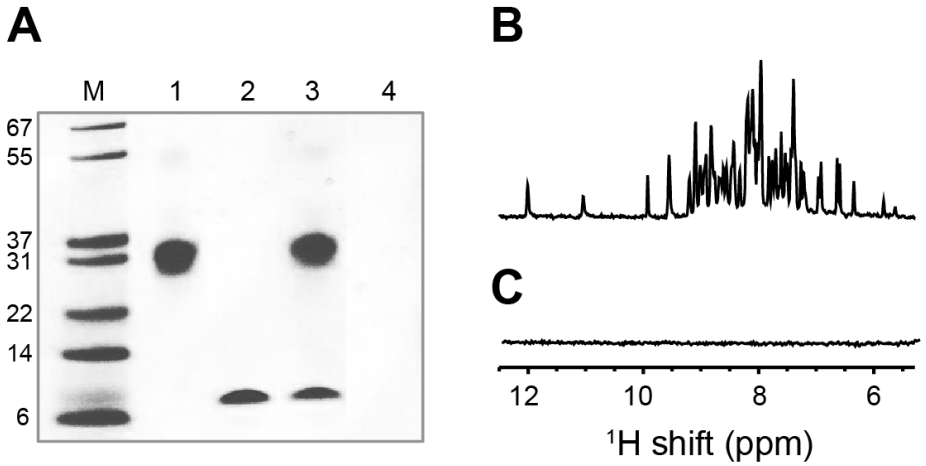

Figure 3.2 IL-8 forms a tight complex with CXCR1 (A) SDS-PAGE analysis of IL-8 (1-66), CXCR1 (1-350), and their 1:1 complex. Lane M: Protein molecular weight marker. Lane 1: CXCR1 (1-350) in phospholipid bilayers. Lane 2: IL-8 (1-66) in aqueous buffer. Lane 3: pellet and Lane 4: supernatant, of a 1:1 molar ratio mixture of IL-8 (1-66) and CXCR1 (1-350) in phospholipid bilayers after 20 h of ultracentrifugation at 645,000 g. Lane 3 demonstrates that IL-8 (1-66) and CXCR1 (1-350) are in the resulting pellet and that neither protein is in the supernatant, indicating that they form a complex in the bilayers. (B and C) One-dimensional ^{15}N-edited ^{1}H solution NMR spectra of uniformly ^{15}N-labeled IL-8 (1-66) obtained at 600 MHz and 40°C. (B) IL-8 (1-66) alone in aqueous solution. (C) 1:1 IL-8 (1-66):CXCR1 (1-350) complex in phospholipid bilayers. The ^{1}H solution NMR signals of IL-8 (1-66) are broadened beyond detection by the slow reorientation of the chemokine bound to CXCR1 in phospholipid bilayers.

3.4.2 Fast-exchanging amide hydrogens of IL-8

A two-dimensional ^{1}H-^{15}N HSQC NMR spectrum of uniformly ^{15}N labeled IL-8 (1-66) in aqueous solution is shown with black contours in Figs. 3.3 A and 3.4 A. This spectrum was obtained with the sample in a standard 5 mm OD solution NMR sample tube that was not spun. All the amide resonances have been assigned to specific residues, with the exception of the mobile C-terminal residue, 66, whose amide hydrogen exchanges rapidly with water at pH 7.3 [129]. A spectrum of the same solution sample obtained in a 1.3 mm rotor spinning at 60 kHz using the same pulse sequence, with minor modifications of the t delay for INEPT transfers and the use of continuous wave irradiation (presaturation) for water signal suppression, is shown with black contours in Fig. 3.3 B and with red contours in Fig. 3.4 A. The observed line widths of amide ^{1}H resonances of IL-8 (1-66) in aqueous solution obtained by conventional solution NMR and obtained by 60 kHz MAS solid-state NMR are 30 and 50 Hz, respectively.

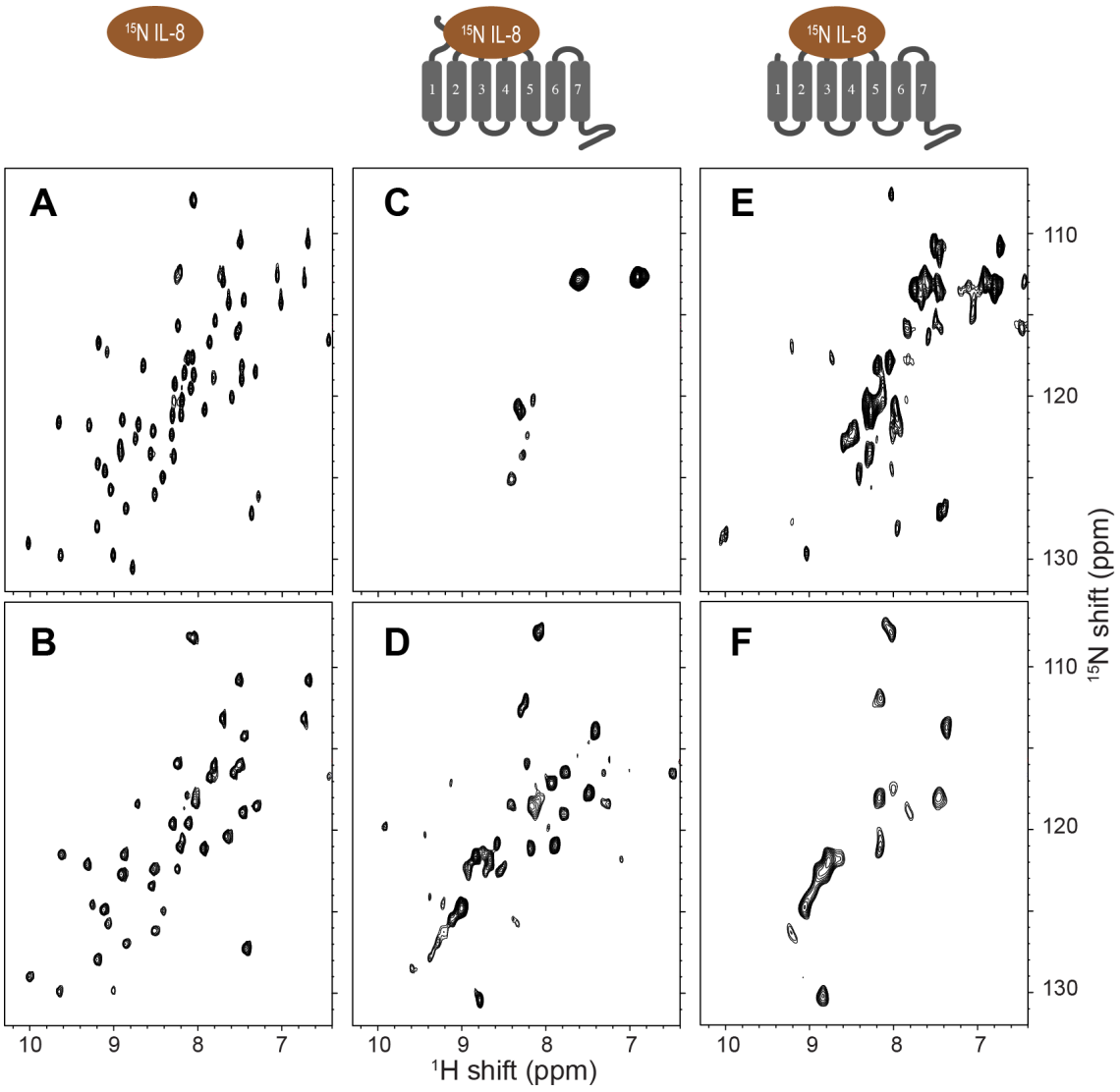

Figure 3.3 Two-dimensional ^{1}H-detected ^{1}H-^{15}N correlation NMR spectra of uniformly [^{2}H, ^{15}N-HN] labeled IL-8 (1-66). The cartoons at the top represent the samples: IL-8 (1-66) alone (left), the IL-8 (1-66):CXCR1(1-350) complex (center), and the IL-8 (1-66):NT-CXCR1(39-350) complex (right). (A) HSQC solution NMR spectrum of IL-8 (1-66) alone in aqueous solution obtained at 600 MHz and 40°C. (B–F) ^{1}H-detected 60 kHz MAS solid-state NMR spectra of IL-8 (1-66) in the absence (B) and presence (C–F) of CXCR1 constructs in phospholipid bilayers obtained at 900 MHz and 30°C. (B) IL-8 (1-66) alone in aqueous solution. (C and D) 1:1 IL-8 (1-66):CXCR1 (1-350) complex in phospholipid bilayers. (E and F) 1:1 IL-8 (1-66):NT-CXCR1 (39-350) in phospholipid bilayers. (A–C and E) were obtained with INEPT and (D and F) with CP magnetization transfers, enabling the separate observation of signals from mobile (A–C and E) and immobile (D and F) sites.

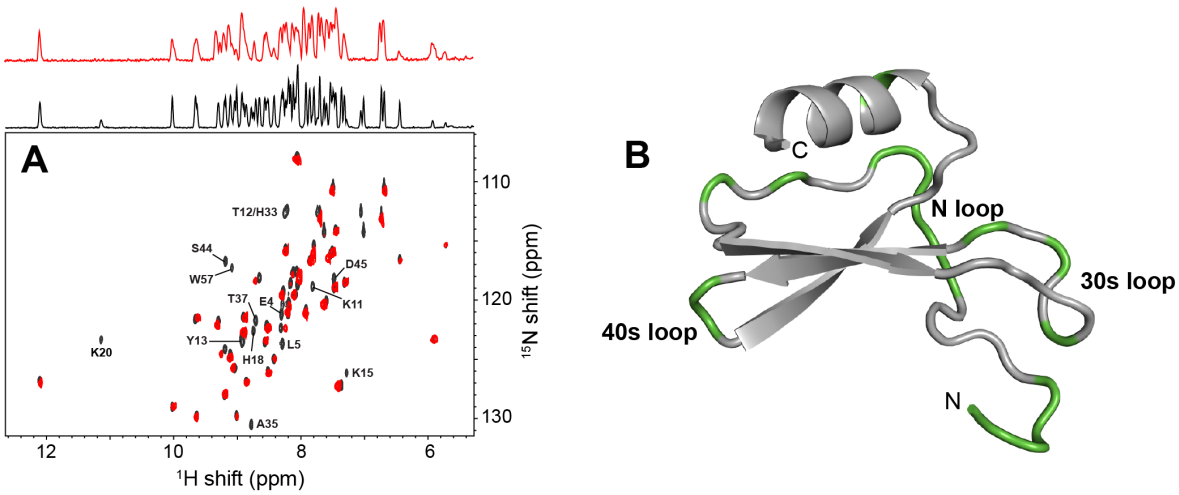

Figure 3.4 Fast-exchanging protons in IL-8 (A) Comparison of one-dimensional ^{15}N-edited ^{1}H NMR and two-dimensional ^{1}H-detected ^{1}H-^{15}N correlation NMR spectra of uniformly ^{15}N-labeled IL-8 (1-66) in aqueous solution obtained by solution NMR (black contours) and solid-state 60 kHz MAS NMR (red contours), respectively. The amide resonances absent in the solid-state MAS NMR spectrum due to fast exchange with water are marked. (B) The fast-exchanging sites in the N-terminal and three loop regions of IL-8 (1-66) are colored in green in the protein structure.

The solution NMR and solid-state NMR spectra in Fig. 3.4 are very similar with extensive overlap of chemical shifts. Importantly, no signals could be observed using CP transfer, indicating that IL-8 (1-66) is not sedimented but remains soluble undergoing isotropic reorientation in solution at 60 kHz MAS, which produces >10^6 g centrifugal force toward the rotor wall. Presaturation for water suppression in the solid-state MAS spectrum results in missing or very weak intensity signals from solvent-accessible residues (1–5, 11–15, 18, 20, 33, 35, 37, 44, 45, and 57) compared to the solution NMR spectrum obtained with the WATERGATE pulse sequence [152] for water suppression. This result was verified by amide hydrogen-deuterium exchange measurements on IL-8 (1-66) in

solution [129]. The residues with fast-exchanging amide hydrogens are represented in green in the IL-8 (1-66) structure (Fig. 3.4 B); they are mainly located in the N-terminal and three loop regions (N-loop, 30s loop, and 40s loop) This result is in agreement with the previously measured amide nitrogen relaxation rates of a monomeric IL-8 mutant in aqueous solution, in which a high degree of mobility was observed for the unstructured N-terminal region, and reduced mobility for several residues in the loop regions (residues 11, 12, 33, 35, 45, and 57) [102].

3.4.3 IL-8 interaction with CXCR1 in phospholipid bilayers

Comparison of MAS solid-state NMR spectra obtained with CP and INEPT magnetization transfers enables the qualitative characterization of residue-specific local dynamics of IL-8 (1-66) bound to CXCR1 in phospholipid bilayers (Figs. 3.3, 3.5, and 3.7). Signals from immobilized residues are observed in the spectra obtained with CP transfers whereas signals from mobile residues are observed in the spectra obtained with INEPT transfers. ^{1}H-detected ^{1}H-^{15}N correlation solid-state MAS NMR spectra of ^{2}H and ^{15}N labeled IL-8 (1-66) bound to unlabeled full-length CXCR1 (1-350) show that signals from most of the IL-8 (1-66) amide backbone sites could be observed in the CP spectrum (Fig. 3.3 D (black contours), and Fig. 3.5 A (red contours)). In contrast, only five backbone and a pair of side-chain signals were observed in the INEPT spectrum (Fig. 3.3 C (black contours), and Fig. 3.5 B (green contours)). Motionally averaged signals of IL-8

(1-66) bound to CXCR1 in phospholipid bilayers were observed in the MAS solid-state NMR spectrum (Figs. 3.3 C and 3.5 B), but not in the solution NMR spectrum (Fig. 3.2 C) because the severe broadening from the dipole-dipole interactions is suppressed by the combination of fast MAS and perdeuteration. Several residues, including those from the C-terminal helical region, which are not observed in either CP or INEPT solid-state NMR experiments, are marked in gray in Fig. 3.5 C. The C-terminal helical region of IL-8 (1-66) does not show evidence of interaction with the receptor. It is known to be responsible for association with the sulfate groups of glycosaminoglycans [153], and local motions might occur on an intermediate timescale, such that neither CP nor INEPT transfers yield signals [154].

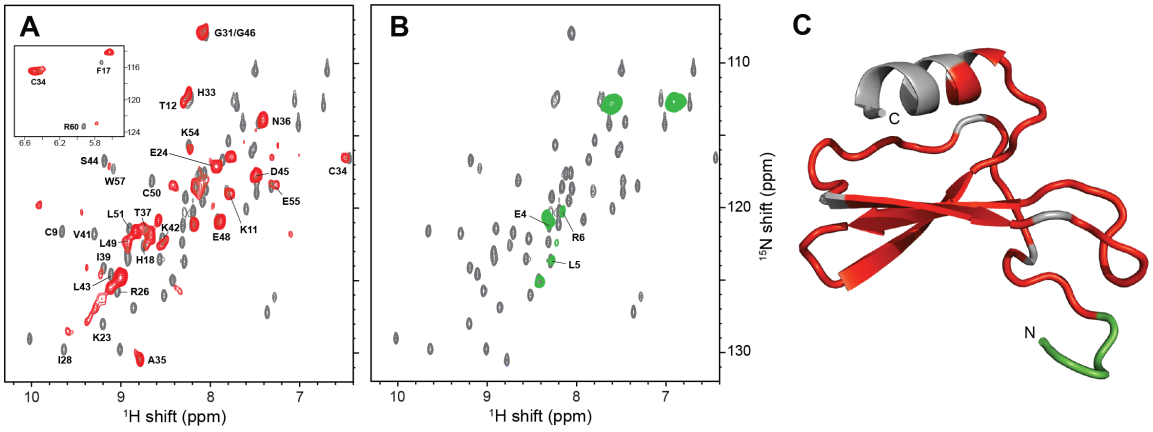

Figure 3.5 (A and B) ^{1}H-detected ^{1}H-^{15}N correlation solid-state 60 kHz MAS NMR spectra of [^{2}H, ^{15}N-HN] labeled IL-8 (1-66) bound to unlabeled CXCR1 (1-350) in phospholipid bilayers obtained with (A) CP (red contours) and (B) INEPT (green contours) magnetization transfers. The solid-state MAS NMR spectra are overlaid on the solution NMR HSQC spectrum (Figs. 3 A and 4 A) of free IL-8 (1-66) (gray contours). Assigned signals are marked. (C) Structure of IL-8 (1-66) with the dynamics of residues in IL-8 (1-66) bound to CXCR1 (1-350) designated by colors. Red represents immobile sites (red contours, A) and green represents mobile sites (green contours, B). Signals from residues in the gray regions are either unassigned or undetected in the solid-state NMR spectra.

The mobile and fast-exchanging IL-8 (1-66) sites in the loops (green sites in Fig. 3.4 B) were immobilized along with the three β-strands upon interaction with CXCR1 (red sites in Fig. 3.5 C). Several fast-exchanging residues (12, 18, 20, 44, 45) in the N-loop and the 40s loop of IL-8 (1-66) contribute to its primary binding site [55, 57, 95-97, 101-103, 118]. Significant chemical shift perturbations of resonances of IL-8 (1-66) upon interaction with CXCR1 (1-350) indicate the locations of the IL-8 (1-66) residues involved in binding. Chemical shift perturbations of five well-resolved resonances of IL-8 (1-66), Gln8, and Lys20 in the downfield (11–12 ppm) region and Phe17, Cys34, and Val58 in the upfield (5.5–6.5 ppm) region are compared in Fig. 3.6. Phe17 and Val58 resonances were significantly perturbed by both CXCR1 (1-350) in phospholipid bilayers and the soluble peptide ND-CXCR1 (1-38) in aqueous buffer, whereas Cys34 was not affected. This result is consistent with solution NMR data on interactions of both monomers and dimers of IL-8 with various N-terminal CXCR1 peptides containing only binding site-I of the receptor [118]. The Gln8 resonance was slightly perturbed by both receptor constructs, but the Lys20 resonance was only perturbed by ND-CXCR1 (1-38) and not by CXCR1 (1-350), suggesting that the IL-8 (1-66) interaction with CXCR1 (1-350) is different from that with ND-CXCR1 (1-38).

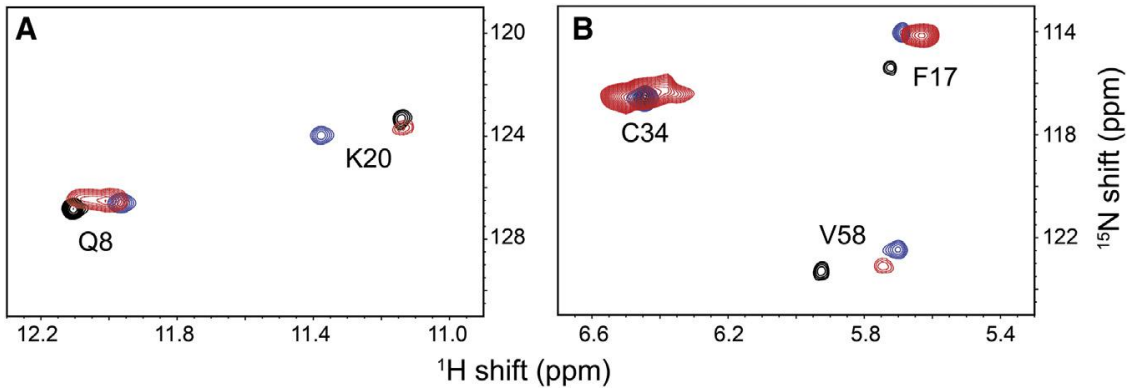

Figure 3.6 Downfield (A) and upfield (B) regions of ^{1}H-^{15}N correlation spectra of IL-8 (1-66). Signals in black contours are from a solution NMR HSQC spectrum of free IL-8 (1-66); blue contours are from a solution NMR HSQC spectrum of IL-8 (1-66) bound to ND-CXCR1 (1-38) (17); and red contours are from a solid-state MAS NMR spectrum of IL-8 (1-66) bound to CXCR1 (1-350). Assigned residues are marked.

3.4.4 IL-8 interaction with NT-CXCR1 in phospholipid bilayers

IL-8 (1-66) binds to NT-CXCR1 (39-350), which lacks the N-terminal 38 residues of the receptor that contribute to binding site-I, but retains binding site-II associated with extracellular loops of the receptor. Significant differences were observed between the ^{1}H-^{15}N correlation spectra of IL-8 (1-66) bound to NT-CXCR1 (39-350) (Figs. 3.3, E and F and 3.7, A and B) and to full-length CXCR1 (1-350) (Figs. 3.3, C and D and 3.5, A and B). From the IL-8 (1-66) and NT-CXCR1 (39-350) complex, 11 backbone amide signals can be observed in the CP spectrum (Fig. 3.3 F, black contours, and Fig. 3.7 A, red contours) compared with 18 signals in the INEPT spectrum (Fig. 3.3 E, black contours, and Fig. 3.7 B, green contours). Out of the 60 expected backbone amide signals, 31 are not detected in either the CP or the INEPT spectra. The corresponding residues are shown in gray on the structure in Fig. 3.7 C. The

observed CP signals are located primarily in the 30s loop, 40s loop, and β3-strand (Fig. 3.7 C, red). The chemical shift perturbations of IL-8 (1-66) resonances by interactions with NT-CXCR1 (39-350) in the CP spectrum are generally smaller than those observed for interactions with full-length CXCR1 (1-350), possibly indicating differences in the nature of the interactions with the extracellular loops of the receptor [31, 115].

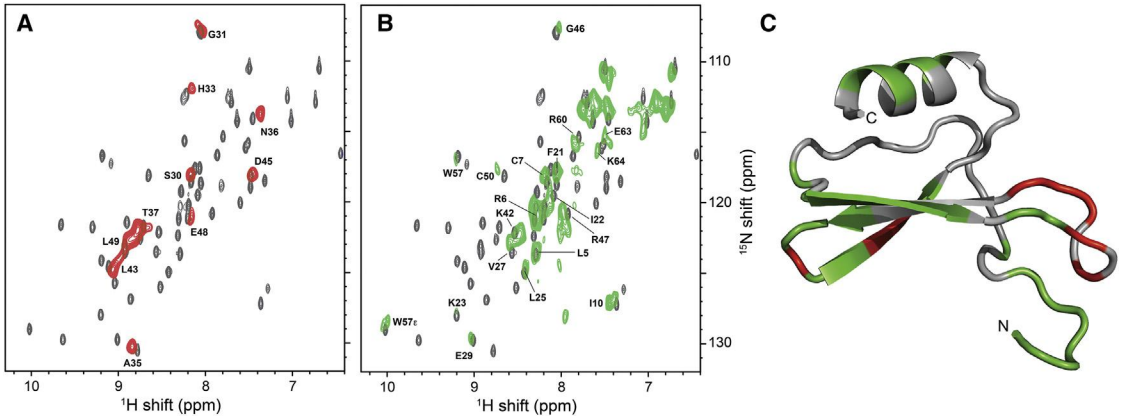

Figure 3.7 (A and B) ^{1}H-detected ^{1}H-^{15}N correlation solid-state 60 kHz MAS NMR spectra of [^{2}H, ^{15}N-HN] labeled IL-8 (1-66) bound to unlabeled NT-CXCR1 (39-350) in phospholipid bilayers obtained with (A) CP (red contours) and (B) INEPT (green contours) magnetization transfers. The solid-state MAS NMR spectra are overlaid on the solution NMR HSQC spectrum (Figs. 3 A and 4 A) of free IL-8 (1-66) (gray contours). Assigned signals are marked. (C) Structure of IL-8 (1-66) with the dynamics of residues in IL-8 (1-66) bound to NT-CXCR1 (39-350) designated by colors. Red represents immobile sites (red signals, A) and green represents mobile sites (green signals, B). Signals from residues in the gray regions are either unassigned or undetected in the solid-state NMR spectra.

3.4.5 Long-range distance restraints from intermolecular PRE of HQA-incorporated CXCR1

The genetic incorporation of the metal-chelating unnatural amino acid HQA [155] into membrane proteins enables the measurement of intra- and intermolecular distance restraints by enabling PRE NMR experiments [109]. The signal intensities in the one-dimensional MAS solid-state ^{15}N-edited ^{1}H NMR spectrum of IL-8 (1-66) bound to W10HQA CXCR1 (1-350) (Fig. 3.8 A) were reduced by the broadening effects of the bound paramagnetic Mn^{2+} ion on nearby ^{1}H nuclei (Fig. 3.8 B). Control experiments show that the presence of free manganese ions in solution has negligible effect on the spectrum of IL-8 (1-66) bound to wild-type CXCR1 (1-350) (Fig. 3.8, C and D). Most likely this is because the CP transferred ^{1}H signals of IL-8 (1-66), which result from the immobilization of its residues due to interactions with CXCR1 (1-350), are shielded from the free manganese ions.

The spectrum of labeled IL-8 (1-66) bound to unlabeled NT-CXCR1(39-350) (Fig. 3.8 E), in which the observed signals are primarily from the immobilized IL-8 (1-66) residues interacting with the extracellular loops of the receptor, is similar to that of IL-8 (1-66) bound to W10HQA-CXCR1 in the presence of manganese ions (Fig. 3.8 B). This suggests that the intermolecular PREs resulting from the $Mn^{2þ}$ bound to residue 10 of CXCR1 selectively broaden the IL-8 (1-66) signals from residues near binding site-I of CXCR1.

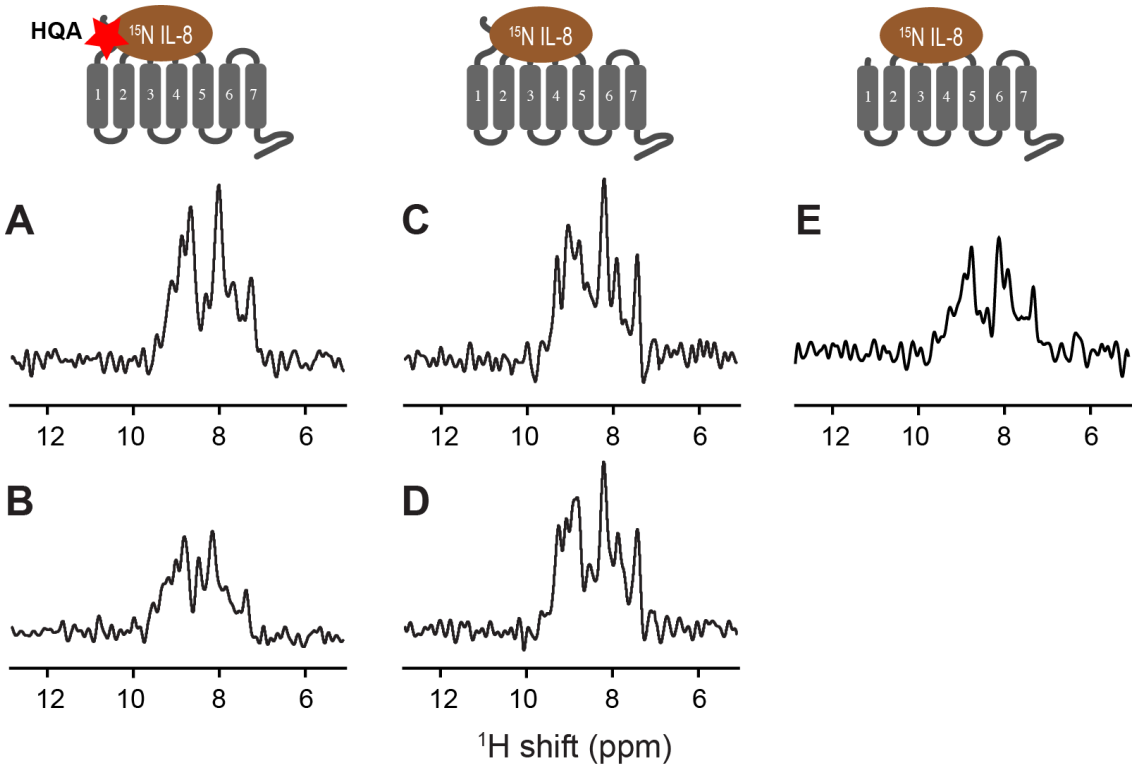

Figure 3.8 One-dimensional ^{15}N-edited ^{1}H-detected 60 kHz MAS solid-state NMR spectra of [^{2}H, ^{15}N-HN] labeled IL-8 (1-66) bound to unlabeled CXCR1 obtained with CP magnetization transfer. The cartoons at the top represent the samples: 1:1 IL-8 (1-66): W10HQA CXCR1 (1-350) complex (left), 1:1 IL-8 (1–66):CXCR1 (1-350) complex (center), and IL-8 (1-66):NT-CXCR1 (39–350) complex (right). The star indicates the location of the metal-chelating unnatural amino acid HQA at residue 10 in the N-terminal domain of CXCR1. (A and B) 1:1 IL-8 (1-66): W10HQA CXCR1 (1-350) complex. (C and D) 1:1 IL-8 (1-66):CXCR1 (1-350) complex. (E) 1:1 IL-8 (1-66):NT-CXCR1 (39-350) complex. (A), (C), and (E) were obtained in the absence of $MnCl_2$. (B) and (D) were obtained in the presence of $MnCl_2$

3.5 Discussion

Residues in the N-terminal domain (binding site-I) and in extracellular loops (binding site-II) of CXCR1 interact with IL-8 [31, 55, 57, 78, 92, 93, 95-97, 102, 103]. Specific residues in the N-terminal domain of CXCR1 contribute to both the selectivity and the affinity of the receptor for IL-8. However, much less is known

about how IL-8 interacts with the extracellular loops of CXCR1, or how the binding of IL-8 activates the receptor and triggers its biological functions. ^{1}H-detected fast MAS solid-state NMR experiments on isotopically labeled IL-8 (1-66) bound to unlabeled constructs of CXCR1 provide new information about the nature of the interactions of IL-8 with CXCR1 in phospholipid bilayers.

IL-8 binds to synthesized and expressed polypeptides with sequences corresponding to the N-terminal region of CXCR1 that contains binding site-I. The K_D values for IL-8 interacting with only binding site-I are in the sub-micromolar to submillimolar range [118], which is significantly weaker than for binding to full-length CXCR1, which includes both binding site-I and binding site-II (K_D = 1–5 nM) [140]. In particular, the binding affinity of IL-8 (1-66) for 1TM-CXCR1 (1-72), which includes N-terminal residues (binding site-I) and the first trans-membrane helix of CXCR1, is 12.5 μM in nanodiscs, which is similar to that for the soluble N-terminal domain alone [ND-CXCR1 (1-38)] in aqueous buffer [129]. Notably, not only IL-8 (1-66) bound to full-length CXCR1 (1-350), which includes binding site-I and binding site-II, but also IL-8 (1-66) bound to the shorter constructs 1TM-CXCR1 (1-72), which includes only binding site-I, and NT-CXCR1 (39-350), which includes only binding site-II, are copelleted by ultracentrifugation. Thus, ligand-receptor complexes in phospholipid bilayers with as low as micromolar binding affinities are copelleted by ultracentrifugation, demonstrating that the complexes are stable and well-suited for NMR experiments. All of the results are consistent

with ‘‘slow exchange’’ of the ligand (IL-8) and the receptor (CXCR1) on the relevant NMR timescales.

GPCRs undergo conformational changes as a result of ligand binding and their dynamics are hypothesized to play an important role in the transmission of signals across membranes [156]. The N- and C-terminal residues of the aporeceptor display evidence of mobility in several different sample preparations and NMR experiments. However, it has also been established that they play roles in the interactions with the extracellular ligand IL-8 and intracellular G-proteins, respectively [72, 108], and these residues become ordered upon interaction with the ligands.

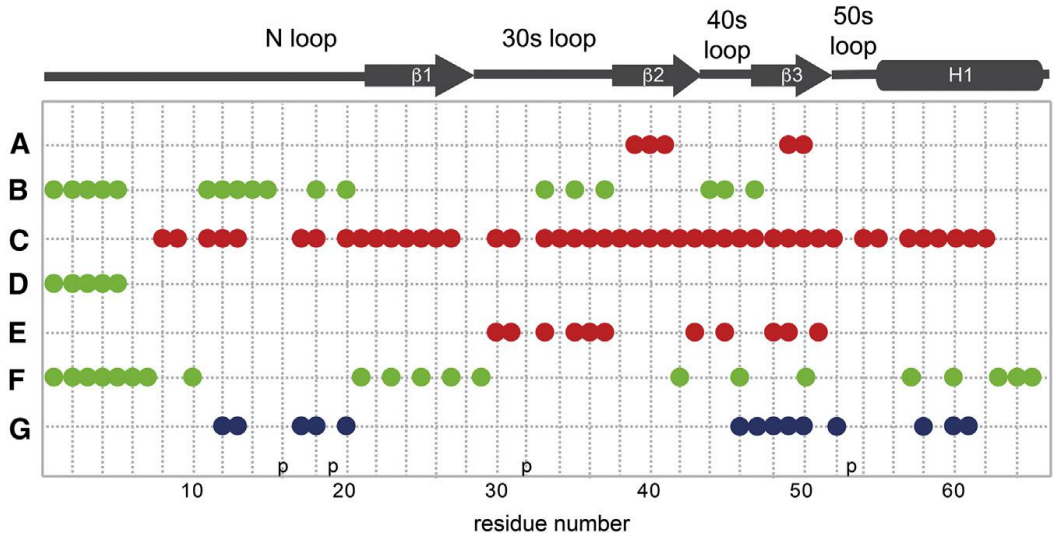

Figure 3.9 Summary of IL-8 (1-66) interactions with CXCR1 (1-350), NT-CXCR1 (39-350), and ND-CXCR1 (1-38). Row A: Non-exchanging amide sites in D_2O. Row B: Fast-exchanging amide sites in H_2O from Fig. 4. (Rows C and D: Immobile and mobile sites by interaction with CXCR1 (1-350), respectively, from Fig. 5. Rows E and F: Immobile and mobile sites by interaction with NT-CXCR1 (39-350), respectively, from Fig. 7. Row G: Most perturbed sites of chemical shifts by interaction with ND-CXCR1 (1-38).

The data summarized in Fig. 3.9 provide an opportunity to focus on the changes in the structure and dynamics of the chemokine IL-8 that result from interactions with its receptor CXCR1. The data in Fig. 3.9, rows C–F, are derived from the spectra in Fig. 3.3; they show that IL-8 (1-66) undergoes significant changes in dynamics upon interaction with full-length CXCR1 (1-350) and the shorter N-terminal truncated construct NT-CXCR1 (39-350).

Previously, the dynamics of monomeric and dimeric IL-8 have been described in the absence and presence of N-terminal CXCR1 peptides by solution NMR [102]; the N-terminus of IL-8, including the conserved ELR motif, is disordered and dynamic, whereas the three loops connecting three β-strands and one C-terminal α-helix are well-structured, even though their amide hydrogens undergo facile exchange with water (the data in row B of Fig. 3.9 are derived from Fig. 3.4). The IL-8 residues that directly interact with various N-terminal CXCR1 constructs, including ND-CXCR1 (1-38) and 1TM-CXCR1 (1-72), are well defined [102, 118]. The residues in the N-loop and 40s loop of IL-8 contribute to its major binding sites and display some evidence of local motions [57, 96, 97, 118]. In combination with the solid-state NMR data obtained on IL-8 (1-66) bound to CXCR1 (1-350) and NT-CXCR1 (39-350) in phospholipid bilayers, this suggests that the dynamics of free and bound IL-8 may play important roles in receptor binding selectivity as well as activation.

Significant changes in IL-8 (1-66) dynamics occur upon binding to wild-type CXCR1 (1-350). A majority of the residues in IL-8 (1-66), including those in the flexible loop regions, are immobilized upon interaction with CXCR1 (1-350). In addition, residue-specific chemical shift perturbations are observed (Fig. 3.5 A). Although many of the resonance assignments of bound IL-8 (1-66) could be obtained by direct comparison to the spectra of unbound IL-8 (1-66), several signals were significantly perturbed by the interaction and independent assignment experiments on the bound form of IL-8 (1-66) will be needed to map out all of the site-specific chemical shift perturbations. This should be feasible using recently developed ^{1}H-detected fast MAS triple resonance solid-state NMR experiments [148].

The solid-state NMR INEPT spectrum in Fig. 3.3 C demonstrates that five backbone amide sites are mobile in IL-8 (1-66) bound to CXCR1 (1-350); the signals from these sites are superimposable on those from the ELR residues of IL-8 (1-66) free in solution as shown in Fig. 3.5 B. The signals of Glu4 and Leu5 are absent in the solution NMR INEPT spectrum of unbound IL-8 (1-66) due to their rapid exchange with water (Fig. 3.4 A). As a result, their presence in the solid-state NMR INEPT spectrum of bound IL-8 (1-66) demonstrates that these residues are protected from solvent exchange by the interactions of IL-8 with CXCR1. The N-terminal ELR motif of IL-8 has been proposed to interact with the extracellular regions of CXCR1 and trigger receptor activation (36). However, no

chemical shift perturbations are observed, and the mobile ELR signals in bound IL-8 (1-66) suggest that the ELR motif does not interact directly with extracellular or transmembrane helical regions of CXCR1, which is consistent with our previous data on the interactions between wild-type IL-8 dimer and full-length CXCR1 in oriented lipid bilayers [97].

Since the N-terminal truncated form of the receptor is missing binding site-I, NMR spectra of the complex of IL-8 (1-66) and NT-CXCR1 (39-350) are informative about the interactions of IL-8 with binding site-II. The relatively small number of IL-8 (1-66) residues that are immobilized by binding are located mainly within the 30s and 40s loops of IL-8 (1-66). They are likely to be involved in direct interactions with residues in extracellular loops of CXCR1. However, most IL-8 residues undergo sufficient motional averaging to yield signals from INEPT experiments in the absence of binding site-I (Fig. 3.7). Thus, IL-8 interacts with both binding site-I and binding site-II of CXCR1. Other efforts to characterize the two-site model of IL-8 binding to CXCR1 have revealed that the N-loop of IL-8 is the major determinant for CXCR1 activation [77]. In contrast, the N-terminus of IL-8 (ELR and CXC) is essential for CXCR2 activation [157], which suggests that this approach has the potential to address the selectivity of chemokines for different receptors.

^{1}H-detected fast MAS solid-state NMR enabled the characterization of IL-8 (1-66)-CXCR1 complexes in phospholipid bilayers, providing insight into the molecular events associated with the first step of the CXCR1-mediated signaling cascade. These studies also served to demonstrate that site-specific incorporation of metal-chelating unnatural amino acid HQA into CXCR1 in combination with high-resolution ^{1}H-detected fast MAS solid-state NMR provide site-specific PRE-derived intermolecular distance restraints in ligand-receptor complex. Thus, solid-state NMR can provide measurements of both intra- and intermolecular distances along with the identification of residues directly involved in binding to specific sites on both the ligand and receptor. Demonstrated here on ligand binding to a GPCR, the approach has the potential to be applicable to a broad range of protein complexes in membranes and other biological supramolecular assemblies.

Chapter 3, in full, is a reprint of the material as it appears in the Biophysical Journal (2017) 113, 2695–2705. Park, S.H., Berkamp, S., Radoicic, J. De Angelis, A. A., and Opella, S. J. The dissertation author was the secondary author of this paper.

CHAPTER 4: NMR STUDIES OF INTERLEUKIN-8 WITH 1TM-CXCR1(1-72) ; CHANGES IN THE STRUCTURE AND DYNAMICS OF BINDING SITE-I OF CXCR1 UPON IL-8 INTERACTION

4.1 Abstract

The interaction between Interleukin-8 (IL-8) and the chemokine receptor CXCR1 are essential for neutrophil activation during inflammation. IL-8 is known to contact two main binding sites on the receptor; Binding Site-I on the flexible N-terminal domain and Binding Site-II on the second and third extracellular loops of CXCR1. We have used a combination of solid-state NMR techniques to map the interactions between interleukin-8 (IL-8) and Binding Site-I in a near-native environment composed of DMPC liposomes. To this end we have designed the construct 1TM-CXCR1(1-72); it has a flexible N-terminal domain, the first transmembrane helix and the first intracellular loop, corresponding to residues 1 through 72 of the wild-type CXCR1 receptor. Using both CP-, and INEPT-based experiments, we have fully assigned the protein and have mapped the binding site of IL-8 on it. We have also studied how the dynamics of 1TM-CXCR1(1-72) change upon interaction with IL-8. Most of the residues in the flexible N-terminal domain underwent chemical shift perturbation, with residues 1-37 also undergoing a change in dynamics upon binding. Little evidence of changes were found in the

transmembrane helix.

4.2. Introduction

G Protein-Coupled Receptors (GPCRs) are the largest family of membrane proteins in the human genome and consist of seven transmembrane-spanning helices separated by alternating intracellular and extracellular loop regions [158-160]. They share a common signaling mechanism in which extracellular stimuli induce conformational changes in the receptor, which in turn activate intracellular heterotrimeric G proteins [158-162]. GPCRs signaling cascades regulate many cellular processes, such as cell differentiation, cell motility and angiogenesis. Due to their connection to a myriad of signaling pathways, misregulation of GPCRs and their ligands are the cause of many diseases, such as cancer, asthma and hypertension. Approximately 30% of all pharmaceuticals target a GPCR [58]. Despite the fact that the structures of around 50 GPCRs have been determined, many questions remain regarding how they interact with their ligands, what conformational changes take place upon receptor activation and how receptor dynamics influence function, as this is likely to play an important role.

CXCR1 is a class A, rhodopsin-like GPCR, which belongs to the family of chemokine receptors. We recently solved the three-dimensional structure of human CXCR1 by rotationally aligned, solid-state NMR spectroscopy in

phospholipid bilayers, without modification to its amino acid sequence and under physiological conditions [72]. CXCR1 is activated by the chemokine interleukin-8 (IL-8, CXCL8), a major mediator of the inflammatory immune response [42, 72, 86, 163]. In case of infection, macrophages secrete IL-8, which then forms a chemotactic gradient. CXCR1 is expressed on the cell surface of several immune cells such as neutrophils and dendritic cells. Interleukin-8 binds to the extracellular domains of CXCR1, which then activates the neutrophil and starts migration towards the site of inflammation, and ultimately leads to neutrophil degranulation [40]. Interleukin-8 (IL-8) has a standard chemokine fold that consists of a disordered N-terminus, the N-loop, one turn of a 3_{10}-helix, three β-strands and a C-terminal α-helix. It has 72 residues in its most common form and forms a homodimer at micromolar concentrations. It can interact with CXCR1 as a monomer and as a dimer, but it is thought that the monomer binds to the N-terminal domain of CXCR1 with higher affinity than the IL-8 dimer [55-57]. An obligatory form of monomeric IL-8 can be obtained by deleting the C-terminal residues 67–72, which contribute to the dimerization interface. This construct, IL-8 (1-66), has been shown to bind CXCR1 with the same affinity as wild-type IL-8, and to have the same potency in neutrophil chemotaxis and Ca^{2+} mobilization assays [84, 85, 95]. The existing model for CXCR1 – IL-8 interaction involves two binding sites on the receptor; residues in both the flexible N-terminal domain (Binding Site-I) as well as the second and third extracellular loops (Binding Site-II) of CXCR1 have been shown to interact with IL-8 [57, 97]. Based on biophysical

and mutational studies, several residues in IL-8 have been found to be important for the interaction with Binding Site-I in CXCR1: mainly residues in the N-loop, in the third β–strand, and a small part of the α-helix [55, 94, 97, 119, 129].

Several NMR, molecular dynamics, and mutational studies set out to characterize the binding pattern between IL-8 and the N-terminal domain of CXCR1. To this end several different constructs of isolated Binding Site-I have been described. These include synthetic peptides with sequences corresponding to portions of the N-terminal domain of CXCR1 interspaced with hexanoic acid, peptides composed of residues 9-29, and ND-CXCR1(1-38), a soluble peptide containing the first 38 residues of CXCR1 developed by our lab [93, 96, 97, 102, 117, 164] The results of these interaction studies largely complement eachother; residues 9-29 are most important for the interaction with IL-8, especially residues D14, G19, P21, P22, D24, E25, D26 and Y27. Interestingly, the N-terminal domain has the highest sequence diversity among all GPCRs and even among chemokine receptors. The N-terminal domain varies in length, and can also undergo post-translational modifications, and can be linked to the extracellular loops through a disulfide bridge. This variety is believed to be the main mechanism by which specific chemokines are selected by chemokine receptors [165]. The N-terminal domain is even linked to receptor internalization rates. When the N-terminal domain of CXCR2 was substituted for the N-terminal domain of CXCR1, the entire receptor internalized faster and matched the internalization

rate of endogenous CXCR2 [77]. To better understand chemokine binding to the N-terminal domain, but also the interplay between N-terminal domain and the remainder of the receptor, several constructs of CXCR1 were produced in our lab. These include the N-terminal truncated CXCR1 (NT-CXCR1 (39-350)), C-terminal truncated CXCR1 (CT-CXCR1 (1-319)), both N- and C-terminal double truncated CXCR1 (DT-CXCR1 (23-319)) in addition to the wild-type CXCR1. Also, 1TM-CXCR1(1–72) was produced; it contains the flexible N-terminus, the first transmembrane helix and the first intracellular loop of CXCR1 [107, 140]. This is the construct used in all experiments described in this chapter.

Solid-state NMR spectroscopy is an emerging tool to study both the dynamics and the structures of membrane proteins at atomic resolution and under near native conditions [166-168]. It also has become a powerful tool to study protein-ligand complexes. Indeed, there are several examples where solid-state NMR has been used to characterize the interaction of ligands bound to GPCRs [169]. Here, we present results on the atomic-level characterization of the interaction between CXCR1 and IL-8, focused on Binding Site–I. We have mapped the interaction site of unlabeled IL-8 on uniformly ^{13}C,^{15}N-labelled 1TM-CXCR1 (1-72) using several CP-based pulse sequences and have studied the change in dynamics upon binding using INEPT(Insensitive nuclei enhanced by polarization transfer) and TOBSY(TOtal through Bond correlation SpectroscopY). All experiments were performed in a near-native environment of hydrated

phospholipid bilayers and at physiological temperatures.

4.3. Materials and Methods

4.3.1 Protein Expression and Purification

The isotopically labeled N-terminal first transmembrane domain of the CXCR1 receptor, 1TM-CXCR1(1-72), was expressed and purified as described previously for similar constructs of the receptor [107, 109]. A pET-31b(+)-vector was modified by including a thrombin cleavage site with a 6-Gly linker between the KSI fusion partner and the polypeptide of interest to facilitate enzymatic cleavage. 100 mL of standard LB medium containing 50 mg/L of carbenicillin and 1% glucose was inoculated with E. coli BL21(DE3)PLysS cells transformed with pET-31b(+)-G-Thr-1TM-CXCR1-6His and shaken at 37 °C and 240 rpm in a shaker for 6 hours. M9 minimal medium contained 1 g/L $(^{15}NH_4)_2SO_4$ as the sole nitrogen source, 3 g/L of 99% ^{13}C6-glucose as carbon source (from Cambridge Isotope Laboratories, www.isotope.com), 50 mg/L of carbenicillin, and trace elements [170] (50 mL of M9 were inoculated with 2 mL of the LB pre-culture and shaken overnight at 37 °C and 240 rpm. A 0.5 L M9 culture was inoculated with 50 mL of M9 overnight pre-culture and shaken at 37 °C and 240 rpm until OD_{600} ~ 0.5-0.6 (typically after 2 hours). At this time expression was induced with a final concentration of 1 mM IPTG. After 5 hours of incubation (37 °C/240 rpm), cells were harvested by centrifugation and stored overnight at -80^{o}C.

The inclusion bodies (IBs) of the KSI-fused 1TM-CXCR1(1-72) resulting from a 1 L bacterial culture were obtained by suspending the cell pellet in 30 mL lysis buffer (20 mM Tris-HCl, 500 mM NaCl, 15% glycerol, pH 8.0) in the presence of ~5 mg lysozyme (Sigma), and tip sonicated on ice for 5 minutes (Fisher Scientific Sonic Dismembrator 550). After adding 6 mL of 10% TritonX-100, the suspension was gently agitated for 10 minutes, centrifuged at 20,000g/4 ^{o}C, for 20 minutes and the supernatant discarded. The IBs from 1L cell culture were solubilized in 30 mL of binding buffer (1X PBS, 1% SDS, 10 mM imidazole, 0.1% TCEP, pH 8.0). The solution was centrifuged at 20,000g/15^{o}C for 20 minutes and the supernatant was immobilized on 10 mL of metal ion affinity chromatography resin (Ni-NTA Superflow; Qiagen, www.qiagen.com), equilibrated in binding buffer, and gently agitated for 2 hours. The column was washed with 5-bed volumes of binding buffer followed by 20-bed volumes of thrombin cleavage buffer (TCB) (0.1% hexadecylphosphocholine (Fos-Choline-16, Sol Grade, Anatrace), 20 mM Tris-HCl, 250 mM NaCl, pH 8.0). Four thousand units of thrombin (Sigma) dissolved in 20 mL of TCB were loaded onto the column to cleave the KSI-fusion protein under gentle agitation overnight at room temperature. The relatively high thrombin concentration used was optimized by SDS-PAGE to ensure complete cleavage of the fusion protein. After cleavage of KSI, the resin-bound protein was washed with 10-bed volumes of washing buffer (0.5% dodecylphosphocholine (Fos-Choline-12, Sol Grade, Anatrace), 20 mM HEPES, 50 mM NaCl, 20-50 mM imidazole, pH 7.0). 1TM-CXCR1(1-72) was eluted with elution buffer (0.5%

dodecylphosphocholine, 20 mM HEPES, 500 mM imidazole, pH 7.0). After elution from the nickel column both size-exclusion chromatography in SDS buffer or HPLC can be used as a final purification step for this GPCR construct. However, in this work HPLC was preferred because it gave higher peptide yields and no protein aggregation. The Fos-Choline-12 detergent was removed by dialysis against solutions containing methyl-β-cyclodextrin in water until a visible precipitate was present, with the final dialysis step in pure water. The protein was then lyophilized, re-dissolved in organic solvent (50% 2,2,2 trifluoroethanol (TFE), 50% water, 0.1% trifluoroacetic acid (TFA)), filtered through a 0.2μM PTFE filter and run through a second purification step by HPLC (Waters C4 Deltapack preparative 300Å, 15 μM column with a linear gradient from 90% solvent A to 95% solvent B, where solvent A: 95% water, 3% isopropanol (IPA), 2% acetonitrile, 0.1% TFA. Solvent B: 47% IPA, 28% acetonitrile, 20% TFE, 5% water, 0.1% TFA). Each purification step was monitored by SDS-PAGE, and there was no oligomerization detected in the eluate. The HPLC eluate was lyophilized to obtain pure protein in powder form, which was stored at -20^{o}C. The final yield 1TM-CXCR1(1-72) was ~3-5 mg of double-labeled pure protein per liter of M9 culture. The resulting construct, 1TM-CXCR1(1-72), was an 83-residue peptide including the first 72 residues of human CXCR1, with the C30S mutation, and including a C-terminal 5-His tag.

4.3.2 NMR Samples

Different lipid-to-protein weight ratios were evaluated for sample stability by MAS solid-state NMR by measuring uniaxial rotational diffusion of the peptide around the bilayer normal and overall signal intensity. Samples with lipid:protein > 12:1 (w:w) were stable at room temperature at 11kHz MAS speeds for over 2 months. To prepare proteoliposome NMR samples, lyophilized 1TM-CXCR1(1-72) was dissolved in pure TFE, sonicated at low-power in a bath sonicator for 5 minutes, and filtered through a 0.2 μm PTFE filter. Absorbance A_{280} (0.1% (w/v) is 1.205) was used to determine protein concentration. 60 mg of 1,2-Dimyristoyl-sn-Glycero-3-Phosphocholine (DMPC, Anatrace) powder was weighed and added to the peptide-TFE solution containing 4.5 mg of peptide. This ensured a lipid:protein ratio of approximately 13:1 (w/w), and an optimal compromise between NMR sample stability and protein concentration in the NMR rotor. The organic solvent was evaporated completely under a stream of nitrogen gas, and the protein-lipid transparent film was placed under vacuum for two days. Proteoliposomes were formed by adding 6 mL 20mM HEPES pH=7.4, warming the sample at 40^{o}C for a minute and mixing gently with a syringe until a uniform suspension with pH 7.3 was obtained. Proteoliposomes were concentrated to a volume of approximately 120 μL by ultracentrifugation for 16 hours in a Beckman Optima-90K centrifuge at 90,000 rpm (644,000 g, Beckman NVT90 rotor) at 15^{o}C. The supernatant was removed and approximately 80 μL of the proteoliposome

pellet was transferred to a ZrO_2 NMR rotor with O.D. 4 mm, Vespel cap (Bruker BioSpin) and a removable KelF spacer (Cortecnet) inserted between the sample and the cap.

4.3.3 Solid-state NMR experiments

All of the ssNMR experiments were performed on a Bruker AVANCE-III HD 750 MHz spectrometer with a 4 mm H/C/N triple-resonance Bruker E-free MAS probe (Bruker, https://www.bruker.com). The spinning rate was maintained at 11.11 kHz ± 2 Hz and the temperature controller was set to 7 ± 2 °C; taking into account frictional heating and calibration with the ^{1}H chemical shift of the water resonance. The actual sample temperature was estimated to be 10 ± 2°C. The applied rf fields corresponded to π/2 pulse lengths of 2.5μs, 3.2μs and 5.1μs for ^{1}H, ^{13}C and ^{15}N, respectively. During direct ^{13}C detection, 100 kHz radio frequency (rf) irradiation was used for ^{1}H decoupling with swept frequency two-pulse phase modulation (SW-TPPM)[171, 172]. Cross-polarization (CP)[173] from ^{1}H to ^{15}N was optimized using amplitude-modulated rf irradiation (100–70%) applied on the ^{1}H channel; 50 kHz rf irradiation on the ^{1}H and ~27 kHz rf irradiation on the ^{15}N channels were applied during the 1 ms contact time. Two-dimensional homonuclear ^{13}C-^{13}C correlation spectra were acquired using the PDSD pulse sequence with 10ms, 50ms, and 100ms mixing times [174, 175]. Double cross-polarization from ^{15}N amide to $^{13}C\alpha$ sites using spectrally induced filtering in combination with cross-polarization (SPECIFIC-CP) [176]. Adiabatic

tangential pulses were applied on the ^{13}C channel. For two-dimensional N-C correlation spectra, rf irradiations of ~27 kHz were applied on the ^{15}N channel and ~16 kHz on the ^{13}C channel for band-selective polarization transfer and continuous wave (CW) ^{1}H irradiation (100 kHz rf field strength) was applied for decoupling during the 4.5ms contact time for N-CA and N-CO transfers. Two-dimensional ^{15}N-detected separated local field (SLF) experiments were carried out using a $R18^{7}_{1}$ symmetry based pulse sequence to correlate ^{15}N chemical shift and ^{1}H-^{15}N dipolar coupling[177]. A pair of π pulses with a phase modulation of 70° (π_{70}–π_{70}) was employed for the $R18^{7}_{1}$ scheme [178]. The chemical shift frequencies were referenced externally to the adamantane methylene ^{13}C resonance at 38.48 ppm and the ammonium sulfate ^{15}N resonance at 26.8 ppm. All of the spectra were processed with the Bruker TopSpin 3.2 software package and analyzed with the program CARA (ETH Zürich) [179].

4.3.4 Resonance Assignment

Figure 4.1A shows a one-dimensional, cross-polarization (CP), MAS solid-state NMR spectrum recorded on uniformly ^{13}C, ^{15}N-labeled 1TM-CXCR1(1–72). The peaks in the spectrum are well dispersed, and a well-resolved carbonyl region was present at around 172 ppm. We also utilized INEPT-based experiments to study the mobile regions of 1TM-CXCR1(1-72). Several mobile residues were observed in $^{1}H/^{13}C$ and $^{1}H/^{15}N$ INEPT spectra (Figure 1B and D).

Lipids signals in the ^{13}C-detected INEPT spectrum are marked with an asterisk. A 2D ^{13}C-^{13}C homonuclear correlation spectrum with 10ms PDSD mixing time showed well-resolved aliphatic and carbonyl regions (Figure 4.2 A and B). Various amino acid types can easily be identified by their characteristic correlation pattern and unique chemical shifts, such as threonine, serine valine, alanine and isoleucine. All resonances were further traced using 20, 50, 100, and 500ms mixing times in the ^{13}C-^{13}C homonuclear correlation spectra. The line-widths measured in the direct dimension, for well-resolved ^{13}C signals, such as those from the Cα, Cβ and Cγ atoms of the side-chains, and were in the range of 0.5–0.8 ppm (90–150 Hz at 750 MHz). In NCA and NCO experiments, polarization is transferred from the backbone amide nitrogen atom to the Cα and carbonyl-carbons, which helps in correlating intraresidue and sequential backbone residues. The NCA transfer is intraresidual, which connects the amide ^{15}N and $^{13}C\alpha$ of the same residue; the NCO transfer is interresidual and connects the amide ^{15}N with the CO of the previous residue (Figure 4.2C and D). A 40 ms PDSD mixing scheme, following the SPECIFIC-CP transfer, allowed us to obtain 2D NCACX and NCOCX spectra, which were used to correlate signals from side chain carbons to the backbone Cα, CO and amide N atomic sites.

With the help of 3D NCACX, 3D NCOCX, and 2D PDSD experiments with various contact times, we were able to assign approximately 70% of 1TM-CXCR1(1-72), namely residues 24-72. The remainder of the protein was mobile

and could not be assigned through CP-based methods. The complete assignment of the protein is shown in figure 4.2. The resonances from the mobile regions of 1TM CXCR1(1-72) were assigned using TOBSY (TOtal through-Bond correlation SpectroscopY). TOBSY utilizes J-couplings to correlate ^{13}C atoms, which means it can only be used for residues that are mobile enough to average out the dipolar couplings [180]. Signals from residues 1-23 in 1TM-CXCR1(1-72) were assigned using TOBSY, $^{1}H/^{13}C$ and $^{1}H/^{15}N$ INEPT experiments. Similarly, we repeated the assignment process on samples containing uniformly labeled ^{13}C, ^{15}N 1TM-CXCR1(1–72) with unlabeled IL-8(1–66). Two-dimensional ^{15}N detected SLF was used to measure ^{1}H-^{15}N dipolar coupling. Values of the ^{1}H–^{15}N dipolar coupling were calculated from the experimentally measured perpendicular edge frequencies of the respective rotationally averaged powder patterns. Variations in these dipolar couplings are observed due to the differential rotational alignment of sites in the membrane proteins along the bilayer normal. To obtain the correct dipolar coupling, the perpendicular edge frequencies were multiplied by 4 to obtain the full dipolar coupling value, corresponding to twice the parallel edge frequency.

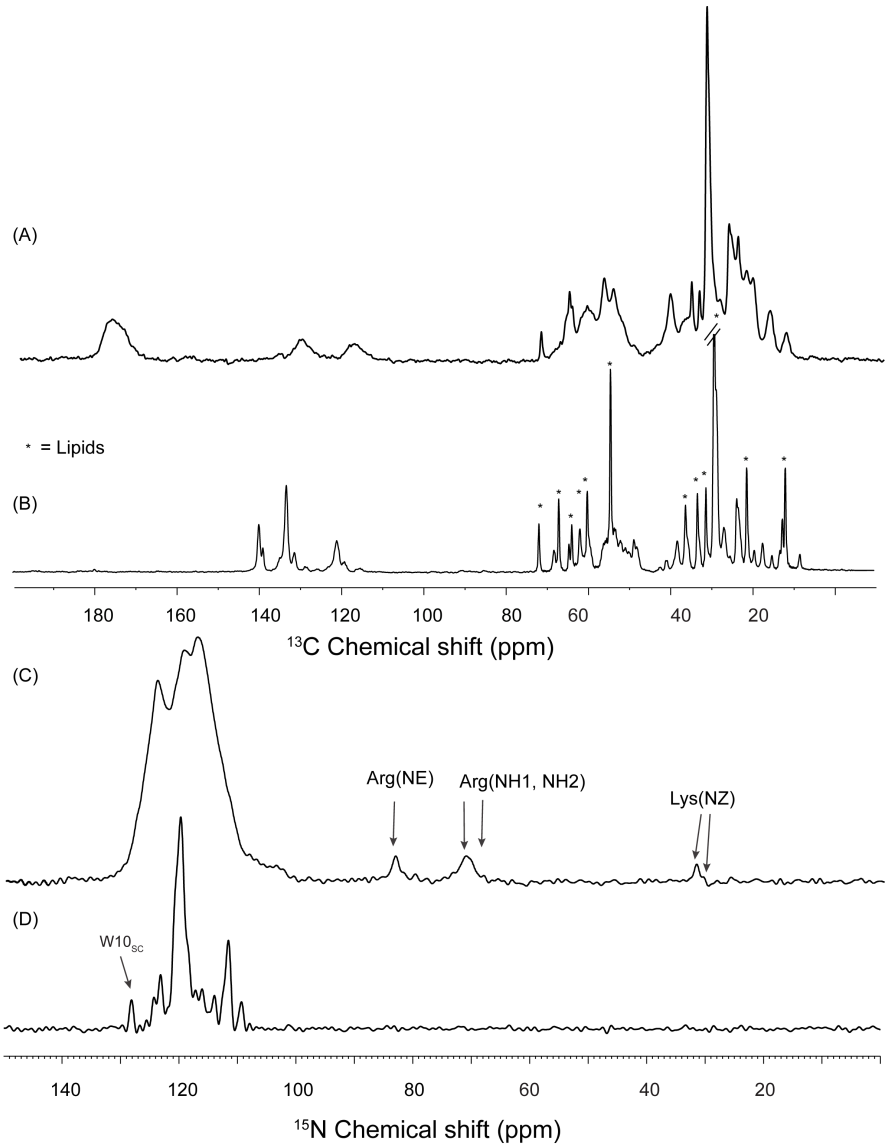

Figure 4.1: Mobile and immobile sites of 1TM-CXCR1(1-72). ^{15}N and ^{13}C NMR spectra of uniformly labeled ^{13}C, ^{15}N 1TM-CXCR1(1–72) in DMPC liposomes. Spectra were obtained at a ^{1}H resonance frequency of 750 MHz at 25°C. (A), (B) 1D ^{13}C CP and 1D ^{13}C refocused INEPT spectrum acquired with 256 scans and 512 scans respectively. (C), (D) 1D ^{15}N CP and 1D ^{15}N refocused INEPT spectrum, acquired with 512 scans and 1k scans respectively. The delay of the refocused INEPT block was chosen so that all ^{13}C and ^{15}N signals are positive.

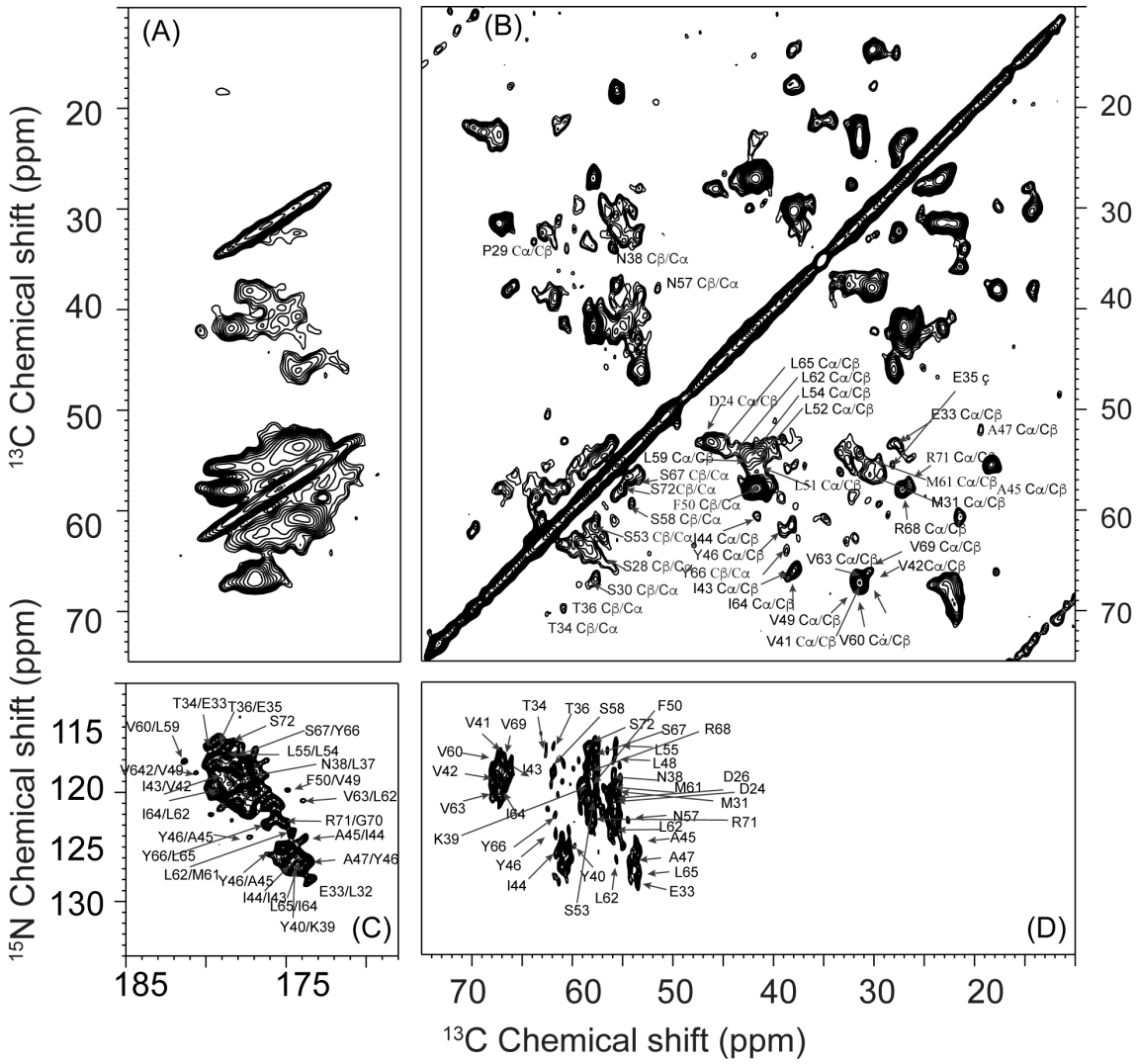

Figure 4.2: Assignments of 1TM-CXCR1(1-72). Contour plot of 2D ^{13}C/^{13}C PDSD (A) carbonyl region (B) aliphatic region, (C) NCO, and (D) NCO recorded using a sample of uniform ^{15}N /^{13}C 1TM-CXCR1(1-72) reconstituted in DMPC proteoliposomes. All spectra were recorded at a field of 750 MHz, a spinning frequency of 11.11 kHz and at 7°C. For the ^{13}C/^{13}C PDSD experiments, magnetization between ^{13}C spins was exchanged using a 10ms PDSD mixing period, resulting in predominantly one-bond correlations and a limited number of two-bond intraresidue correlations. For the 2D NCO and NCA spectra, polarization between ^{1}H and ^{15}N was exchanged using a 1 ms standard cross-polarization (CP) period; selective transfer from ^{15}N to ^{13}C' or ^{13}Cα was achieved by a 4ms SPECIFIC CP pulse.

4.4. Results

NMR is a formidable tool to monitor protein−ligand interactions. By detecting spectral changes, site-specific details of the protein−ligand interaction can be obtained. Binding a ligand will perturb the local chemical environment of the interacting amino acids, which, in turn, will alter the chemical shift of the nuclei close to the binding site. In order to map these chemical shift perturbations, well-resolved signals in NMR spectra of the protein are a prerequisite. We have used MAS solid-state NMR to map site-specific changes in the N-terminal domain of 1TM-CXCR1(1–72) upon binding unlabeled IL-8(1–66) in an attempt to elucidate the exact binding site. Because regions of the protein undergo motion on different time scales, two different types of experiments were used; CP-based experiments were used to study the most rigid residues of 1TM-CXCR1(1-72) and INEPT-based experiments captured the more dynamic residues, such as these located in the N-terminal domain. Figure 4.3 shows two CP-based PDSD $^{13}C/^{13}C$ correlation spectra; the one in panel A was recorded on uniformly labeled ^{13}C, ^{15}N 1TM-CXCR1(1-72), and the spectrum in panel B shows uniformly labeled ^{13}C, ^{15}N 1TM-CXCR1(1–72) with unlabeled IL-8(1–66) bound. All peaks were assigned to specific residues using standard 2D and 3D experiments. Using PDSD only residues 24-72 of 1TM-CXCR1(1-72) could be detected, which includes part of the N-terminal domain closest to the transmembrane helix, the transmembrane helix and the intracellular loop. Differences between the two spectra recorded on 1TM-CXCR1(1-72) with and without IL-8(1-66) bound are highlighted with a red

box. Additional signals were detected in the spectrum of 1TM-CXCR1(1-72) with IL-8(1-66) bound, indicating several residues were immobilized upon interaction. Comparison of panel A and B in figure 4.3 also shows that, upon interaction with IL-8(1-66), several peaks in the CP-based PDSD $^{13}C/^{13}C$ correlation spectrum undergo a chemical shift perturbation. These perturbations are likely due to changes in the chemical environment upon protein–ligand interaction. The reproducibility of the solid-state NMR data in terms of chemical shift and line width was evaluated by repeating the measurements multiple times on different samples using the same protocol and experimental conditions. The data sets showed chemical shifts from well-resolved peaks deviate from each other less than 0.1 ppm.

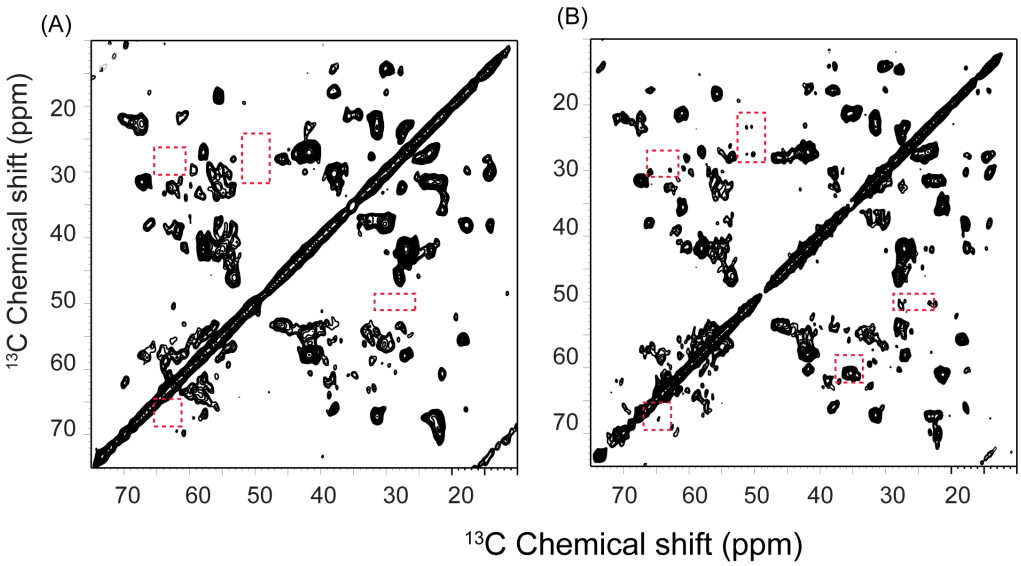

Figure 4.3: Changes upon IL-8(1-66) binding detected by 2D $^{13}C-^{13}C$ correlation experiments. (A) Aliphatic region of ^{13}C, ^{13}C proton-driven spin diffusion (PDSD) spectrum recorded on uniformly $^{13}C/^{15}N$-labeled 1TM-CXCR1(1-72) (B) Aliphatic region of ^{13}C, ^{13}C proton-driven spin diffusion (PDSD) spectrum recorded on uniformly $^{13}C/^{15}N$-labeled 1TM-CXCR1(1-72) in the presence of unlabeled IL-8. Aliphatic regions of $^{13}C/^{13}C$ correlation spectra were obtained with 10 ms mixing. Differences between the two spectra are highlighted using red boxes.

The first 23 residues of the N-terminal domain of 1TM-CXCR1(1–72) could not be observed in CP-based experiments, due to motion. Therefore INEPT and TOBSY were used to provide insight into possible changes upon complex formation between 1TM-CXCR1(1-72) and unlabeled IL-8. Significant changes were observed in $^{1}H/^{15}N$ and $^{1}H/^{13}C$ INEPT experiments recorded on uniformly ^{15}N, ^{13}C labeled 1TM-CXCR1(1–72) upon interaction with unlabeled IL-8(1-66), (Compare Figure 4.4A,C to Figure 4.4B,D). Remarkably few residues in 1TM-CXCR1(1–72) were immobilized after binding to IL-8(1-66). Immobilization is distinguished by a disappearance of peaks due to incompatible rotational correlations times with INEPT-based experiments. For instance, one of the residues easily identified in the spectra due to its distinct chemical shift, the Trp10 side chain, became immobilized after binding to IL-8(1-66) and its corresponding signal could no longer be detected. Sharp lines in $^{1}H/^{13}C$ INEPT spectra due to natural abundance ^{13}C in lipids were marked with an asterisk. To get better resolution two–dimensional versions of the INEPT spectra from figure 4.4 were recorded (Figure 4.5). Several well-separated peaks in $^{1}H/^{15}N$ 2D inept spectra illustrate the effect of IL-8(1-66) binding to the receptor. For instance, peaks assigned to W10, G19 and T18 are present in the spectra recorded on 1TM-CXCR1(1-72) by itself, (Figure 4.5A, C), but absent in the spectra recorded on the 1TM-CXCR1(1-72) – IL-8(1-66) complex (Figure 4.5B, D).

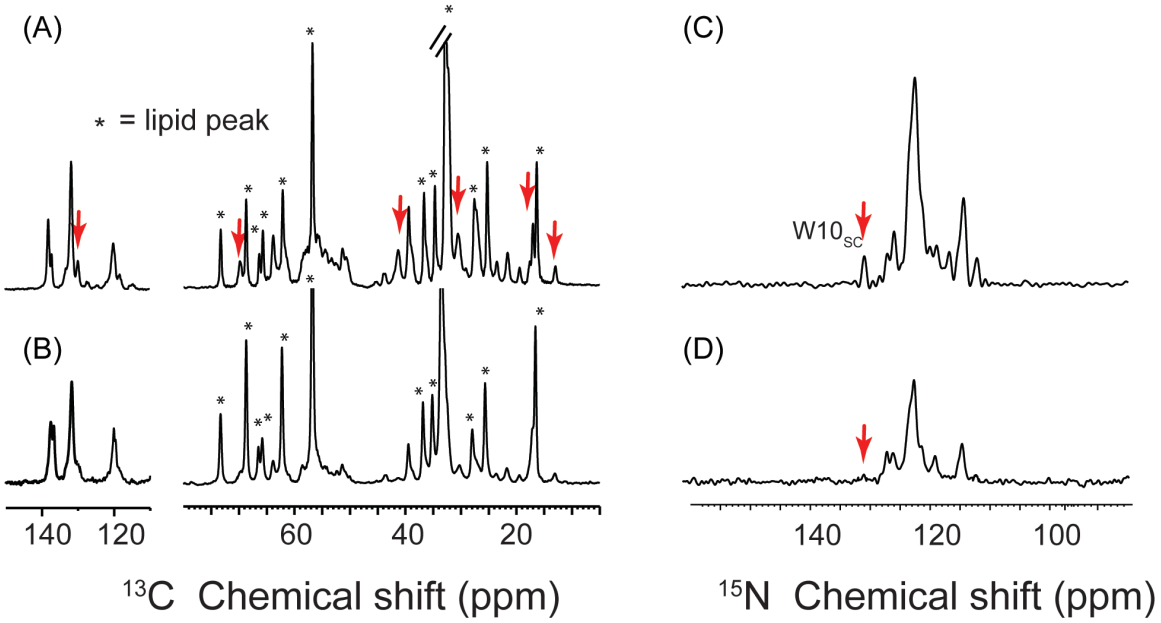

Figure 4.4: INEPT experiments show reduced dynamics in 1TM-CXCR1 upon binding of IL-8(1-66). (A, C) MAS solid-state NMR: INEPT experiments performed on uniform $^{15}N/^{13}C$ 1TM-CXCR1 reconstituted in DMPC proteoliposomes. (B, D) same as in (A) and (C), but with an equimolar amount of ^{14}N IL-8 (1-66) added to the sample. INEPT experiments only show peaks corresponding to mobile residues. The 110-160 ppm region corresponds to aromatic residues. A big loss in sensitivity is seen in this region upon binding to IL-8(1-66). The 10-75 ppm region corresponds to aliphatic residues and lipids. Signals from the lipid environment are indicated with asterisk.
s

To further analyze the structural changes taking place in the flexible N-terminal domain of 1TM-CXCR1(1-72) upon interaction with IL-8(1-66), we performed TOBSY experiments. In TOBSY experiments, aliphatic intra-residue carbon resonances of dynamic regions are correlated using a polarization transfer through ^{13}C-^{13}C resonances via J-couplings. We successfully assigned the first 23 residues of the flexible N-terminal domain in 1TM-CXCR1(1-72) using this method (Figure 4.6A). Upon binding IL-8(1–66), only a few peaks were detected in TOBSY spectra of 1TM-CXCR1(1-72), in stark contrast to that of the apo-

receptor. These changes are likely due to restricted motions of residues that are in contact with IL-8(1-66). The residues that could no longer be detected in TOBSY spectra upon binding IL-8(1-66) are all located in the middle of the N-terminal domain: M9, W10, D11, F12, D13, D14, L15, N16, F17, T18, G19, and M20. Interestingly, residues P21, P22 and A23 could still be observed in the TOBSY spectrum of the complex, indicating they retain their higher mobility. Also, the first eight residues of 1TM-CXCR1(1-72) are still flexible upon binding to IL-8(1–66), but undergo a significant chemical shift perturbation of 0.2 -1.6 ppm. IL-8(1-66) binding to the N-terminal domain of 1TM-CXCR1(1-72) perturbed the environment of these amino acids close to the interaction site and thus altered the chemical shift.

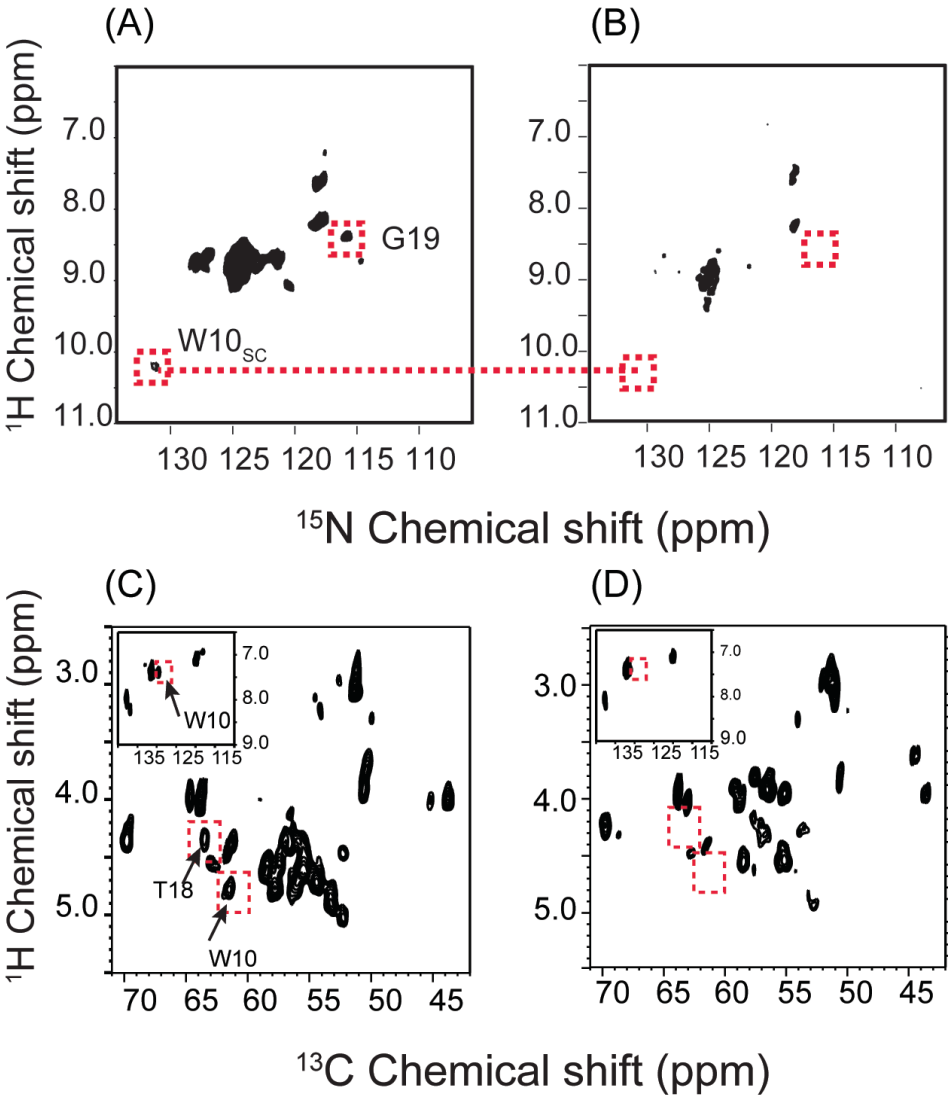

Figure 4.5: Two-dimensional INEPT was used to resolve flexible residues in 1TM-CXCR1(1-72) - IL-8(1-66) complex. (A, C) 11.11kHz MAS ssNMR: ^{1}H/^{15}N 2D-INEPT and ^{1}H/^{13}C 2D-INEPT experiments performed on uniform ^{15}N/^{13}C 1TM-CXCR1(1-72) reconstituted in DMPC proteoliposomes at 25 °C. (B,D) same as in (A) and (C), but with an equimolar amount of ^{14}N IL-8 (1-66) added in the sample. (C, D) Spectra are focused on the chemical shift region for aliphatic carbons. The boxed zoomed spectra in the upper left corner depict the aromatic region of ^{1}H/^{13}C INEPT spectra. Lipid peaks have subtracted in both 2D ^{1}H/^{13}C INEPT spectra.

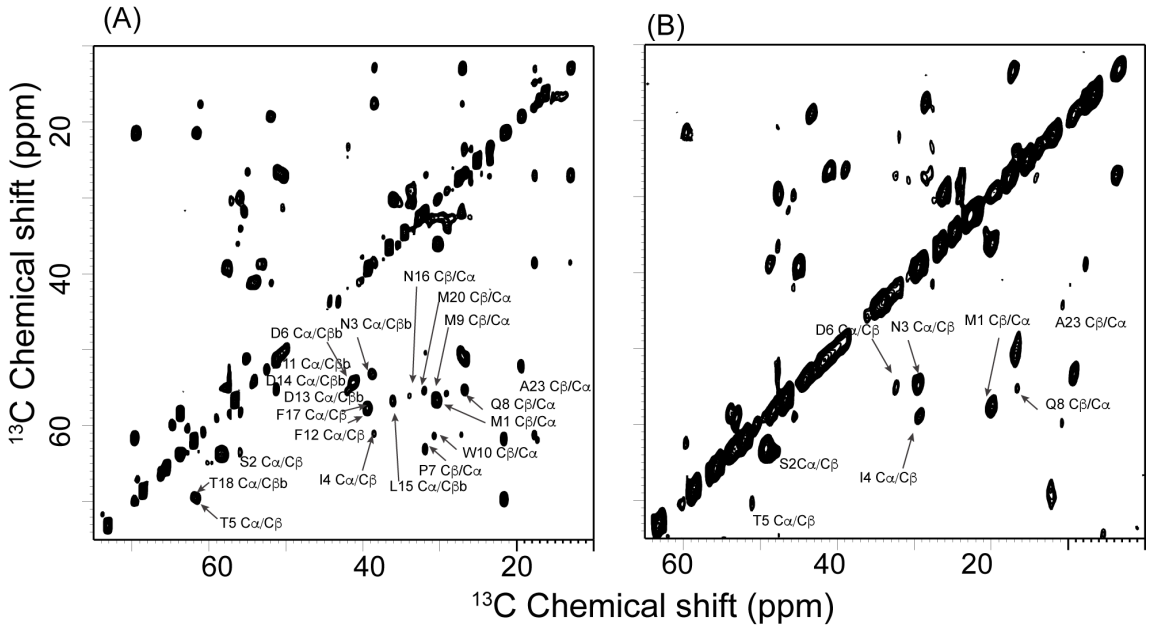

Figure 4.6: TOBSY ^{13}C/^{13}C correlation spectra were used to resolve flexible residues in 1TM-CXCR1 (1-72) upon IL-8(1-66) complex formation. TOBSY experiments correlate aliphatic intra-residue carbon peaks of dynamic regions, transferring the polarization through ^{13}C-^{13}C resonances via J couplings. (A) ^{13}C/^{13}C TOBSY spectrum recorded on uniformly ^{15}N ^{13}C labeled 1TM-CXCR1(1-72). (B) Same as in (A), but with an equimolar amount of ^{14}N IL-8 (1-66) present in the sample. Experiments were carried out at 25 °C.

4.5 Discussion

IL-8(1-66) is one of the most studied chemokines of the chemokine protein family. It recruits neutrophils during the inflammatory immune response by binding and activating the chemokine receptors CXCR1 and CXCR2 [44, 86]. IL-8 is thought to interact with two main regions of the GPCR; Binding Site-I is located on the flexible N-terminal domain and Binding Site-II is composed of extracellular loops 2 and 3. In previous studies the main focus has been to identify which residues in IL-8(1–66) interact with Binding Site-I on CXCR1. This has been

mainly done using mutational analysis and NMR spectroscopy [55, 94, 97, 102, 118, 119, 129]. Three main regions of IL-8(1–66) were shown to interact with the N-terminal domain of CXCR1, the N-loop, the third β-strand, and the N-terminal part of the α-helix [129]. On the other hand, very few studies have explored the effect that IL-8 binding has on CXCR1. All experimental studies that have been carried out have used soluble peptides: one used the first 38 residues of the N-terminal domain of CXCR1 in proteoliposomes [97]. Another used a synthetic peptide corresponding to the first 40 residues of the N-terminal domain of CXCR1 [103], and several studies have been done using a construct corresponding to residues 9-29 of CXCR1 where residues 15-19 were replaced with a hexanoic acid moiety [93, 96, 97, 102]. All of these studies found that residues 9-29 are most important for the interaction with IL-8(1-66), especially residues D14, G19, P21, P22, D24, E25, D26 and Y27. We designed a construct termed 1TM-CXCR1(1-72), which has the entire flexible N-terminal domain, the first transmembrane helix and the first intracellular loop of CXCR1. This construct was used to map the interaction of IL-8(1-66) on Binding Site-I on the receptor, to study the change in dynamics and to study possible tilt angle changes in the helix using solid-state NMR spectroscopy. This is the first time that changes in dynamics in CXCR1 upon IL-8 interaction with Binding Site-I have been studied. We observed chemical shift perturbations in 1TM-CXCR1(1-72) upon binding to IL-8 using $^{13}C/^{13}C$ correlation spectra. The magnitude of all chemical shift changes was quantified using the equation $\Delta\delta = 1/2\sqrt{(\Delta C/2)^2 + (\Delta N/5)^2}$ where ΔC and

ΔN are the change in carbon and nitrogen chemical shifts, respectively. The chemical shift perturbation upon interaction with IL-8 is summarized in Figure 4.7A. Most differences map to the N-terminal domain, in particular residues D24, Y27, M31 L32 and L37, but resonances from amino acids in the transmembrane helix itself remained largely unperturbed.

Capturing dynamics of proteins is always challenging for solid-state NMR spectroscopy. Several pulse sequences, including TOBSY, which rely on J-coupling to transfer magnetization, have been developed as tools to investigate dynamics [180]. TOBSY requires that motions of the residues are faster than the μs range in order to average out the dipolar couplings. This dynamics range is close to the lower-limit of measurements of T_1, T_2. Based on the resonance assignments made of 1TM-CXCR1(1-72) using TOBSY and 2D INEPT spectra, the first 23 residues located in the N-terminal domain are mobile, with residues 24-37 undergoing an intermediate timescale motion that could not be detected using INEPT, nor with CP-based experiments. Even when the receptor interacts with IL-8(1-66), the first 8 residues and residue A23 were found to be still mobile, whereas some resides were immobilized to such an extent that they could be detected using CP-based experiments. Previous observations made by our group show that, upon interaction with IL-8, the N-terminal domain is not associated with the lipid membrane, so it is unlikely that this immobilization is due to interaction with both IL-8 and the DMPC liposomes [97, 129]

Chemical shift perturbation data suggest that the entire N-terminal domain of 1TM-CXCR1(1-72) is affected upon binding IL-8 (1–66). Residues N3, T5, D6, A23, D24, Y27, S30, M31, L32 and L37 showed the largest chemical shift perturbation (Figure 4.7A, B). These results are largely consistent with previous experimental studies performed on various N-terminal domain peptides. These results also correlate well with two molecular dynamics simulations that attempted to dock IL-8 to a N-terminal domain peptide [164] and with full length CXCR1 in POPC bilayers [117]. Some residues, such as residues N3, T5, D6 and L37, that we have found to undergo chemical shift perturbation upon interaction with IL-8(1-66) have not been described before,. It is likely that the chemical shift perturbation of L37 is due to its close proximity to the transmembrane helix, which starts at residue 39, and the presence of a lipid bilayer.

To date, no structure of CXCR1, or any other chemokine receptor, in an active conformation has been solved. However, several other class A GPCR structures have been determined in active conformations and compared to their inactive conformations to gain insight into the structural rearrangement that is needed to initiate a signaling cascade inside the cell. In all of those structures, several transmembrane helices, mainly helix 3, helix 5 and helix 6, changed tilt angles [181]. Dipolar waves can be obtained by plotting measured values of the $^{1}H–^{15}N$ dipolar couplings versus residue number. Dipolar waves have characteristic features that allow helix length, helix orientation in the membrane,

and presence of any kinks to be easily identified [182]. Two separate dipolar waves with distinct amplitudes were found, indicating that the transmembrane helix of 1TM-CXCR1(1-72) has a kink in it at a position roughly halfway through the membrane. Upon interaction with IL-8(1-66) no tilt angle changes were observed in 1TM-CXCR1(1-72) (Figure 4.7C, D) Both chemical shift perturbation and dipolar waves analysis indicate that the transmembrane helix is not involved in binding IL-8 and does not undergo any conformational change upon binding to IL-8(1-66). All differences were observed in the N-terminal domain (in particular in residues 9-20), which was completely immobilized upon binding to IL-8(1-66) and residues N3, T5, D6, A23, D24, Y27, M31 L32 and L37, which underwent a large chemical shift perturbation.

Chapter 4 is currently being prepared for submission for the publication of the material, Rai, R. K, de Angelis, A.A., Berkamp, S., Park, S.H. and Opella, S.J. The dissertation author was the tertiary author of this material.

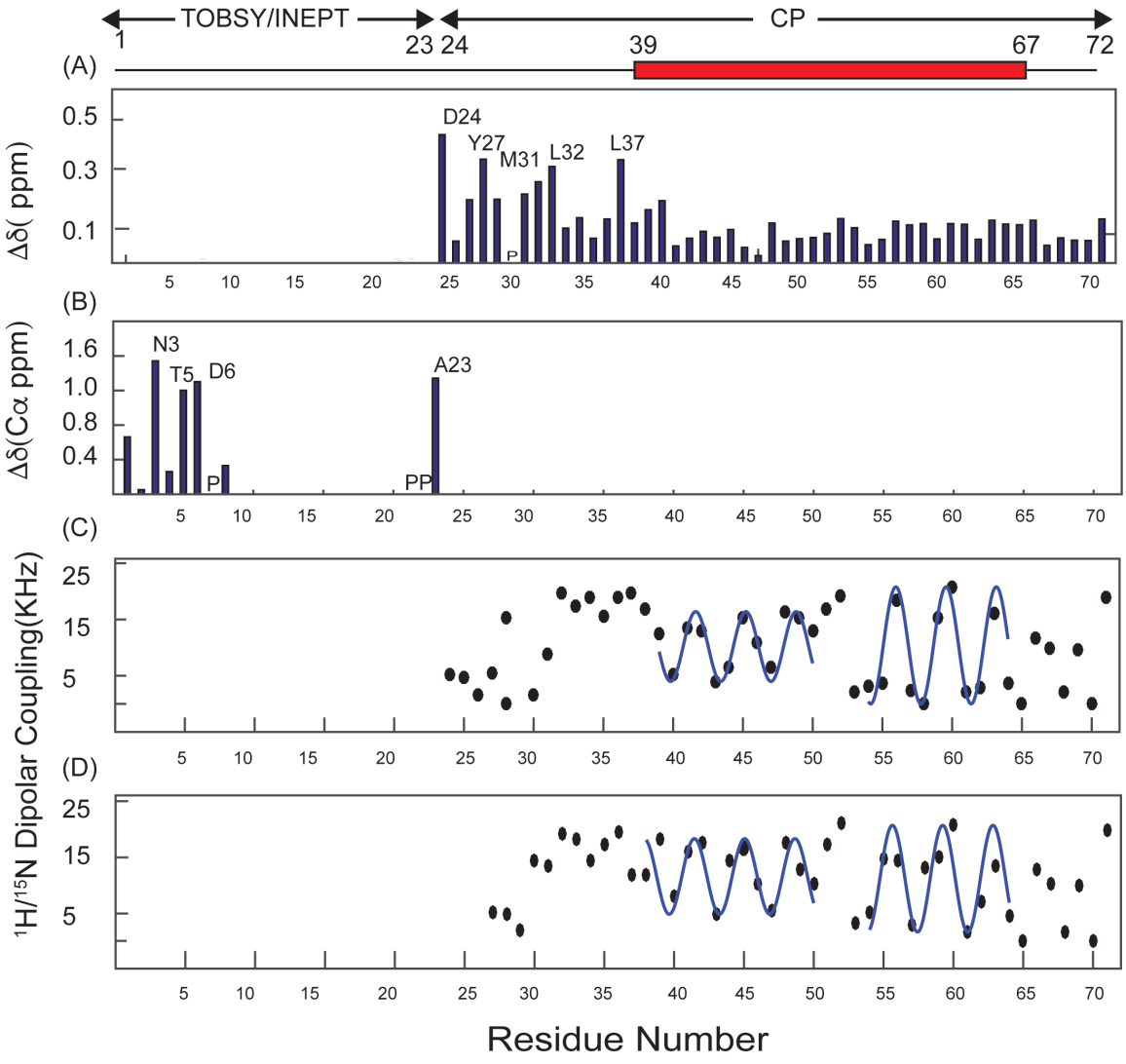

Figure 4.7. Interaction with IL-8(1–66) causes major chemical shift perturbations.(A) 1TM-CXCR1(1-72) chemical shift perturbation plot due to protein ligend binding. NCA data were used to make this plot (Figure 4.2). (B) Chemical shift perturbation in mobile region of 1TM-CXCR1 (1–72) due to ligend binding. TOBSY data were used to make this plot (Figure 4.6). (C) Dipolar waves obtained by plotting measured values of the $^{1}H–^{15}N$ DC versus residue number for 1TM-CXCR1 (1–72). (D) Dipolar waves of 1TM-CXCR1(1-72) in the presence of unlabeled IL-8.

CHAPTER 5: ORIENTATION OF INTERLEUKIN-8 BOUND TO CXCR1 STUDIED BY ORIENTED SAMPLE SOLID-STATE NMR

5.1 Abstract

The globular protein Interleukin-8 (IL-8) binds and activates the G Protein-Coupled Receptor (GPCR) CXCR1 that is expressed on neutrophils and other immune cells. IL-8 interacts with two main sites on CXCR1: Binding Site-I is located on the flexible N-terminal domain and Binding Site-II is located on the second and third extracellular loops of the receptor. Many studies have explored how IL-8 interacts with Binding Site-I, but little information is known about the IL-8 – CXCR1 structure. We previously showed that IL-8 does not undergo a large conformational change upon interaction with CXCR1. Here, orientation dependent parameters were measured on IL-8 immobilized on CXCR1 in bicelles using oriented sample, solid-state NMR spectroscopy. The experimental values obtained for the dipolar couplings and chemical shift anisotropy were compared to that of simulated NMR spectra. IL-8 is shown to adopt a orientation in which its β-sheet core points towards the receptor at a slight angle.

5.2 Introduction

Interleukin-8 (IL-8) is a 72-residue globular protein that belongs to the class of CXC-chemokines. All CXC chemokines adopt a so-called “chemokine-fold” that is characterized by the presence of long flexible N-loop terminated by one turn of

a 3_{10}-helix, followed by three anti-parallel β-strands connected by short loops and a C-terminal α-helix. IL-8 plays an important function in the innate immune response; after secretion by macrophages and other immune cells, it forms a chemotactic gradient. It binds and activates the class A G protein-coupled receptors, CXCR1 and CXCR2, expressed on the cell surfaces of neutrophils. Several biochemical responses are then initiated in the cell ultimately leading to the neutrophil leaving the blood stream, traveling along the IL-8 gradient and degranulating to combat infection [40].

IL-8 dimerizes at micromolar concentrations, but it is thought that the monomeric form is predominantly involved in binding the chemokine receptor CXCR1 [55-57]. An IL-8 obligatory monomer can be created in several ways; 1) by placing the unnatural amino acid, N-methyl leucine, near the dimerization interface; 2) by mutating several residues known to stabilize the dimer; or 3) by removal of the last six residues of the protein [82-85]. This last truncation is not known to influence the interaction with CXCR1 or perturb its structure in any major way [84, 129]. This construct; IL-8 (1-66), is the protein used in all the experiments described here. Experimental data suggest that IL-8 interacts with two main binding sites on CXCR1; Binding Site-I is located within the extracellular, 38-residue, N-terminal region of the receptor whereas Binding Site-II includes extracellular loops 2 and loop 3 [31, 78, 92, 93]. We have previously solved the solution NMR structure of a monomeric version of IL-8 and mapped the

interaction between IL-8 and Binding Site-I using truncated constructs of CXCR1 [129]. We found that several residues in the N-loop (residues 10-19), in the third β-strand (residues 47-51) and a small part of the α-helix (residues 56-66) are affected by binding to Binding Site-I. These results nicely correlate with the result of others [95, 96, 102, 118, 119]. In another study by our lab, proton-detected ultrafast MAS solid-state NMR spectroscopy was used to map the residues that are important for the interaction with Binding Site-II and with the full length receptor and we studied the change in protein dynamics associated with IL-8 binding to CXCR1. We found that most backbone amide sites of IL-8 were immobilized upon binding CXCR1, and chemical shift perturbation was be used to map the residues of IL-8 that interact with both Binding Site-I and Binding Site-II in CXCR1 [100]. Most noticeably, the overall pattern of chemical shifts was not altered significantly, suggesting that IL-8 does not undergo a major conformational change when it interacts with CXCR1.

The X-ray crystal structure of several chemokine receptors have been solved [74, 87-91] and the solid-state NMR structure of CXCR1 in phospholipid bilayers was solved by our lab [72]. The flexible, N-terminal domain of CXCR1 could not be observed, but structural restraints were obtained for the seven transmembrane helices, the intracellular and extracellular loops and part of the intracellular C-terminal domain. The overall fold was similar to that of another chemokine receptor, CXCR4, which was described by other groups [74]. The

largest differences between the two structures occured in the intracellular C-terminal domain, which is the location of the heterotrimeric G-protein interaction site. All of the structures of chemokine receptors determined to date are of receptors in the inactive states, so little information is available on the conformational changes that take place upon activation. However, several structures of other class A GPCR structures have been solved to examine the conformational change in both active and inactive state. Upon activation in all class A GPCRs described to date, transmembrane helix 6 undergoes a change of tilt angle and moves away from the rest of the helical bundle, which itself undergoes some rearrangements. This movement induces changes in the hydrogen bond network between the other helices and exposes a pocket that is important for the interaction with the G-protein [181, 183, 184]. The most important residues found in the structures of active conformation class A GCPRs are the D-R-Y motif in TM3, several residues in TM6 and the N-P-x-x-Y motif in TM7 [185]. These same residues are also thought to be important in the activation of CXCR1; mutation of D134 in the D-R-Y motif of CXCR1 abolishes IL-8 binding and receptor activation [29] whereas mutation of V247 in TM6 of CXCR1 leads to a constitutively active receptor [30]. Molecular modeling has been used to try to dock IL-8 to CXCR1. In the models, the charged residues in the N-loop of IL-8 interact with Binding Site-I, then IL-8 rotates to enable its the hydrophobic residues in IL-8 to contact Binding Site-I, and finally the residues in the ELR motif of IL-8 interact with Binding Site-II [94, 117]. This ELR motif is required for

receptor activation, but not for the interaction with the receptor [84]. This modeled rotation of IL-8 upon interaction with Binding Site-II had yet to be studied using experimental methods, and hence this motivated the current study described here.

We have used oriented sample, solid state NMR to derive the relative orientation of IL-8 bound to the receptor. IL-8 was immobilized onto CXCR1 reconstituted in triton bicelles and orientation dependent parameters were measured using SAMPI-4 experiments. The ^{1}H-^{15}N dipolar couplings and the ^{15}N anisotropic chemical shifts of both ^{15}N uniform and ^{15}N selectively labeled leucine and valine labeled IL-8 were then matched to that of simulated spectra of IL-8 in different orientations. Using a vector that is defined as running parallel through the α-helix, from its N-terminus to its C-terminal end, IL-8 makes an angle of 72°±2° and -30°±2° degrees relative to the bilayer normal.

5.3 Material and Methods

5.3.1 Protein Expression and Purification

The gene for human IL-8 (1-66) was cloned and expressed as described previously [106]. Uniformly ^{15}N-labeled, selectively ^{15}N-leucine labeled, selectively ^{15}N-valine labeled and uniformly ^{15}N, 2-^{13}C labeled samples were obtained by growing bacteria in standard M9 cell growth media, supplemented with 1g/L ^{15}N ammonium sulfate (Cambridge Isotope Laboratories, 15N2, 99%), 4g/L 2-^{13}C

glucose (Cambridge Isotope Laboratories, 2-^{13}C D-glucose, 99%) or 100mg/L leucine of valine (Cambridge Isotope Laboratories, 15N, 98%). Uniform ^{15}N, 2-^{13}C labeled IL-8 was expressed using a media exchange protocol to enhance yield; the cells were grown in LB medium up to OD_{600}=0.5-0.6, the cells were then pelleted using centrifugation and resuspended in one-quarter volume equivalent ^{15}N, 2-^{13}C glucose M9 media. After 1 hour, protein purification was induced using IPTG and the cells harvested after 4-5 hours. Selective labeled IL-8 was grown in unlabeled M9 media until OD_{600}=0.4, an amino acid mix was then added (100mg/L labeled amino acid, 500mg/L Glu, Asp, Asn and Gln, 300mg/L Leu, Ala, Val, Ile and Thr, 200mg/L Ser, Tyr, Phe, Trp, Cys, Met, Lys, Arg, His, Gly and Pro) and protein expression induced after 1 hour using IPTG. The cells were harvested 2 hours after induction. After protein purification IL-8 was stored as a lyophilized powder at -20°C. The gene for human CXCR1 was cloned and expressed as described previously [108, 186]. The purified unlabeled protein was reconstituted in 1,2-dimyristoyl-sn-glycero-3-phosphocholine (DMPC) lipid bilayers and stored at -80°C. The final lipid:protein ratio was 10:1 by weight, or ~600:1 by molar ratio.

5.3.2 Sample Preparation

Interleukin-8 and CXCR1 in DMPC liposomes were mixed in an equimolar ratio and incubated for 15 minutes at room temperature. The proteoliposomes were then pelleted using a NVT90 Beckman rotor in an ultracentrifuge 90,000 rpm

for 3 hours at 15°C. To form q=5 DMPC/triton X-100 bicelles, a 5 molar excess of triton was added directly to the pellet and incubated for at least 1 hour. To form bicelles, the sample was vortexed and intermittently placed on ice and at 40°C. Final samples contained on average 4.5 mg of unlabeled CXCR1, 0.9 mg labeled IL-8, 45 mg DMPC and 8.5 mg of triton X-100 in 180μL sample volume.

5.3.3 NMR Spectroscopy

All solid-state NMR experiments were performed on a 700MHz spectrometer with a Bruker Avance console and on a 900MHz spectrometer with a Bruker Avance III HD console. Both spectrometers were equipped with home-built probes. ^{31}P-detected experiments were done at 700MHz using a double-channel probe with a scroll coil configuration (grant 2010). ^{13}C-detected experiments were performed at 700MHz using a triple-channel probe equipped with a cross coil configuration using a solenoid coil to detect the heteronuclei and a MAGC coil for proton [187]. ^{15}N-detected experiments were performed at 900MHz using a home-built, triple-channel probe with a 5mm solenoid coil and a modified Alderman-grant resonator in a cross coil configuration [188]. All of the experiments were performed at 40°C. All two-dimensional spectra were obtained using the SAMPI4 pulse sequence [16, 17] with 1ms CP contact time and SPINAL-16 decoupling during acquisition [189]. One-dimensional ^{15}N and ^{13}C detected spectra were recorded using the CP-MOIST pulse sequence [190]. ^{15}N-detected experiments were performed using a B_1 field strength between 42 and

50kHz, a recycle delay of 3 seconds and carriers on 120 ppm and 9ppm for ^{15}N and ^{1}H, respectively. For uniform ^{15}N labeled IL-8 64 t_1 and 1024 t_2 points were acquired, for selective labeled IL-8 32 t_1 and 512 t_2 points were acquired. ^{13}C-detected experiments were performed using a B_1 field strength of 40kHz, a recycle delay of 6 seconds and carriers on 50 ppm and 8.5ppm for ^{13}C and ^{1}H, respectively. All spectra were referenced externally relative to phosphoric acid at 0 ppm, ammonium sulfate at 26.8 ppm and adamantane methylene at 38.48 ppm. The data were processed using Topspin using a zero-filling function and a phase-shifter sine-bell in both dimensions before Fourier transform.

5.3.4. Simulations on IL-8 Orientations

One-dimensional and two-dimensional oriented sample, solid-state NMR spectra of IL-8 were simulated using a modified version of the MATLAB script described by Nevzorov et al. [191]. The script takes atomic coordinates from the protein structure, peptide plane geometry angles and distances, amide nitrogen chemical shift tensor elements and an order parameter to calculate the ^{15}N chemical shift and ^{1}H-^{15}N dipolar coupling for the given protein orientation, which is then plotted in a way to resemble the NMR spectra. The following values were used to describe the amino acid geometry: H-N-Cα = 118.2°, N-C'-Cα = 115.6°, H-N-C' = 119.5°, tetrahedral angle = 111.65° with an amide bond length of 1.05 Å. The following values were used to describe the principal values of the ^{15}N amide chemical shift tensor: σ11 = 64 ppm, σ22 = 77 ppm, σ33 = 217 ppm, and the following values for the glycine^{15}N amide chemical shift tensor: σ11=41 ppm, σ22

= 64 ppm, σ33 = 210 ppm, the angle between the tensor and amide bond was set as H-N- σ33 = 18.5°. A value of 0.3 for the order parameter was used for all the simulations, which is less than the standard value of 0.8 for perpendicular aligned bicelles to compensate for increased dynamics in the protein complex. After every simulation, the IL-8 structure was rotated in MOLMOL, and the atomic coordinates used to rerun the simulation.

5.4 Conclusions and Discussion

The orientation of IL-8 in the IL-8 – CXCR1 complex was determined by measuring orientation-dependent parameters such as anisotropic chemical shifts and dipolar couplings. Oriented sample, solid-state NMR is uniquely suited for addressing this research question, since only one experiment needs to be performed to obtain both of these parameters. Samples were prepared by mixing isotopically labeled IL-8 with unlabeled CXCR1 reconstituted in DMPC liposomes. The complex was pelleted using ultracentrifugation after which the detergent Triton-X100 was added in order to form q=5 DMPC/triton X-100 bicelles [192]. ^{31}P-detected solid state NMR spectroscopy was used to confirm alignment of the bicelles in the magnetic field; upon uniaxial alignment a single, narrow peak can be detected (Figure 5.1G). DMPC bicelles naturally align with bilayer normal perpendicular to the magnetic field. Upon perpendicular alignment, the phosphorus atom in the lipid head group will resonate at approximately -15 ppm. Isotropic micelles will have a single, sharp peak at approximately 0 ppm, whereas

unaligned bilayers display the full powder pattern. One-dimensional CP-MOIST experiments [190] recorded on a sample containing uniform ^{15}N labeled IL-8, unlabeled CXCR1 in bicelles, show a lot of intensity in the range from 100-140 ppm, attributed to the ^{15}N amide residues in the backbone of the protein (Figure 5.1A). The sharper peaks around 35 ppm, 75 ppm and 90 ppm were tentatively assigned as lys, arg and trp sidechains, respectively because their isotropic chemical shifts are resonate at these approximate frequencies. This result suggests that IL-8 is immobilized upon interaction with CXCR1 and aligned relative to the magnetic field. INEPT experiments were recorded on the same sample to study mobile residues that may be present. Little to no signal intensity was found in the INEPT spectra, which indicates that the entire protein is immobilized and it undergoes motion on a timescale slower than what is compatible with this pulse sequence (Figure 5.1B). To ensure that IL-8 had not precipitated or bound to the bicelles, the same set of experiments was run on samples containing just ^{15}N IL-8 and q=5 bicelles (Figure 5.1C,D). A small amount of signal was present in both CP and INEPT spectra, suggesting that the protein is weakly aligned by the bicelles, but does not otherwise interact with them. Cross-polarization spectra on IL-8 in aqueous environment did not produce any signal, whereas the INEPT showed intensity at the isotropic chemical shift frequencies (figure 5.1E,F). These results indicate that, upon interaction with CXCR1, IL-8 is fully immobilized and that the orientation of IL-8 in the IL-8 –

CXCR1 complex can be determined by measuring both orientation-dependent, anisotropic chemical shifts and dipolar couplings.

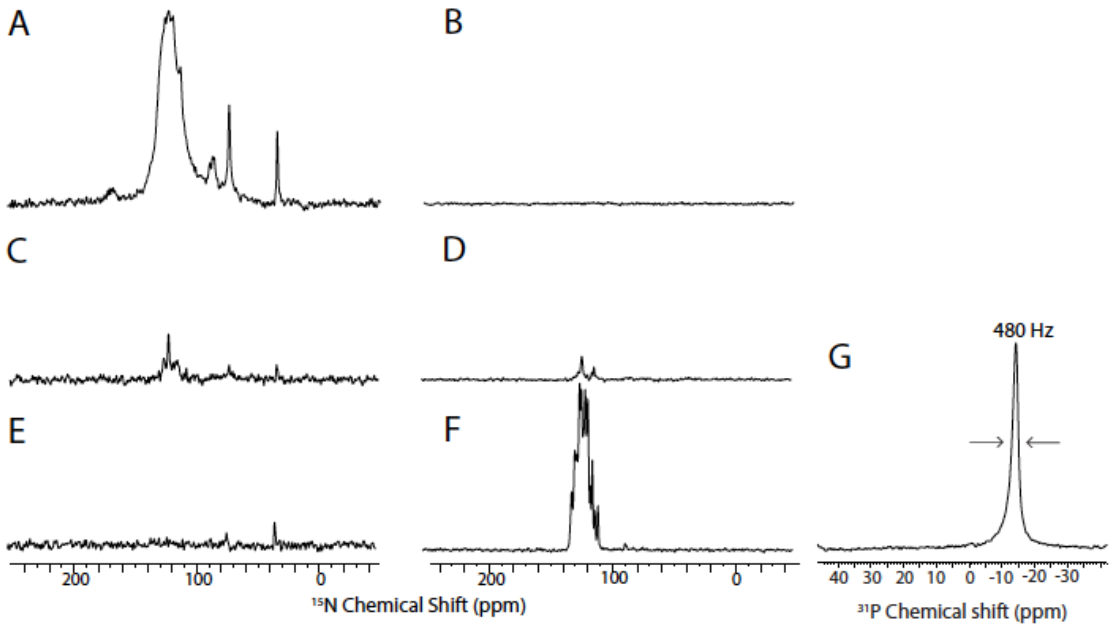

Figure 5.1: IL-8(1-66) is immobilized upon binding CXCR1 (A) ^{15}N CP-MOIST spectrum recorded on a sample containing ^{15}N IL-8 and an equimolar amount of unlabeled CXCR1 in q=5 bicelles. (B) ^{15}N INEPT spectrum recorded on the sample described in (A). (C) ^{15}N CP-MOIST spectrum recorded on a sample containing ^{15}N IL-8 and q=5 bicelles. (D) ^{15}N INEPT spectrum recorded on the sample described in (C). (E) ^{15}N CP-MOIST spectrum recorded on a sample containing ^{15}N IL-8 in HEPES buffer. (F) ^{15}N INEPT spectrum recorded on the sample described in (E). (G) ^{31}P spectrum to demonstrate the bicelles are aligned perpendicular to the external magnetic field. All ^{15}N- detected spectra recorded at 313K, 900MHz, 50kHz ^{1}H field, 1ms contact time. ^{31}P spectrum recorded at 313K, 700MHz. (A), (C), (E) and (B), (D), (F) recorded using the same experimental setup.

One-dimensional ^{13}C-detected CP-MOIST experiments were recorded on samples containing ^{15}N 2-^{13}C glucose IL-8 and unlabeled CXCR1 in q=5 triton bicelles [193]. IL-8 labeling was optimized to minimize line-broadening caused by the strong C-C dipolar couplings present in uniformly ^{13}C labeled proteins [194, 195]. Figure 5.2B shows a sharp peak at ~35ppm in control samples containing

unlabeled CXCR1 reconstituted in q=5 bicelles. Chemical shifts in this region have been assigned to natural abundance ^{13}C in the DMPC acyl chains [196]. The spectrum in Figure 5.2A shows this same sharp peak attributed to the lipids, as well as additional intensity in the 45-80 ppm range, a region typically associated with signals from the alpha carbon region. Unfortunately, some intensity in this region could also be seen in the control experiment (Figure 5.2B), which is likely due to natural abundance ^{13}C labeling in the unlabeled CXCR1 protein. Little intensity in the regions typical for carbon sidechain and carbonyl chemical shift can be observed, because 2-^{13}C glucose was used to isotopically label IL-8. These regions could be explored by switching to a different labeling strategy, such as 2-^{13}C glycerol, 1,3-^{13}C glycerol or 1-^{13}C pyruvate [197].

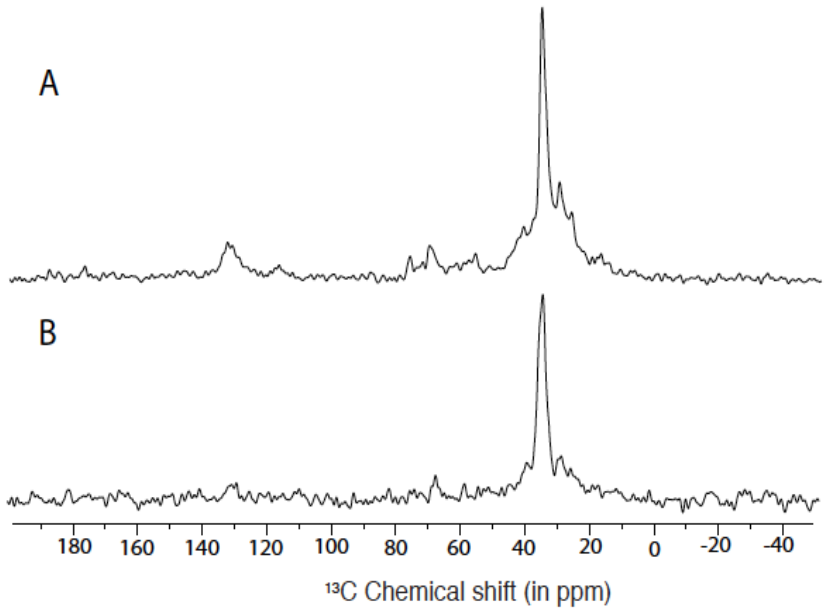

Figure 5.2: CP spectrum recorded on ^{13}C labeled IL-8(1-66) (A) ^{13}C CP-MOIST spectrum recorded on a sample containing ^{15}N 2-^{13}C glucose IL-8 and an equimolar amount of unlabeled CXCR1 in q=5 bicelles. (B) ^{13}C CP-MOIST spectrum recorded on a sample containing ^{14}N CXCR1 in q=5 bicelles. All spectra recorded at 313K, 700MHz, 40kHz ^{1}H field, 1ms contact time.

Two-dimensional SAMPI-4 experiments [17] were recorded on samples containing ^{15}N uniformly labeled IL-8 and unlabeled CXCR1, ^{15}N-leucine labeled IL-8 and unlabeled CXCR1, and ^{15}N-valine-labeled IL-8 and unlabeled CXCR1. SAMPI-4 belongs to the class of separated-local-field (SLF) experiments, such as PISEMA [15], SAMMY [16] and HIMSELF [198]. SAMPI-4 works by averaging out the proton homonuclear dipolar coupling using a magic-sandwich sequence [199], observing the heteronuclear dipolar coupling in the indirect dimension and measuring the chemical shift anisotropy in the direct dimension. About 55-60 partially overlapped peaks could be observed in the spectrum of ^{15}N uniformly labeled IL-8 (Figure 5.3A). However, single-site resolution was obtained on the

selective labeled samples (Figure 5.3 B,C). At least three distinct peaks can be observed in SAMPI-4 spectrum recorded on ^{15}N leucine IL-8 bound to CXCR1. Interleukin-8 has six leucine residues, one near the N-terminus (L5), four in the β-sheet core (L25, L43, L49 and L51) and one at the C-terminus (L66). Due to local motion in IL-8, it is unlikely that L5 and L66 are sufficiently immobilized upon interaction with CXCR1 that they appear in cross-polarization based experiments [100, 129]. Slightly more signal overlap was observed in SMAPI-4 spectra recorded on ^{15}N valine IL-8 bound to CXCR1. Interleukin-8 has five valine residues; two in the β-sheet core (V27 and V41) and three in the α-helix (V58, V61 and V62). Leucine and valine were selected owing to their distribution in the IL-8 amino acid sequence as well as owing to their labeling efficiency in proteins expressed in E. coli cells.

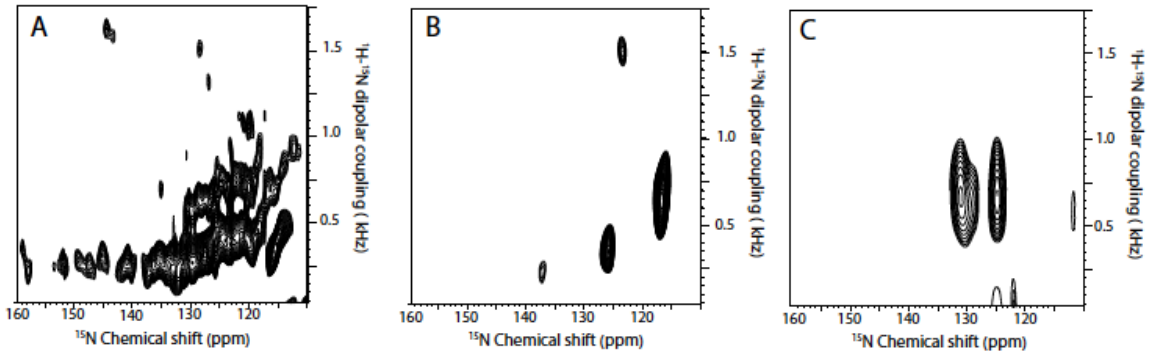

Figure 5.3: Two-dimensional SAMPI-4 experiments recorded on IL-8 bound to CXCR1 (A) ^{15}N SAMPI-4 spectrum recorded on a sample containing ^{15}N IL-8 and an equimolar amount of unlabeled CXCR1 in q=5 bicelles. (B) ^{15}N SAMPI-4 spectrum recorded on a sample containing ^{15}N-leucine labeled IL-8 and an equimolar amount of unlabeled CXCR1 in q=5 bicelles. (C) ^{15}N SAMPI-4 spectrum recorded on a sample containing ^{15}N-valine labeled IL-8 and an equimolar amount of unlabeled CXCR1 in q=5 bicelles. All spectra recorded at 313K, 900MHz, 50kHz ^{1}H field, 1ms contact time.

Several protein structures have been solved using oriented sample, solid-state NMR spectroscopy. Full resonance assignment is helpful but not always necessary. Resonance assignment in oriented sample, solid-state NMR can be achieved using several techniques; such as triple resonance experiments [193, 200], using pulse sequences that try to correlate residues using dilute spin exchange [19, 201] or through correlation of resonances obtained with solution or MAS solid-state NMR [20]. Incomplete resonance assignments can still be useful when combined with theoretical predictions on secondary structure elements; experimental α-helices and β-sheets result in characteristic patterns such as PISA wheels [18, 202]. By taking ideal representations of α-helices and β-sheets, helix tilt angles and sheet rotation and twists can be predicted without the use of assignments. Partial resonance assignments obtained using the "shotgun approach" can be combined with simulations to obtain protein structure [203]. IL-8 contains on several loops, 3 β-strands and one α-helix, so predictions from ideal representations can not be used to predict the entire IL-8 structure and orientation. However, we have previously solved the solution NMR structure of IL-8 [129] and have also found that the structure does not change upon interaction with CXCR1 [100]. A rigid body simulation of IL-8 was performed using a MATLAB script that used standard dihedral angles, and standard values for the chemical shift anisotropy. From previous work we know the structure of IL-8 (PDB: 5WDZ) and we know it does not undergo a large conformational change upon interaction with CXCR1 [100, 129]. The IL-8 structure was used to simulate

one-dimensional and two-dimensional spectra at different orientations relative to the magnetic field. For each nitrogen atom in an amide bond in the IL-8 structure the orientation was calculated and the chemical shift estimated using the literature values for the chemical shift anisotropy[204]. The dipolar coupling was estimated in a similar fashion and the entire process repeated for all backbone nitrogen amide atoms in the protein structure. Both the maximum magnitude of the dipolar coupling as well as the maximum value for the nitrogen chemical shift scale with the order parameter of the system. The more motion there is, the smaller the order parameter gets and the smaller the breadth of the chemical shift tensor and the smaller the size of the dipolar coupling. A standard value for a protein embedded in a bicelle with a large q value is 0.85 [205]. During the simulations, the order parameter that best fit the experimental data was 0.3. This indicates that IL-8 bound to CXCR1 still undergoes significant motion.

Comparisons between the experimental and simulated two-dimensional spectra recorded on uniformly ^{15}N labeled IL-8 bound to CXCR1, as well as the data obtained on ^{15}N-leucine and ^{15}N-valine-labeled IL-8 bound to CXCR1 are shown in figure 5.4. Several different orientations are show to illustrate the sensitivity of the technique. Panels D, E, F, and G show the orientation that most closely matched the experimental data shown in figure 5.4A-C.

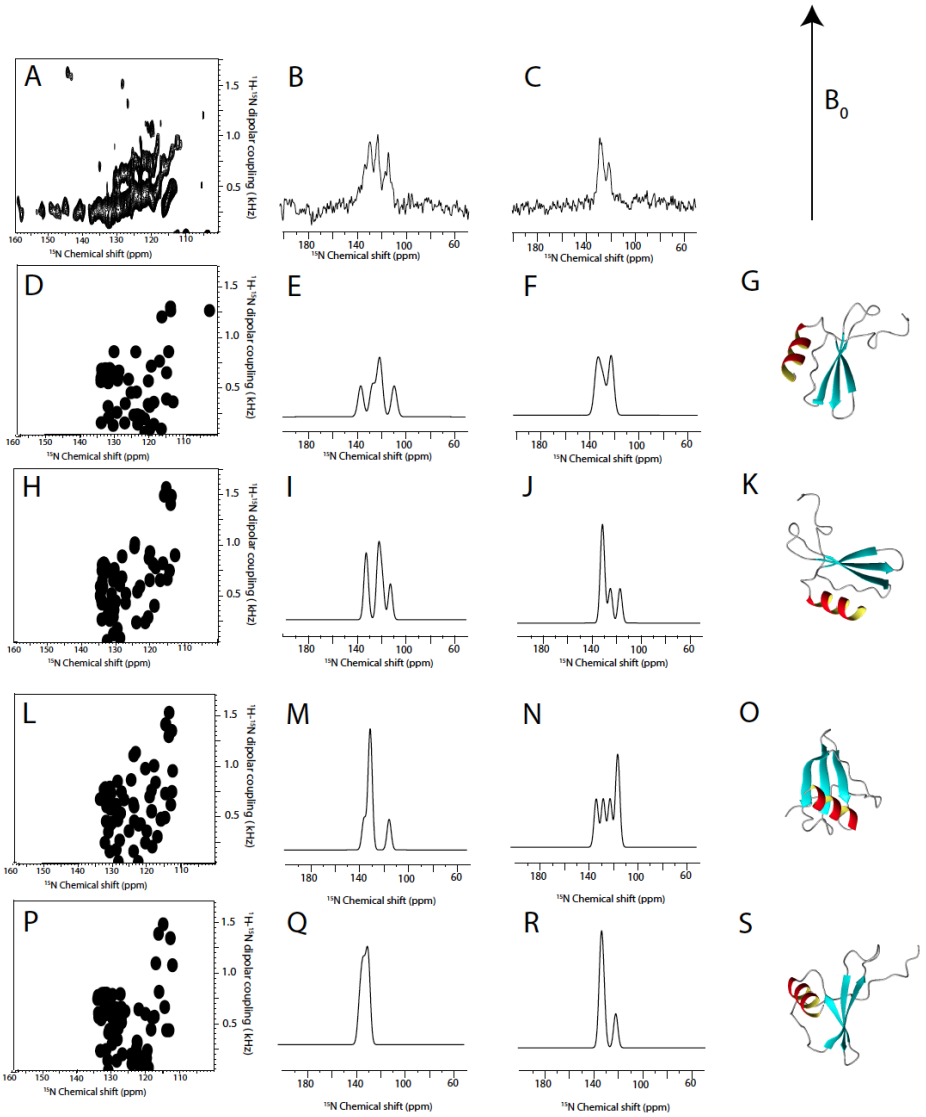

Figure 5.4: Comparison between experimental data and simulated data (A) ^{15}N SAMPI-4 spectrum recorded on a sample containing ^{15}N IL-8 and an equimolar amount of unlabeled CXCR1 in q=5 bicelles. (B) ^{15}N CP-MOIST spectrum of ^{15}N-leucine-labeled IL-8 bound to an equimolar amount of unlabeled CXCR1 in q=5 bicelles. (C) ^{15}N CP-MOIST spectrum of ^{15}N-valine-labeled IL-8 bound to an equimolar amount of unlabeled CXCR1 in q=5 bicelles. (D) Simulated SAMPI-4 spectrum of orientation of IL-8 that best matches experimental data. (E) Simulated one-dimensional CP spectrum corresponding to the orientation in (D) only displaying the leucine residues. (F) Simulated one-dimensional CP spectrum corresponding to the orientation in (D) only displaying the valine residues. (G) structure of IL-8 in orientation relative to magnetic field corresponding to that of simulated spectra in panels (D, E, F). Panels H through S follow the same order as in D through G, all showing orientations that do not match the experimental data, illustrating the sensitivity of the technique.

An intramolecular vector was defined as running through the center of the α-helix of IL-8 from the N-terminal side to the C-terminal side. In the orientation that matched best with all the experimental data, this vector makes an angle of 72°±2° and -30°±2° relative to the bilayer normal (Figure 5.5). In this orientation the β-sheet core of IL-8 points downward towards the receptor. Several residues in this β-sheet core and the loops surrounding it (i.e. residues K11, S30, G31, A35, N36, T37, L43, D45, E48 and L49) have been shown to be important for the interaction with Binding Site-II on extracellular loops 2 and 3 of CXCR1[206]. In this orientation, all these residues lie on the side of IL-8 facing the loops of CXCR1 (Figure 5.5). The relative rotation of IL-8 around the bilayer normal relative to the orientation of CXCR1 and the distance of IL-8 to the receptor could not be determined from the current data. Such distance measurements could be made by incorporating a paramagnetic tag in the receptor and studying selective line-broadening in IL-8. Several distance measurements would need to be made to get a reliable determination of the orientation. For a CXCR1 – IL-8 complex structure, additional experiments are necessary to solve the structure of CXCR1 in an active conformation. Structures from other class A GPCRs that have been solved in both active and an inactive conformations show that significant changes take place in the transmembrane helices. Most helices change their tilt angles during this process. How this large conformational change is induced by binding of a ligand on the extracellular loops is not well understood.

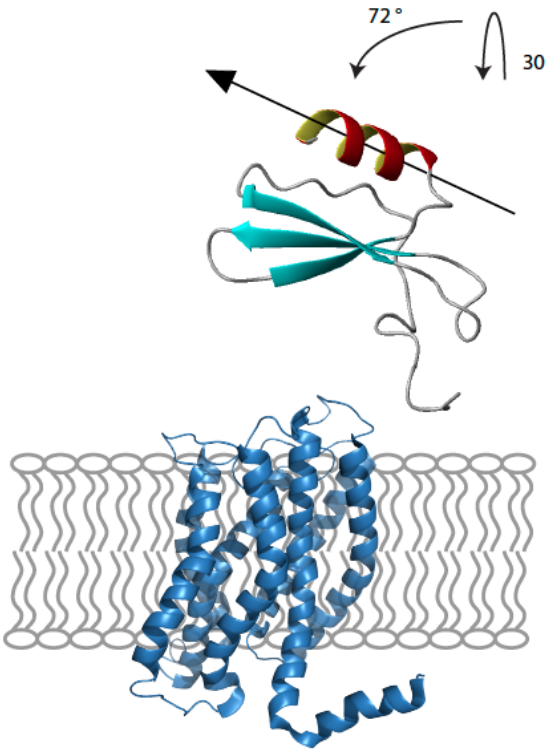

Figure 5.5: The orientation of IL-8 when bound to CXCR1 (A) Solution NMR structure of IL-8 (1-66) (PDB 5WDZ) displayed in the orientation that best matches the experimental oriented sample, solid-state NMR data presented here. A vector through IL-8 was defined as running through the through the center of the α-helix from the N-terminal side to the C-terminal side, shown here using an arrow. This vector makes an angle of 72°±2° and -30°±2° relative to the bilayer normal, as indicated with the arrows. To indicate the biological significance of this orientation, the structure of CXCR1 (PDB 2LNL) is shown placed in a depiction of a membrane. Note the structure of IL-8 and CXCR1 are not drawn to scale.

Chapter 5 is currently being prepared for submission for the publication of the material, Berkamp, S., Radoicic, J., Tian, Y, Park, S.H. and Opella, S.J. The dissertation author was the primary author of this material.

CHAPTER 6: NANODISCS VERSUS MACRODISCS FOR NMR OF MEMBRANE PROTEINS

6.1 Abstract

It is challenging to find membrane mimics that stabilize the native structures, dynamics, and functions of membrane proteins. In a recent advance, nanodiscs have been shown to provide a bilayer environment compatible with solution NMR. We show that increasing the lipid to " belt" peptide ratio expands their diameter, slows their reorientation rate, and allows the protein-containing discs to be aligned in a magnetic field for oriented sample solid state NMR. The spectroscopic properties of membrane proteins with one to seven transmembrane helices in q = 0.1 isotropic bicelles, ~ 10 nm diameter isotropic nanodiscs, ~ 30 nm diameter magnetically aligned macrodiscs, and q = 5 magnetically aligned bicelles are compared.

6.2 Materials and Methods

6.2.1 Sample preparation

Preparation of micelle, isotropic bicelle, and magnetically alignable bicelle samples of Pf1 [203], p7 [207], and CXCR1 [107, 108, 140] were described previously. The 14-residue peptide (>98% purity, Ac-DYLKAFYDKLKEAF-NH2) was purchased from NEO Peptide (www.NEO-Peptide.com). DMPC was purchased from Anatrace (www.affymetrix.com), DHPC from Avanti Polar Lipids

(www.avantilipids.com), and Triton X-100 from Sigma-Aldrich (www.sigmaaldrich.com). The procedure for the preparation of nanodisc and macrodisc samples is similar to that of bicelle samples. Lyophilized powder of the 14-residue peptide was dissolved in an aqueous buffer at a concentration of 80mg/ml. Nanodisc and macrodisc samples were prepared by adding appropriate amounts of an aqueous solution of the 14-residue peptide to DMPC liposomes (for empty bilayer discs) or DMPC proteoliposomes (for protein-containing bilayer discs) to a final molar ratio (DMPC/peptide) of 1.67 and 13.3, respectively. Final lipid contents in the nanodiscs and macrodiscs were 5% (w/v) and 10% (w/v), respectively. Pf1, p7, and MerE proteoliposomes was prepared by mixing 2-3 mg protein solubilized in 500 µl trifluoroethanol with 20 mg DMPC solubilized in 500 µl chloroform at a ratio of 1:1 (v/v). The organic solvent was then evaporated under a stream of nitrogen gas to obtain a thin, transparent protein-lipid film, which was placed under high vacuum overnight. An aqueous solution of the 14-residue peptide was added to the dry film and vortexed and cool-heated (ice/40°C) several times and then allowed to equilibrate to room temperature. Preparation of CXCR1 proteoliposomes was described previously [186]. Upon macrodisc formation, the previously white dispersion of proteoliposomes becomes a clear and non-viscous solution between 0°C and 20°C. Weakly aligned interleukin-8 (IL-8) sample was prepared by mixing IL-8 with macrodiscs in 20 mM HEPES, pH 5.5 at a final concentration of 0.5 mM IL-8 and 10% DMPC (w/v) macrodiscs.

6.2.2 NMR Spectroscopy

The solution NMR experiments were performed at 50°C on a Bruker DRX 600 MHz spectrometer equipped with 5 mm triple-resonance cold probe and z-axis gradient. ^{15}N edited 1H NMR experiments were performed on uniformly ^{15}N labeled samples incorporated in 100 mM DHPC micelles, isotropic DMPC:DHPC bicelles, and nanodisc with a protein concentration of 50-100 μM. IPAP-HSQC spectra [208] obtained on isotropic and weakly aligned IL-8 were used to measure the ^{1}H–^{15}N residual dipolar couplings. The ^{15}N and ^{31}P solid-state NMR spectra were obtained on a Bruker Avance spectrometer with a ^{1}H resonance frequency of 700 MHz. The homebuilt ^{1}H/^{15}N double-resonance probe had 5 mm inner diameter solenoid coil tuned to the ^{15}N frequency, and an outer MAGC coil tuned to the ^{1}H frequency [188]. The ^{31}P solid-state NMR spectra were obtained using a homebuilt ^{1}H/^{31}P double-resonance probe equipped with double-tuned scroll coil [209]. The one-dimensional ^{31}P NMR spectra were obtained by direct excitation with a single pulse using a 6 s recycle delay. 64 scans were signal averaged with a 10 ms acquisition time for each spectrum. Continuous wave ^{1}H decoupling utilized a B1 radio frequency field strength of 42 kHz during the acquisition period. The one dimensional ^{15}N solid-state NMR spectra were obtained by spin-lock cross-polarization with a contact time of 1 ms, a recycle delay of 6 s, and an acquisition time of 10 ms. 2048 transients were co-added, and an exponential function corresponding to 50 Hz of line broadening was applied prior to Fourier

transformation.

6.2.3 Electron Microscopy

A 2.5 ml solution of the sample was absorbed to a carbon-coated copper grid, washed with deionized water and stained with 0.75% uranyl acetate. Micrographs were taken in a 120 kV CM120 electron transmission electron microscope at a magnification of 50,000X and a defocus value of 1.5 mm. Images were digitized with a Nikon SuperCool 9000 scanner using a step size of 6.25 mm. All digitized micrographs were initially binned over 3 x 3 pixels yielding a pixel size on the specimen level of 3.81 Å. Particles were manually selected using the display program WEB and the SPIDER program was used for the subsequent image-processing steps [210]. A total of 3064 nanodisc particles were selected and windowed into 80 x 80 pixels and 2754 150 x 150 pixels macrodiscs particles. Images were normalized and eight cycles of multi-reference alignment, multivariant statistical analysis and classification into 50 class averages were performed.

6.3 Results

Substantial progress has been made in determining the structures of membrane proteins in recent years. However, the major obstacles to application of NMR spectroscopy and X-ray crystallography to helical membrane proteins at the beginning of the field 35 years ago [211] are still present; these are primarily

the identification and optimization of detergent/lipid environments that meet the strict sample requirements of the methods and stabilize the structures of the proteins. Micelles [212], isotropic bicelles [213], and other detergent/lipid assemblies are used as membrane mimics in solution NMR. Solid-state NMR is distinguished by its ability to study immobilized membrane proteins in proteoliposomes [214] and in magnetically aligned bilayers [215]. Most X-ray diffraction structures have been obtained from membrane proteins crystallized from monoolein in lipid cubic phase [216] or from detergents or bicelles [217].

Bicelles are characterized by q, the molar ratio of the “longchain” phospholipid (e.g., DMPC) to the “short-chain” phospholipid (e.g., DHPC) or detergent (Triton X-100 or CHAPSO). Isotropic bicelles have $q < 1.5$, although even for small membrane proteins, $q < 0.5$ is required for the protein to give tractable solution NMR spectra. Magnetically aligned bicelles have $q > 2.5$, that are useful for oriented sample (OS) solid-state NMR because the integral membrane protein is immobilized and aligned along with the phospholipids in the bilayers.

Recently, protein-containing nanodiscs have been introduced as a soluble bilayer environment compatible with many biophysical experiments, including solution NMR [218]. A nanodisc is a synthetic model membrane system with a diameter of ~10 nm, consisting of ~150 phospholipids surrounded by a

membrane scaffold protein (MSP) or amphipathic α-helical peptides derived from apolipoprotein A-1 [110]. Integral membrane proteins can be inserted into the bilayer portion of the nanodiscs. Nanodiscs can accommodate a wide variety of saturated or unsaturated phospholipids. Significantly, protein-containing nanodiscs are “detergent-free”, which minimizes the possibility that the membrane environment will cause the distortion or denaturation of the native protein structure.

Because nanodiscs reorient relatively rapidly in aqueous solution, they have received particular attention in the quest for conditions that yield high-resolution solution NMR spectra of membrane proteins in bilayer environments [219-222]. The principal alternatives are detergent micelles and isotropic bicelles. In solution NMR, the line widths and spectral resolution reflect the size and shape of the polypeptide, its oligomeric state, the nature of the detergent/lipid assembly, especially the q value of isotropic bicelles, and the temperature. Most efforts have been aimed at minimizing the apparent size of the protein−lipid complexes in order to decrease the rotational correlation time and obtain spectra with resonances having the narrowest line widths. In general, the line widths of resonances from membrane proteins in nanodiscs are broader than those in micelles or low-q bicelles.

The opportunities presented by increasing the diameter from ∼10 nm

(nanodiscs) to ~30 nm (macrodiscs) are shown in Figure 6.1.

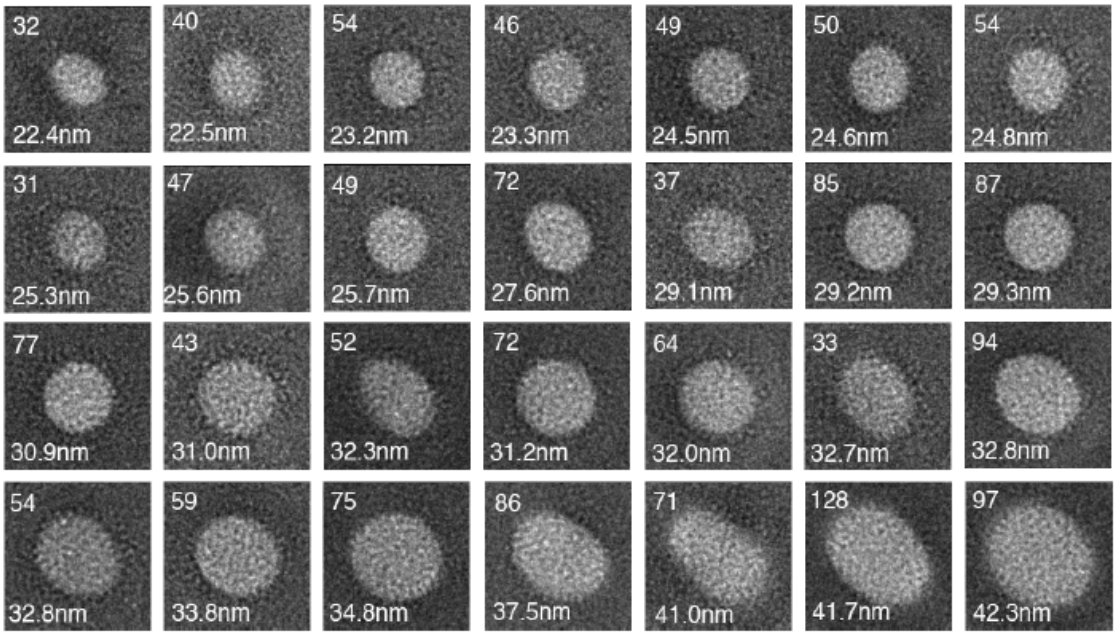

Figure 6.1. Single particle electron microscopy of macrodiscs. The length of the panels is 57.2 nm per side. The molar ratio of DMPC to 14-residue peptide was 13.3. The number of particles (top) and average size (bottom) of macrodiscs are shown in each panel.

The discs consist of long-chain phospholipid bilayers encircled by a 14-residue peptide (Ac-DYLKAFYDKLKEAF-NH2), a truncated analogue of class a A amphipathic α-helical peptide 18A that forms a discoidal bilayer particle when mixed with phospholipids used previously as a model for apolipoprotein A-I [223]. The diameter of the phospholipid bilayer disc can be adjusted by changing the length of the MSP [224] or the molar ratio of the phospholipids and the 14-residue peptide. The increase in diameter alters the behavior of the bilayer discs in aqueous solution. Proteins in nanodiscs undergo isotropic reorientation similar to approximately the same frequency as q = 0.5 isotropic bicelles; in contrast,

protein-containing macrodiscs form magnetically alignable bilayers at temperatures above the gel-to-liquid crystalline transition temperature of the phospholipids (Figure 6.2), similar to the behavior of q > 2.5 bicelles. [225]

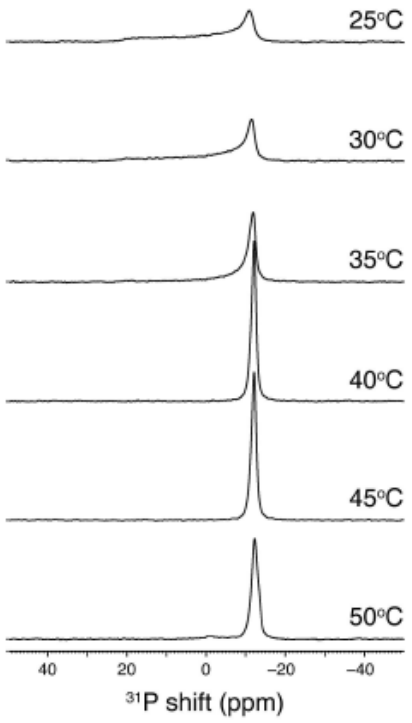

Figure 6.2. One-dimensional solid-state ^{31}P NMR spectra of the membrane protein containing macrodisc at various temperatures recorded at 284 MHz. 64 acquisitions were collected for each spectrum.

In Figure 6.3, single-particle electron microscopy shows that a nanodisc has a diameter of ~10 nm and that a typical macrodisc has a larger diameter of ~30 nm. The difference in diameters has a dramatic effect on their ^{31}P NMR spectra. In the case of nanodiscs, the ^{31}P NMR chemical shift corresponds to the isotropic value of a phosphodiester group. In contrast, macrodiscs have their ^{31}P resonance shifted by ~ 12 ppm. This frequency shift is crucial evidence that the

phospholipids in macrodiscs align with their normals perpendicular to the direction of the magnetic field. Moreover, it is possible to **“** flip**”** the direction of alignment of the macrodisc from perpendicular to parallel by adding lanthanide ions, as previously demonstrated for q > 2.5 bicelles. The narrow line widths in the ^{31}P NMR spectra demonstrate that the phospholipids are arranged homogeneously, and that the macrodiscs are uniformly aligned in the magnetic field. The ^{31}P NMR data indicate that the isotropic reorientation of protein-containing nanodiscs is rapid enough for solution NMR experiments. In contrast, the macrodiscs immobilize and align the proteins along with the phospholipids for OS solid-state NMR experiments. Unoriented macrodiscs can also be used in magic angle spinning (MAS) solid-state NMR experiments [226, 227].

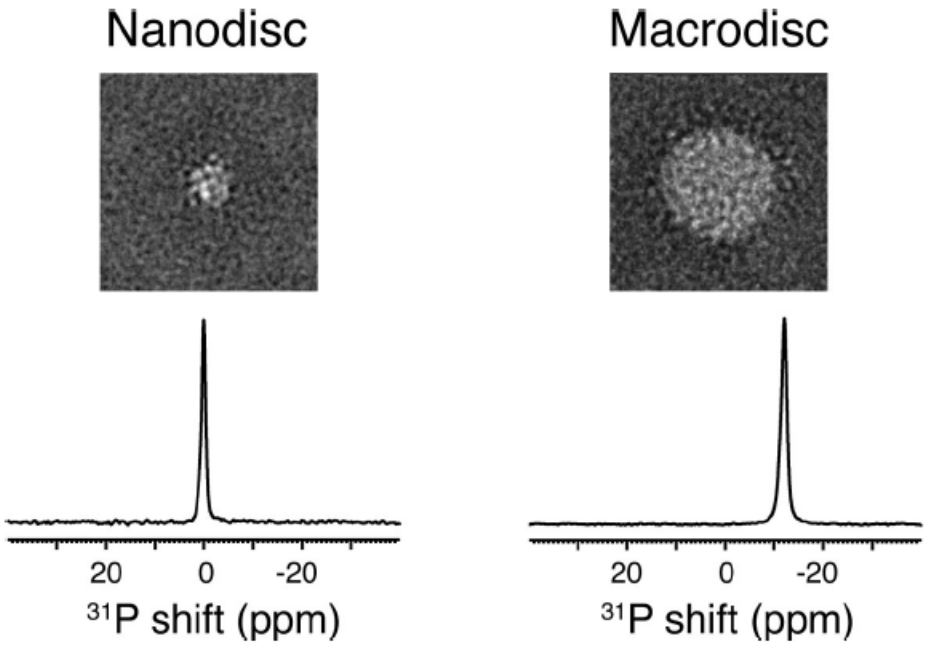

Figure 6.3. Electron micrographs and ^{31}P NMR spectra of nanodiscs and macrodiscs. Representative two-dimensional class average of negatively stained single particle electron micrographs of protein-containing DMPC nanodiscs (left) and macrodiscs (right). Each side of the panel is 57.2 nm. (top). ^{31}P solid-state NMR spectra of protein-containing DMPC nanodiscs (left) and macrodiscs (right) at 40^{o}C. The molar ratios of DMPC to the 14-residue peptide are 1.67 for nanodiscs and 13.3 for macrodiscs.

^{15}N-labeled membrane proteins are compared in Figure 6.4. Micelle samples (q = 0) with high detergent concentrations generally give solution NMR spectra with the best apparent resolution; however, there are now multiple examples where the addition of a small amount of long-chain phospholipid improves the spectral quality. In particular, resonances missing in q = 0 micelle spectra can often be observed in q = 0.1 isotropic bicelle spectra. Both micelles and q = 0.1 bicelles act as effectively spherical assemblies of detergents, and the line widths of the protein resonances are similar; however, they are both

problematic in terms of providing an environment conducive to the membrane protein retaining its native structure and function, especially at the high detergent concentrations and high temperatures required to obtain the best resolved spectra [228]. The membrane proteins compared in Figure 6.4 contain between 46 and 350 residues, and between one and seven transmembrane helices. Therefore, they represent a broad range of the helical membrane proteins found in bacteria, viruses, and humans. The top row of Figure 6.4 contains spectra from the membrane-bound form of Pf1 coat protein, which has 46 residues and one hydrophobic transmembrane helix [203]. The middle row contains spectra of the p7 protein from human hepatitis C virus, which has 63 residues and two transmembrane helices [229]. The bottom row contains spectra of the human chemokine receptor CXCR1, a G-protein-coupled receptor (GPCR), with 350 residues and seven transmembrane helices [140].

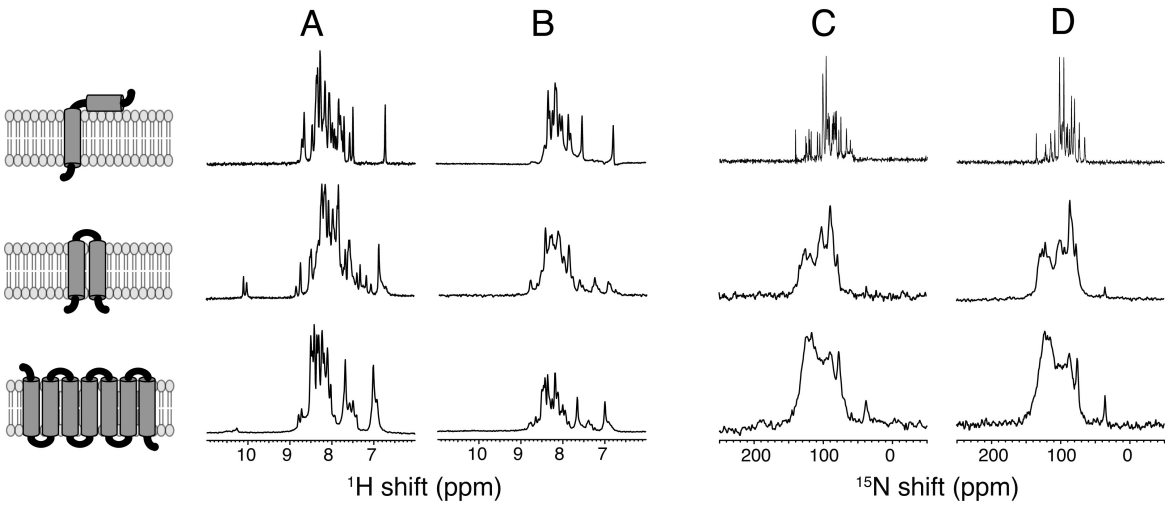

Figure 6.4. NMR spectra of uniformly ^{15}N-labeled membrane proteins in four different membrane-mimic environments: (A) q = 0.1 bicelles, (B) nanodiscs, (C) macrodiscs, and (D) q = 5 bicelles. From top to bottom, the left-most column contains cartoon representations of the membrane proteins with one (Pf1 coat protein), two (p7 protein), and seven (CXCR1) transmembrane helices. (A and B) ^{15}N-edited ^{1}H solution NMR spectra. (C and D) OS solid-state ^{15}N NMR spectra.

For the smaller membrane proteins, signals from all amide sites are observed in the solution NMR spectra (as verified by completely assigned two-dimensional HSQC spectra). However, the resonances from the nanodisc samples are considerably broader than those from the isotropic bicelles samples. In general, protein resonances from nanodisc samples have approximately the same line widths and numbers of observable signals as in q = 0.5 isotropic bicelles (Figure 6.5). While the line widths obtained from the same protein in nanodiscs are broader than those from the same protein in q =0.1 isotropic bicelles, the loss of spectral resolution may be offset by the advantages of working in a detergent-free environment. Nonetheless, it is unlikely that nanodiscs will be the optimal choice for resolution in solution NMR spectra of small

membrane proteins.

The situation for CXCR1 is quite different. The only signals that can be observed in panels A and B of Figure 6.4 are from mobile residues at the termini of the protein [108]. Forty-four signals have been assigned to individual residues. The spectrum in Figure 6.4B is considerably broader and weaker. In any event, GPCRs are unlikely to yield solution NMR spectra with sufficient resolution to be useful in structural studies. We have already shown that no significant improvements result from high levels of deuteration and application of " TROSY-class" pulse sequences to CXCR1 in q = 0.1 isotropic bicelles [108].

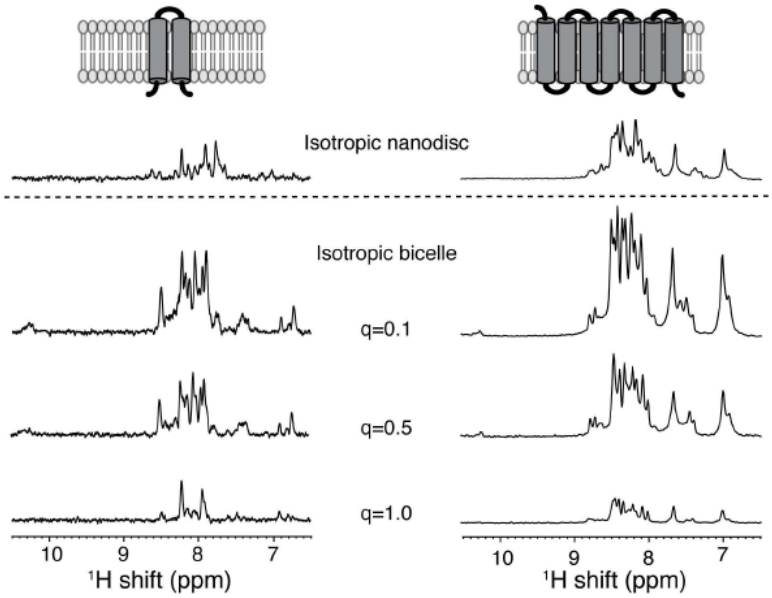

Figure 6.5. Comparison of ^{15}N edited ^{1}H solution NMR spectra of two transmembrane protein MerE (left) and seven transmembrane protein CXCR1 (right) reconstituted into isotropic nanodiscs and isotropic bicelles.

One-dimensional ^{15}N solid-state NMR spectra of the three membrane proteins are compared in macrodiscs (Figure 6.4C) and q = 5 magnetically aligned bilayers (Figure 6.4D). In general, the spectra appear to have slightly better resolution when the protein is immobilized and aligned in DMPC:Triton X-100 q = 5 bicelles [192](Figure 6.4D) than in macrodiscs (Figure 6.4C). However, the macrodiscs have the advantage of being detergent-free; therefore, the samples have the potential to be more stable and less likely to induce distortions or denaturation of the proteins.

An entirely different use of macrodiscs in solution NMR is as an alignment medium to measure residual dipolar couplings (RDCs) of soluble, globular proteins. RDCs are an important source of structural constraints in solution NMR studies. Much like high-q bicelles [230], macrodiscs induce weak alignment in soluble, globular proteins in aqueous solution. As an example, the measurement of $^{1}H-^{15}N$ RDCs for chemokine interleukin- 8 weakly aligned by the presence of macrodiscs in aqueous solution is illustrated in Figure 6.6. Importantly, there is no detectable line broadening or chemical shifts of the resonances caused by the presence of the macrodiscs in the sample.

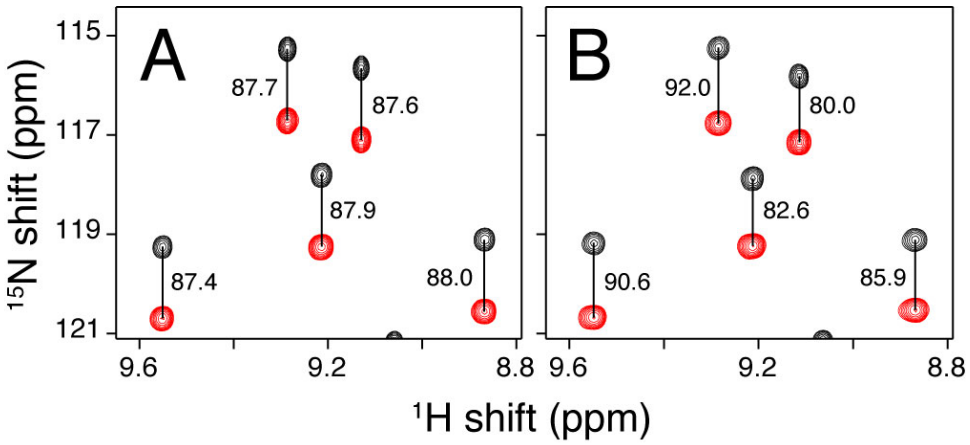

Figure 6.6. Representative region of $^{1}H-^{15}N$ IPAP-HSQC spectra of uniformly ^{15}N-labeled interleukin-8 at 40 °C: (A) isotropic in aqueous solution and (B) weakly aligned in aqueous solution by the addition of macrodiscs at a final DMPC concentration of 10% (w/v). The measured values of one-bond $^{1}H-^{15}N$ splitting are marked in Hertz.

The diameter of bilayer discs encircled by the 14-residue peptides derived from apolipoprotein A-1 can be varied by at least 3-fold by changing the lipid:peptide molar ratio. Nanodiscs and macrodiscs provide complementary lipid environments for NMR and other physical and functional studies of membrane proteins. The NMR spectra in the figures demonstrate that nanodiscs with an ~ 10 nm diameter and macrodiscs with an ~ 30 nm diameter bridge between solution NMR spectroscopy and OS solid-state NMR spectroscopy. Although nanodiscs do not compete well with micelles and low q isotropic bicelles for optimal resolution in solution NMR spectra, the resolution that can be attained with macrodiscs is similar to that of the best high-q bicelles in OS solid-state NMR spectra. Both nanodiscs and macrodiscs have the advantage of providing a detergent-free bilayer environment that reduces the likelihood of distorting or denaturing the protein structures. Finally, macrodiscs provide an alignment

medium for soluble, globular proteins, allowing the measurement of RDCs. Thus, macrodiscs have the potential to play several complementary roles in NMR studies of membrane proteins.

Chapter 6, in full, is a reprint of the material as it appears in Biochemistry, (2011), 50, 8983–8985. Park, S.H., Berkamp, S., Cook, G. A., Chan, M. K., Viadiu, H. and Opella, S. J. The dissertation author was the secondary author of this paper.

CHAPTER 7: CONCLUSIONS

During an infection or inflammation macrophages and other immune cells secrete Interleukin-8 (IL-8), which then diffuses away and forms a chemotactic gradient. On the surface of neutrophils, mast cells, and NK cells, several proteins are expressed, including the G Protein-Coupled Receptors (GPCR) CXCR1 and CXCR2. When IL-8 binds these chemokine receptors several intracellular signaling cascades are set in motion through the heterotrimeric G Proteins that interact with the intracellular segments of CXCR1 and CXCR2. These signaling pathways cause the cell to leave the blood stream, travel up the IL-8 gradient and combat the infection by degranulation. The exact molecular mechanism behind this process is not well understood. Both the structure of IL-8 and the structure of CXCR1 have been solved, but exactly how these two proteins interact, what kind of conformational change they undergo upon activation and how this activation signal is passed to the other side of the membrane to the G Proteins is not well understood. It is known that IL-8 has two main interaction sites on the receptor: Binding Site-I is located on the flexible, N-terminal domain of CXCR1 and Binding Site-II is located on the second and third extracellular loops. Binding Site-I is thought to be involved in the initial recognition of the chemokine and is a high affinity site. Binding Site-II is thought to be related to receptor activation and is lower affinity. We have performed several solution NMR, oriented sample solid-state NMR, and MAS solid-state NMR studies to try to better understand this interaction between IL-8 and CXCR1.

We have solved the solution NMR structure of a monomeric version of IL-8 composed of the first 66 residues out of the 72-residue wildtype protein. The structure of this monomeric form did not deviate much from that of the wildtype dimeric protein; only the location of the N-loop was slightly different. Next, we mapped the interaction between IL-8 and ND-CXCR1(1-38) and 1TM-CXCR1(1-72). ND-CXCR1(1-38) is a soluble peptide composed of the entire N-terminal domain of CXCR1, which forms Binding Site-I. 1TM-CXCR1(1-72) is a construct that has the N-terminal domain, the first transmembrane helix and the first intracellular loop of CXCR1. Chemical shift perturbations were recorded using samples of labeled IL-8 and different molar ratios of unlabeled ND-CXCR1(1-38) or unlabeled 1TM-CXCR(1-72) reconstituted in nanodiscs. Three main interaction regions in IL-8 were identified: the N-loop region, the third β-strand and the α-helix. No difference was found in how IL-8 interacts with ND-CXCR1(1-38) and 1TM-CXCR(1-72), indicating that the presence of the transmembrane helix and membrane does not matter.

We also studied the interaction between IL-8 and Binding Site-II using proton detected, fast MAS, solid-state NMR. To this end two constructs were used: NT-CXCR1 and wildtype CXCR1, both reconstituted in DMPC liposomes. NT-CXCR1 is a construct that lacks the flexible N-terminal domain that makes up Binding Site-I, and only has Binding Site-II. Upon interaction with NT-CXCR1 only

about 11 residues in IL-8 were immobilized and could be studied using CP-based experiments. Most residues could be detected using INEPT, indicating that they undergo fast motion. When IL-8 was bound to full-length CXCR1 we found that almost all residues were visible in the CP-spectrum, so almost the entire protein is immobilized upon interaction with both binding sites. Interestingly, IL-8 does not undergo a large conformational change upon binding CXCR1.

Magic Angle Spinning (MAS) solid-state NMR was used to study the location of the IL-8 binding site on 1TM-CXCR1(1-72) and study changes in dynamics upon binding IL-8. All the residues in 1TM-CXCR1(1-72) in the presence and in the absence of IL-8 were assigned. The first 23 residues in the apo-receptor were mobile and were assigned using INEPT and TOBSY experiments, whereas residues 24-72 were immobile and could be assigned using standard CP-based experiments. Upon binding IL-8, chemical shift perturbations were mapped, all localized to the first 38 residues that make up the entire N-terminal domain. Large changes in receptor dynamics were also found: upon interaction with IL-8, only a few residues in the N-terminal domain remained mobile enough to be detected using INEPT and TOBSY and some additional resonances appeared in CP-based spectra. Interestingly, no change in tilt angle of the transmembrane helix was observed.

Oriented sample, solid-state NMR was used to determine the orientation of IL-8 upon interaction with CXCR1. Samples were made using labeled IL-8 and unlabeled CXCR1 reconstituted in uniaxially aligned q=5 triton bicelles. We found that IL-8 was fully immobilized and aligned on the receptor. Orientation dependent parameters such as the anisotropic chemical shift and dipolar couplings were measured. Experimental spectra were compared to simulated spectra of IL-8 in different orientations. In the orientation that matched the experimental data best, the β-sheet core of the protein points down toward the bilayer.

A new membrane mimetic was developed based on the nanodisc system. In traditional nanodiscs the hydrophobic acyl chains of the long-chain lipid are shielded from the aqueous environment by a membrane scaffold protein. The size of the nanodisc is determined by the length of the scaffold protein. We developed the so-called macrodisc by shortening the membrane scaffold protein to a 14 residue peptide. By varying the peptide to lipid ratio different sizes of discs can be made. These large macrodiscs were found to align in a magnetic field, making them a detergent-free alternative to aligned bicelles in oriented sample, solid-state NMR.

Bibliography

[1] M. Caffrey, V. Cherezov, Crystallizing membrane proteins using lipidic mesophases, Nature Protocols, 4 (2009).

[2] C.R. Sanders, C.L. Landis, Reconstitution of membrane proteins into lipid-rich bilayered mixed micelles for NMR studies, Biochemistry, (1995).

[3] F. Hagn, M. Etzkorn, T. Raschle, G. Wagner, Optimized phospholipid bilayer nanodiscs facilitate high-resolution structure determination of membrane proteins, Journal of the American Chemical Society, 135 (2013) 1919-1925.

[4] C. Tribet, R. Audebert, J.-L. Popot, Amphipols: Polymers that keep membrane proteins soluble in aqueous solutions, Proceedings of the National Academy of Sciences, 93 (1996) 15047-15050.

[5] T.J. Knowles, R. Finka, C. Smith, Y.-P. Lin, T. Dafforn, M. Overduin, Membrane Proteins Solubilized Intact in Lipid Containing Nanoparticles Bounded by Styrene Maleic Acid Copolymer, Journal of the American Chemical Society, 131 (2009) 7484-7485.

[6] H.-X. Zhou, T.A. Cross, Influences of Membrane Mimetic Environments on Membrane Protein Structures, Annual Review of Biophysics, 42 (2013) 361-392.

[7] D.S. Wishart, B.D. Sykes, R.-F.M. Biochemistry, The chemical shift index: a fast and simple method for the assignment of protein secondary structure through NMR spectroscopy, Biochemistry, (1992).

[8] H.-J. Sass, G. Musco, S.J. Stahl, P.T. Wingfield, S. Grzesiek, Solution NMR of proteins within polyacrylamide gels: Diffusional properties and residual alignment by mechanical stress or embedding of oriented purple membranes, Journal of Biomolecular NMR, 18 (2000) 303-309.

[9] S.H. Park, W.S. Son, R. Mukhopadhyay, H. Valafar, S.J. Opella, Phage-induced alignment of membrane proteins enables the measurement and

structural analysis of residual dipolar couplings with dipolar waves and lambda-maps, Journal of the American Chemical Society, 131 (2009) 14140-14141.

[10] S. Gaemers, A. Bax, Morphology of Three Lyotropic Liquid Crystalline Biological NMR Media Studied by Translational Diffusion Anisotropy, Journal of the American Chemical Society, 123 (2001) 12343-12352.

[11] S.M. Douglas, J.J. Chou, W.M. Shih, DNA-nanotube-induced alignment of membrane proteins for NMR structure determination, Proceedings of the National Academy of Sciences, 104 (2007) 6644-6648.

[12] P. Güntert, Automated structure determination from NMR spectra, European biophysics journal : EBJ, 38 (2009) 129-143.

[13] B.B. Das, H.J. Nothnagel, G.J. Lu, W.S. Son, Y. Tian, F.M. Marassi, S.J. Opella, Structure determination of a membrane protein in proteoliposomes, Journal of the American Chemical Society, 134 (2012) 2047-2056.

[14] S.J. Opella, J.S. Waugh, Two-dimensional 13C NMR of highly oriented polyethylene, The Journal of Chemical Physics, 66 (1977).

[15] C.H. Wu, A. Ramamoorthy, S.J. Opella, High-resolution heteronuclear dipolar solid-state NMR spectroscopy, High-resolution heteronuclear dipolar solid-state NMR spectroscopy, (1994).

[16] A.A. Nevzorov, S.J. Opella, A “Magic Sandwich” pulse sequence with reduced offset dependence for high-resolution separated local field spectroscopy, Journal of Magnetic Resonance, 164 (2003) 182186.

[17] A.A. Nevzorov, S.J. Opella, Selective averaging for high-resolution solid-state NMR spectroscopy of aligned samples, J Magn Reson, 185 (2007) 59-70.

[18] F.M. Marassi, S.J. Opella, A solid-state NMR index of helical membrane protein structure and topology, Journal of magnetic resonance (San Diego, Calif. : 1997), 144 (2000) 150-155.

[19] W. Tang, R.W. Knox, A.A. Nevzorov, A spectroscopic assignment technique for membrane proteins reconstituted in magnetically aligned bicelles, J Biomol NMR, 54 (2012) 307-316.

[20] G.J. Lu, W.S. Son, S.J. Opella, A general assignment method for oriented sample (OS) solid-state NMR of proteins based on the correlation of resonances through heteronuclear dipolar couplings in samples aligned parallel and perpendicular to the magnetic field, Journal of magnetic resonance (San Diego, Calif. : 1997), 209 (2011) 195-206.

[21] S.P. Alexander, A.P. Davenport, E. Kelly, N. Marrion, J.A. Peters, H.E. Benson, E. Faccenda, A.J. Pawson, J.L. Sharman, C. Southan, J.A. Davies, C. Collaborators, The Concise Guide to PHARMACOLOGY 2015/16: G protein-coupled receptors, Br J Pharmacol, 172 (2015) 5744-5869.

[22] M.N. Devalaraja, A. Richmond, Multiple chemotactic factors: fine control or redundancy?, Trends Pharmacol Sci, 20 (1999) 151-156.

[23] A. Mantovani, The chemokine system: redundancy for robust outputs, Immunology today, 20 (1999) 254-257.

[24] I.V. Nesmelova, Y. Sham, A.Z. Dudek, L.I. van Eijk, G. Wu, A. Slungaard, F. Mortari, A.W. Griffioen, K.H. Mayo, Platelet factor 4 and interleukin-8 CXC chemokine heterodimer formation modulates function at the quaternary structural level, The Journal of biological chemistry, 280 (2005) 4948-4958.

[25] J. Carlson, S.A. Baxter, D. Dreau, I.V. Nesmelova, The heterodimerization of platelet-derived chemokines, Biochim Biophys Acta, 1834 (2013) 158-168.

[26] A. Levoye, K. Balabanian, F. Baleux, F. Bachelerie, B. Lagane, CXCR7 heterodimerizes with CXCR4 and regulates CXCL12-mediated G protein signaling, Blood, 113 (2009) 6085-6093.

[27] F.M. Decaillot, M.A. Kazmi, Y. Lin, S. Ray-Saha, T.P. Sakmar, P. Sachdev, CXCR7/CXCR4 heterodimer constitutively recruits beta-arrestin to enhance cell migration, J Biol Chem, 286 (2011) 32188-32197.

[28] M. Mellado, J.M. Rodriguez-Frade, A.J. Vila-Coro, S. Fernandez, A. Martin de Ana, D.R. Jones, J.L. Toran, A.C. Martinez, Chemokine receptor homo- or heterodimerization activates distinct signaling pathways, EMBO J, 20 (2001) 2497-2507.

[29] X. Han, Y. Feng, X. Chen, C. Gerard, W.A. Boisvert, Characterization of G protein coupling mediated by the conserved D1343.49 of DRY motif, M2416.34, and F2516.44 residues on human CXCR1, FEBS Open Bio, 5 (2015).

[30] X. Han, S.D. Tachado, H. Koziel, W.A. Boisvert, Leu128(3.43) (I128) and Val247(6.40) (V247) of CXCR1 are critical amino acid residues for g protein coupling and receptor activation, PloS one, 7 (2012).

[31] E.F. Barter, M.J. Stone, Synergistic interactions between chemokine receptor elements in recognition of interleukin-8 by soluble receptor mimics, Biochemistry, 51 (2012) 1322-1331.

[32] J.A. Katancik, A. Sharma, E. de Nardin, Interleukin 8, neutrophil-activating peptide-2 and GRO-alpha bind to and elicit cell activation via specific and different amino acid residues of CXCR2, Cytokine, 12 (2000) 1480-1488.

[33] C.T. Veldkamp, C. Seibert, F.C. Peterson, N.B. De la Cruz, J.C. Haugner, 3rd, H. Basnet, T.P. Sakmar, B.F. Volkman, Structural basis of CXCR4 sulfotyrosine recognition by the chemokine SDF-1/CXCL12, Sci Signal, 1 (2008) ra4.

[34] Y. Kofuku, C. Yoshiura, T. Ueda, H. Terasawa, T. Hirai, S. Tominaga, M. Hirose, Y. Maeda, H. Takahashi, Y. Terashima, K. Matsushima, I. Shimada, Structural basis of the interaction between chemokine stromal cell-derived factor-1/CXCL12 and its G-protein-coupled receptor CXCR4, The Journal of biological chemistry, 284 (2009) 35240-35250.

[35] J. Ye, L.L. Kohli, M.J. Stone, Characterization of binding between the chemokine eotaxin and peptides derived from the chemokine receptor CCR3, J Biol Chem, 275 (2000) 27250-27257.

[36] C. Blanpain, B.J. Doranz, A. Bondue, C. Govaerts, The core domain of chemokines binds CCR5 extracellular domains while their amino terminus

interacts with the transmembrane helix bundle, Journal of Biological …, 278 (2003) 5179-5187.

[37] M. Baggiolini, Chemokines and leukocyte traffic, Nature, 392 (1998) 565-568.

[38] S. Zaja-Milatovic, A. Richmond, CXC chemokines and their receptors: a case for a significant biological role in cutaneous wound healing, Histology and histopathology, 23 (2008) 1399-1407.

[39] K. Rajarathnam, B.D. Sykes, C.M. Kay, B. Dewald, T. Geiser, M. Baggiolini, I. Clark-Lewis, Neutrophil activation by monomeric interleukin-8, Science (New York, N.Y.), 264 (1994) 90-92.

[40] M. Rosenkilde Mette, W. Schwartz Thue, The chemokine system – a major regulator of angiogenesis in health and disease, APMIS, 112 (2004) 481-495.

[41] P. Panina, M. Mariani, D. Dambrosio, Chemokine receptors in chronic obstructive pulmonary disease (COPD), Current drug targets, (2006).

[42] D.J. Waugh, C. Wilson, The interleukin-8 pathway in cancer, Clin Cancer Res, 14 (2008) 6735-6741.

[43] P.M. Murphy, M. Baggiolini, I.F. Charo, C.A. Hébert, R. Horuk, K. Matsushima, L.H. Miller, J.J. Oppenheim, C.A. Power, International union of pharmacology. XXII. Nomenclature for chemokine receptors, Pharmacological reviews, 52 (2000) 145-176.

[44] P.M. Murphy, H.L. Tiffany, Cloning of complementary DNA encoding a functional human interleukin-8 receptor, Science, 253 (1991) 1280-1283.

[45] E.T. Baldwin, I.T. Weber, R. St Charles, J.C. Xuan, E. Appella, M. Yamada, K. Matsushima, B.F. Edwards, G.M. Clore, A.M. Gronenborn, Crystal structure of interleukin 8: symbiosis of NMR and crystallography, Proceedings of the National Academy of Sciences of the United States of America, 88 (1991) 502-506.

[46] G.M. Clore, E. Appella, M. Yamada, K. Matsushima, A.M. Gronenborn, Determination of the secondary structure of interleukin-8 by nuclear magnetic

resonance spectroscopy, The Journal of biological chemistry, 264 (1989) 18907-18911.

[47] G.M. Clore, E. Appella, M. Yamada, K. Matsushima, A.M. Gronenborn, Three-dimensional structure of interleukin 8 in solution, Biochemistry, 29 (1990) 1689-1696.

[48] C. Eigenbrot, H.B. Lowman, L. Chee, D.R. Artis, Structural change and receptor binding in a chemokine mutant with a rearranged disulfide: X-ray structure of e38C/C50A IL-8 at 2 Å resolution, Proteins: Structure, Function, and Genetics, 27 (1997).

[49] N. Gerber, H. Lowman, D.R. Artis, C. Eigenbrot, Receptor-binding conformation of the "ELR" motif of IL-8: X-ray structure of the L5C/H33C variant at 2.35 A resolution, Proteins, 38 (2000) 361-367.

[50] K. Rajarathnam, I. Clark-Lewis, B.D. Sykes, 1H NMR solution structure of an active monomeric interleukin-8, Biochemistry, 34 (1995) 12983-12990.

[51] S.D. Burrows, M.L. Doyle, K.P. Murphy, S.G. Franklin, J.R. White, I. Brooks, D.E. McNulty, M.O. Scott, J.R. Knutson, D. Porter, Determination of the monomer-dimer equilibrium of interleukin-8 reveals it is a monomer at physiological concentrations, Biochemistry, 33 (1994) 12741-12745.

[52] B. Goger, Y. Halden, A. Rek, R. Mösl, D. Pye, J. Gallagher, A.J. Kungl, Different Affinities of Glycosaminoglycan Oligosaccharides for Monomeric and Dimeric Interleukin-8: A Model for Chemokine Regulation at Inflammatory Sites†, Biochemistry, 41 (2002) 16401646.

[53] S. Das, L. Rajagopalan, A. Guerrero-Plata, J. Sai, A. Richmond, R.P. Garofalo, K. Rajarathnam, Monomeric and dimeric CXCL8 are both essential for in vivo neutrophil recruitment, PLoS One, 5 (2010).

[54] P.R. Joseph, P.D. Mosier, U.R. Desai, K. Rajarathnam, Solution NMR characterization of chemokine CXCL8/IL-8 monomer and dimer binding to glycosaminoglycans: structural plasticity mediates differential binding interactions, The Biochemical journal, 472 (2015) 121-133.

[55] H. Fernando, C. Chin, J. Rösgen, K. Rajarathnam, Dimer dissociation is essential for interleukin-8 (IL-8) binding to CXCR1 receptor, The Journal of biological chemistry, 279 (2004) 36175-36178.

[56] K. Rajarathnam, G.N. Prado, H. Fernando, I. Clark-Lewis, J. Navarro, Probing receptor binding activity of interleukin-8 dimer using a disulfide trap, Biochemistry, 45 (2006) 7882-7888.

[57] A. Ravindran, P.R. Joseph, K. Rajarathnam, Structural basis for differential binding of the interleukin-8 monomer and dimer to the CXCR1 N-domain: role of coupled interactions and dynamics, Biochemistry, 48 (2009) 8795-8805.

[58] A.S. Hauser, S. Chavali, I. Masuho, L.J. Jahn, K.A. Martemyanov, D.E. Gloriam, M.M. Babu, Pharmacogenomics of GPCR Drug Targets, Cell, 172 (2018) 41-54.e19.

[59] J.R. Hepler, A.G. Gilman, G proteins, Trends in biochemical sciences, 17 (1992) 383-387.

[60] W.M. Oldham, H.E. Hamm, Heterotrimeric G protein activation by G-protein-coupled receptors, Nature Reviews Molecular Cell Biology, 9 (2008) 60-71.

[61] K.M. Druey, Advances in Immunology, Advances in Immunology, 136 (2017) 315-351.

[62] M.M. Ahmadzai, D. Broadbent, C. Occhiuto, C. Yang, R. Das, H. Subramanian, Canonical and Noncanonical Signaling Roles of beta-Arrestins in Inflammation and Immunity, Adv Immunol, 136 (2017) 279-313.

[63] B. Holst, R. Nygaard, L. Valentin-Hansen, A. Bach, M.S. Engelstoft, P.S. Petersen, T.M. Frimurer, T.W. Schwartz, A Conserved Aromatic Lock for the Tryptophan Rotameric Switch in TM-VI of Seven-transmembrane Receptors, Journal of Biological Chemistry, 285 (2010) 3973-3985.

[64] R. Liu, D. Nahon, B. Roy, E.B. Lenselink, A.P. Ijzerman, Scanning mutagenesis in a yeast system delineates the role of the NPxxY (x) 5, 6 F motif

and helix 8 of the adenosine A 2B receptor in G protein coupling, Biochemical pharmacology, (2015).

[65] A. Ravindran, K.V. Sawant, J. Sarmiento, J. Navarro, K. Rajarathnam, Chemokine CXCL1 Dimer Is a Potent Agonist for the CXCR2 Receptor, Journal of Biological Chemistry, 288 (2013) 1224412252.

[66] D. Rajasekaran, C. Keeler, M.A. Syed, M.C. Jones, J.K. Harrison, D. Wu, V. Bhandari, M.E. Hodsdon, E.J. Lolis, A Model of GAG/MIP-2/CXCR2 Interfaces and Its Functional Effects, Biochemistry, 51 (2012) 5642-5654.

[67] S.K. Ahuja, P.M. Murphy, The CXC chemokines growth-regulated oncogene (GRO) alpha, GRObeta, GROgamma, neutrophil-activating peptide-2, and epithelial cell-derived neutrophil-activating peptide-78 are potent agonists for the type B, but not the type A, human interleukin-8 receptor, The Journal of biological chemistry, 271 (1996) 20545-20550.

[68] S.A. Jones, M. Wolf, S. Qin, C.R. Mackay, M. Baggiolini, Different functions for the interleukin 8 receptors (IL-8R) of human neutrophil leukocytes: NADPH oxidase and phospholipase D are activated through IL-8R1 but not IL-8R2, Proceedings of the National Academy of Sciences, 93 (1996) 6682-6686.

[69] R.M. Richardson, R.A. DuBose, H. Ali, E.D. Tomhave, B. Haribabu, R. Snyderman, Regulation of human interleukin-8 receptor A: identification of a phosphorylation site involved in modulating receptor functions, Biochemistry, 34 (1995) 14193-14201.

[70] S.K. Raghuwanshi, Y. Su, V. Singh, K. Haynes, A. Richmond, R.M. Richardson, The chemokine receptors CXCR1 and CXCR2 couple to distinct G protein-coupled receptor kinases to mediate and regulate leukocyte functions, Journal of immunology (Baltimore, Md. : 1950), 189 (2012) 2824-2832.

[71] M.W. Nasser, S.K. Raghuwanshi, K.M. Malloy, P. Gangavarapu, J.-Y.Y. Shim, K. Rajarathnam, R.M. Richardson, CXCR1 and CXCR2 activation and regulation. Role of aspartate 199 of the second extracellular loop of CXCR2 in CXCL8-mediated rapid receptor internalization, The Journal of biological chemistry, 282 (2007) 6906-6915.

[72] S.H. Park, B.B. Das, F. Casagrande, Y. Tian, H.J. Nothnagel, M. Chu, H. Kiefer, K. Maier, A.A. De Angelis, F.M. Marassi, S.J. Opella, Structure of the chemokine receptor CXCR1 in phospholipid bilayers, Nature, 491 (2012) 779-783.

[73] S.H. Park, B.B. Das, A.A. De Angelis, M. Scrima, S.J. Opella, Mechanically, magnetically, and "rotationally aligned" membrane proteins in phospholipid bilayers give equivalent angular constraints for NMR structure determination, The journal of physical chemistry. B, 114 (2010) 13995-14003.

[74] B. Wu, E.Y. Chien, C.D. Mol, G. Fenalti, W. Liu, V. Katritch, R. Abagyan, A. Brooun, P. Wells, F.C. Bi, D.J. Hamel, P. Kuhn, T.M. Handel, V. Cherezov, R.C. Stevens, Structures of the CXCR4 chemokine GPCR with small-molecule and cyclic peptide antagonists, Science, 330 (2010) 1066-1071.

[75] G.J. LaRosa, J. Navarro, Amino terminus of the interleukin-8 receptor is a major determinant of receptor subtype specificity, J Biol Chem, (1992).

[76] R.B. Gayle, P.R. Sleath, S. Srinivason, C.W. Birks, K.S. Weerawarna, D.P. Cerretti, C.J. Kozlosky, N. Nelson, V.T. Bos, M.P. Beckmann, Importance of the amino terminus of the interleukin-8 receptor in ligand interactions, The Journal of biological chemistry, 268 (1993) 7283-7289.

[77] G.N. Prado, K. Suetomi, D. Shumate, C. Maxwell, A. Ravindran, K. Rajarathnam, J. Navarro, Chemokine Signaling Specificity: Essential Role for the N-Terminal Domain of Chemokine Receptors, Biochemistry, 46 (2007) 8961-8968.

[78] K. Suetomi, D. Rojo, J. Navarro, Identification of a signal transduction switch in the chemokine receptor CXCR1, J Biol Chem, 277 (2002) 31563-31566.

[79] L. Bendall, Chemokines and their receptors in disease, Histology and Histopathology, 20 (2005) 907-926.

[80] C. Bizzarri, A.R. Beccari, R. Bertini, M.R. Cavicchia, S. Giorgini, M. Allegretti, ELR+ CXC chemokines and their receptors (CXC chemokine receptor 1 and CXC chemokine receptor 2) as new therapeutic targets, Pharmacol Ther, 112 (2006) 139-149.

[81] M. Baggiolini, CXCL8-the first chemokine, Front Immunol, 6 (2015).

[82] P.R. Joseph, K.M. Poluri, P. Gangavarapu, L. Rajagopalan, S. Raghuwanshi, R.M. Richardson, R.P. Garofalo, K. Rajarathnam, Proline substitution of dimer interface β-strand residues as a strategy for the design of functional monomeric proteins, Biophysical journal, 105 (2013) 1491-1501.

[83] H.B. Lowman, W.J. Fairbrother, P.H. Slagle, R. Kabakoff, J. Liu, S. Shire, C.A. Hebert, Monomeric variants of IL-8: effects of side chain substitutions and solution conditions upon dimer formation, Protein Sci, 6 (1997) 598-608.

[84] I. Clark-Lewis, C. Schumacher, M. Baggiolini, B. Moser, Structure-activity relationships of interleukin-8 determined using chemically synthesized analogs. Critical role of NH2-terminal residues and evidence for uncoupling of neutrophil chemotaxis, exocytosis, and receptor binding activities, The Journal of biological chemistry, 266 (1991) 23128-23134.

[85] K. Rajarathnam, C.M. Kay, I. Clark-Lewis, B.D. Sykes, Characterization of quaternary structure of interleukin-8 and functional implications, in: Methods in Enzymology, Academic Press, 1997, pp. 89-105.

[86] W.E. Holmes, J. Lee, W.J. Kuang, G.C. Rice, W.I. Wood, Structure and functional expression of a human interleukin-8 receptor, Science (New York, N.Y.), 253 (1991) 1278-1280.

[87] L. Qin, I. Kufareva, L.G. Holden, C. Wang, Y. Zheng, C. Zhao, G. Fenalti, H. Wu, G.W. Han, V. Cherezov, R. Abagyan, R.C. Stevens, T.M. Handel, Structural biology. Crystal structure of the chemokine receptor CXCR4 in complex with a viral chemokine, Science (New York, N.Y.), 347 (2015) 1117-1122.

[88] Y. Zheng, L. Qin, N.V. Zacarias, H. de Vries, G.W. Han, M. Gustavsson, M. Dabros, C. Zhao, R.J. Cherney, P. Carter, D. Stamos, R. Abagyan, V. Cherezov, R.C. Stevens, I.J. AP, L.H. Heitman, A. Tebben, I. Kufareva, T.M. Handel, Structure of CC chemokine receptor 2 with orthosteric and allosteric antagonists, Nature, 540 (2016) 458-461.

[89] C. Oswald, M. Rappas, J. Kean, A.S. Dore, J.C. Errey, K. Bennett, F. Deflorian, J.A. Christopher, A. Jazayeri, J.S. Mason, M. Congreve, R.M. Cooke,

F.H. Marshall, Intracellular allosteric antagonism of the CCR9 receptor, Nature, 540 (2016) 462-465.

[90] Q. Tan, Y. Zhu, J. Li, Z. Chen, G.W. Han, I. Kufareva, T. Li, L. Ma, G. Fenalti, J. Li, W. Zhang, X. Xie, H. Yang, H. Jiang, V. Cherezov, H. Liu, R.C. Stevens, Q. Zhao, B. Wu, Structure of the CCR5 chemokine receptor-HIV entry inhibitor maraviroc complex, Science (New York, N.Y.), 341 (2013) 1387-1390.

[91] J.S. Burg, J.R. Ingram, A.J. Venkatakrishnan, K.M. Jude, A. Dukkipati, E.N. Feinberg, A. Angelini, D. Waghray, R.O. Dror, H.L. Ploegh, C.K. Garcia, Structural basis for chemokine recognition and activation of a viral G protein–coupled receptor, Science, 347 (2015) 1113-1117.

[92] C.A. Hébert, A. Chuntharapai, M. Smith, T. Colby, J. Kim, R. Horuk, Partial functional mapping of the human interleukin-8 type A receptor. Identification of a major ligand binding domain, The Journal of biological chemistry, 268 (1993) 18549-18553.

[93] S.R. Leong, R.C. Kabakoff, C.A. Hébert, Complete mutagenesis of the extracellular domain of interleukin-8 (IL-8) type A receptor identifies charged residues mediating IL-8 binding and signal transduction, The Journal of biological chemistry, 269 (1994) 19343-19348.

[94] D. Helmer, I. Rink, J.A.R. Dalton, K. Brahm, M. Jost, T.M. Nargang, W. Blum, P. Wadhwani, G. Brenner-Weiss, B.E. Rapp, J. Giraldo, K. Schmitz, Rational design of a peptide capture agent for CXCL8 based on a model of the CXCL8:CXCR1 complex, Rsc Adv, 5 (2015) 25657-25668.

[95] H. Fernando, G.T. Nagle, K. Rajarathnam, Thermodynamic characterization of interleukin-8 monomer binding to CXCR1 receptor N-terminal domain, The FEBS journal, 274 (2007) 241-251.

[96] N.J. Skelton, C. Quan, D. Reilly, H. Lowman, Structure of a CXC chemokine-receptor fragment in complex with interleukin-8, Structure (London, England : 1993), 7 (1999) 157-168.

[97] S.H. Park, F. Casagrande, L. Cho, L. Albrecht, S.J. Opella, Interactions of interleukin-8 with the human chemokine receptor CXCR1 in phospholipid bilayers by NMR spectroscopy, J Mol Biol, 414 (2011) 194-203.

[98] S. Haldar, H. Raghuraman, T. Namani, K. Rajarathnam, A. Chattopadhyay, Membrane interaction of the N-terminal domain of chemokine receptor CXCR1, Biochimica et biophysica acta, 1798 (2010) 1056-1061.

[99] C.A. Hebert, R.V. Vitangcol, J.B. Baker, Scanning mutagenesis of interleukin-8 identifies a cluster of residues required for receptor binding, J Biol Chem, 266 (1991) 18989-18994.

[100] S.H. Park, S. Berkamp, J. Radoicic, A.A. De Angelis, S.J. Opella, Interaction of Monomeric Interleukin-8 with CXCR1 Mapped by Proton-detected Fast MAS Solid-state NMR and Intermolecular Paramagnetic Relaxation Enhancement, SUBMITTED, (2017).

[101] G. Williams, N. Borkakoti, G.A. Bottomley, I. Cowan, A.G. Fallowfield, P.S. Jones, S.J. Kirtland, G.J. Price, L. Price, Mutagenesis studies of interleukin-8. Identification of a second epitope involved in receptor binding, J Biol Chem, 271 (1996) 9579-9586.

[102] A.A. Kendrick, M.J. Holliday, N.G. Isern, F. Zhang, C. Camilloni, C. Huynh, M. Vendruscolo, G. Armstrong, E.Z. Eisenmesser, The dynamics of interleukin-8 and its interaction with human CXC receptor I peptide, Protein Sci, 23 (2014) 464-480.

[103] R.T. Clubb, J.G. Omichinski, G.M. Clore, A.M. Gronenborn, Mapping the binding surface of interleukin-8 complexed with an N-terminal fragment of the Type 1 human interleukin-8 receptor, FEBS Letters, 338 (1994) 93-97.

[104] M.E. Hammond, V. Shyamala, M.A. Siani, C.A. Gallegos, P.H. Feucht, J. Abbott, G.R. Lapointe, M. Moghadam, H. Khoja, J. Zakel, P. Tekamp-Olson, Receptor recognition and specificity of interleukin-8 is determined by residues that cluster near a surface-accessible hydrophobic pocket, The Journal of biological chemistry, 271 (1996) 8228-8235.

[105] I. Kufareva, M. Gustavsson, Y. Zheng, B.S. Stephens, T.M. Handel, What Do Structures Tell Us About Chemokine Receptor Function and Antagonism?, Annu Rev Biophys, 46 (2017) 175-198.

[106] L. Rajagopalan, K. Rajarathnam, Ligand selectivity and affinity of chemokine receptor CXCR1. Role of N-terminal domain, J Biol Chem, 279 (2004) 30000-30008.

[107] F. Casagrande, K. Maier, H. Kiefer, S.J. Opella, S.H. Park, Expression and purification of G-protein coupled receptors for NMR structural studies, Production of membrane proteins. Wiley-vch; Weinheim, (2011).

[108] S.H. Park, F. Casagrande, B.B. Das, L. Albrecht, M. Chu, S.J. Opella, Local and global dynamics of the G protein-coupled receptor CXCR1, Biochemistry, 50 (2011) 2371-2380.

[109] S.H. Park, V.S. Wang, J. Radoicic, A.A. De Angelis, S. Berkamp, S.J. Opella, Paramagnetic relaxation enhancement of membrane proteins by incorporation of the metal-chelating unnatural amino acid 2-amino-3-(8-hydroxyquinolin-3-yl)propanoic acid (HQA), J Biomol NMR, 61 (2015) 185-196.

[110] T.K. Ritchie, Y.V. Grinkova, T.H. Bayburt, I.G. Denisov, J.K. Zolnerciks, W.M. Atkins, S.G. Sligar, Chapter 11 - Reconstitution of membrane proteins in phospholipid bilayer nanodiscs, Methods in enzymology, 464 (2009) 211-231.

[111] C.D. Schwieters, J.J. Kuszewski, G. Marius Clore, Using Xplor,ÄìNIH for NMR molecular structure determination, Progress in Nuclear Magnetic Resonance Spectroscopy, 48 (2006) 47-62.

[112] Y. Tian, C.D. Schwieters, S.J. Opella, F.M. Marassi, A Practical Implicit Membrane Potential for NMR Structure Calculations of Membrane Proteins, Biophys J, 109 (2015) 574-585.

[113] B.L. Grasberger, A.M. Gronenborn, M.G. Clore, Analysis of the Backbone Dynamics of Interleukin-8 by< sup> 15</sup> N Relaxation Measurements, Journal of molecular biology, 230 (1993) 364-372.

[114] M.F. Mesleh, S. Lee, G. Veglia, D.S. Thiriot, F.M. Marassi, S.J. Opella, Dipolar waves map the structure and topology of helices in membrane proteins, Journal of the American Chemical Society, 125 (2003) 8928-8935.

[115] L. Wu, N. Ruffing, X. Shi, W. Newman, D. Soler, C.R. Mackay, S. Qin, Discrete steps in binding and signaling of interleukin-8 with its receptor, J Biol Chem, 271 (1996) 31202-31209.

[116] S.-J. Jiang, J.-W. Liou, C.-C. Chang, Y. Chung, L.-F. Lin, H.-J. Hsu, Peptides derived from CXCL8 based on in silico analysis inhibit CXCL8 interactions with its receptor CXCR1, Scientific reports, 5 (2015) 18638.

[117] J.W. Liou, F.T. Chang, Y. Chung, W.Y. Chen, W.B. Fischer, H.J. Hsu, In silico analysis reveals sequential interactions and protein conformational changes during the binding of chemokine CXCL-8 to its receptor CXCR1, PLoS One, 9 (2014) e94178.

[118] P.R. Joseph, K. Rajarathnam, Solution NMR characterization of WT CXCL8 monomer and dimer binding to CXCR1 N-terminal domain, Protein Sci, 24 (2015) 81-92.

[119] P.R.B. Joseph, J.M. Sarmiento, A.K. Mishra, S.T. Das, R.P. Garofalo, J. Navarro, K. Rajarathnam, Probing the Role of CXC Motif in Chemokine CXCL8 for High Affinity Binding and Activation of CXCR1 and CXCR2 Receptors, Journal of Biological Chemistry, 285 (2010) 29262-29269.

[120] F.S. Monteclaro, I.F. Charo, The amino-terminal domain of CCR2 is both necessary and sufficient for high affinity binding of monocyte chemoattractant protein 1 - Receptor activation by a pseudo-tethered ligand, Journal of Biological Chemistry, 272 (1997) 23186-23190.

[121] A. Chaudhuri, P. Basu, S. Haldar, M. Kombrabail, G. Krishnamoorthy, K. Rajarathnam, A. Chattopadhyay, Organization and Dynamics of the N-Terminal Domain of Chemokine Receptor CXCR1 in Reverse Micelles: Effect of Graded Hydration, The Journal of Physical Chemistry B, 117 (2013) 12251233.

[122] M.W. Nasser, S.K. Raghuwanshi, D.J. Grant, V.R. Jala, K. Rajarathnam, R.M. Richardson, Differential activation and regulation of CXCR1 and CXCR2 by CXCL8 monomer and dimer, J Immunol, 183 (2009) 3425-3432.

[123] K. Möbius, K. Nordsieck, A. Pichert, S.A. Samsonov, L. Thomas, J. Schiller, S. Kalkhof, M. Teresa Pisabarro, A.G. Beck-Sickinger, D. Huster, Investigation of lysine side chain interactions of interleukin-8 with heparin and other glycosaminoglycans studied by a methylation-NMR approach, Glycobiology, 23 (2013) 1260-1269.

[124] E. Krieger, E. Geretti, B. Brandner, B. Goger, T.N. Wells, A.J. Kungl, A structural and dynamic model for the interaction of interleukin-8 and glycosaminoglycans: support from isothermal fluorescence titrations, Proteins, 54 (2004) 768-775.

[125] K.A. Jacobson, New paradigms in GPCR drug discovery, Biochem Pharmacol, 98 (2015) 541-555.

[126] V. Katritch, V. Cherezov, R.C. Stevens, Structure-function of the G protein-coupled receptor superfamily, Annu Rev Pharmacol Toxicol, 53 (2013) 531-556.

[127] Y.L. Liang, M. Khoshouei, M. Radjainia, Y. Zhang, A. Glukhova, J. Tarrasch, D.M. Thal, S.G.B. Furness, G. Christopoulos, T. Coudrat, R. Danev, W. Baumeister, L.J. Miller, A. Christopoulos, B.K. Kobilka, D. Wootten, G. Skiniotis, P.M. Sexton, Phase-plate cryo-EM structure of a class B GPCR-G-protein complex, Nature, 546 (2017) 118-123.

[128] Y. Zhang, B. Sun, D. Feng, H. Hu, M. Chu, Q. Qu, J.T. Tarrasch, S. Li, T. Sun Kobilka, B.K. Kobilka, G. Skiniotis, Cryo-EM structure of the activated GLP-1 receptor in complex with a G protein, Nature, 546 (2017) 248-253.

[129] S. Berkamp, S.H. Park, A.A. De Angelis, F.M. Marassi, S.J. Opella, Structure of monomeric Interleukin-8 and its interactions with the N-terminal Binding Site-I of CXCR1 by solution NMR spectroscopy, J Biomol NMR, 69 (2017) 111-121.

[130] B.J. Rollins, Where the confusion began: cloning the first chemokine receptors, J Immunol, 183 (2009) 2893-2894.

[131] L. Rajagopalan, K. Rajarathnam, Structural basis of chemokine receptor function--a model for binding affinity and ligand selectivity, Bioscience reports, 26 (2006) 325-339.

[132] L.S. Brown, V. Ladizhansky, Membrane proteins in their native habitat as seen by solid-state NMR spectroscopy, Protein Sci, 24 (2015) 1333-1346.

[133] B.B. Das, S.H. Park, S.J. Opella, Membrane protein structure from rotational diffusion, Biochimica et Biophysica Acta (BBA)- …, (2015).

[134] S.K. Hansen, K. Bertelsen, B. Paaske, N. Nielsen, T. Vosegaard, Solid-state NMR methods for oriented membrane proteins, Progress in Nuclear Magnetic Resonance Spectroscopy, 88-89 (2015) 4885.

[135] S.J. Opella, Solid-state NMR and membrane proteins, Journal of Magnetic Resonance, (2015).

[136] J.J. Lopez, A.K. Shukla, C. Reinhart, H. Schwalbe, H. Michel, C. Glaubitz, The structure of the neuropeptide bradykinin bound to the human G-protein coupled receptor bradykinin B2 as determined by solid-state NMR spectroscopy, Angew Chem Int Ed Engl, 47 (2008) 1668-1671.

[137] S. Luca, J.F. White, A.K. Sohal, D.V. Filippov, J.H. van Boom, R. Grisshammer, M. Baldus, The conformation of neurotensin bound to its G protein-coupled receptor, Proceedings of the National Academy of Sciences of the United States of America, 100 (2003) 10706-10711.

[138] M.A. Verhoeven, A.F.L. Creemers, P.H.M. Bovee-Geurts, W.J. De Grip, J. Lugtenburg, H.J.M. de Groot, Ultra-high-field MAS NMR assay of a multispin labeled ligand bound to its G-protein receptor target in the natural membrane environment: Electronic structure of the retinylidene chromophore in rhodopsin, Biochemistry, 40 (2001) 3282-3288.

[139] C.A. Whittaker, S.G. Patching, M. Esmann, D.A. Middleton, Ligand orientation in a membrane-embedded receptor site revealed by solid-state NMR with paramagnetic relaxation enhancement, Org Biomol Chem, 13 (2015) 2664-2668.

[140] S.H. Park, S. Prytulla, A.A. De Angelis, J.M. Brown, H. Kiefer, S.J. Opella, High-resolution NMR spectroscopy of a GPCR in aligned bicelles, Journal of the American Chemical Society, 128 (2006) 7402-7403.

[141] A. Marchetti, S. Jehle, M. Felletti, M.J. Knight, Backbone Assignment of Fully Protonated Solid Proteins by 1H Detection and Ultrafast Magic‐Angle‐Spinning NMR Spectroscopy, Angewandte ⋯, (2012).

[142] D.H. Zhou, G. Shah, M. Cormos, C. Mullen, D. Sandoz, C.M. Rienstra, Proton-detected solid-state NMR spectroscopy of fully protonated proteins at 40 kHz magic-angle spinning, Journal of the American Chemical Society, 129 (2007) 11791-11801.

[143] L.B. Andreas, T. Marchand, K. Jaudzems, G. Pintacuda, High-resolution proton-detected NMR of proteins at very fast MAS, Journal of Magnetic Resonance, 253 (2015) 3649.

[144] B. Reif, Ultra-high resolution in MAS solid-state NMR of perdeuterated proteins: implications for structure and dynamics, Journal of magnetic resonance (San Diego, Calif. : 1997), 216 (2012) 1-12.

[145] A.J. Nieuwkoop, W.T. Franks, K. Rehbein, A. Diehl, U. Akbey, F. Engelke, L. Emsley, G. Pintacuda, H. Oschkinat, Sensitivity and resolution of proton detected spectra of a deuterated protein at 40 and 60 kHz magic-angle-spinning, J Biomol NMR, 61 (2015) 161-171.

[146] S.H. Park, C. Yang, S.J. Opella, L.J. Mueller, Resolution and measurement of heteronuclear dipolar couplings of a noncrystalline protein immobilized in a biological supramolecular assembly by proton-detected MAS solid-state NMR spectroscopy, Journal of magnetic resonance (San Diego, Calif. : 1997), 237 (2013) 164-168.

[147] D. Mance, T. Sinnige, M. Kaplan, An Efficient Labelling Approach to Harness Backbone and Side‐Chain Protons in 1H‐Detected Solid‐State NMR Spectroscopy, Angewandte ⋯, (2015).

[148] E. Barbet-Massin, A.J. Pell, J.S. Retel, L.B. Andreas, K. Jaudzems, W.T. Franks, A.J. Nieuwkoop, M. Hiller, V. Higman, P. Guerry, A. Bertarello, M.J.

Knight, M. Felletti, T. Le Marchand, S. Kotelovica, I. Akopjana, K. Tars, M. Stoppini, V. Bellotti, M. Bolognesi, S. Ricagno, J.J. Chou, R.G. Griffin, H. Oschkinat, A. Lesage, L. Emsley, T. Herrmann, G. Pintacuda, Rapid proton-detected NMR assignment for proteins with fast magic angle spinning, J Am Chem Soc, 136 (2014) 12489-12497.

[149] H.R. Dannatt, G.F. Taylor, K. Varga, V.A. Higman, M.P. Pfeil, L. Asilmovska, P.J. Judge, A. Watts, (1)(3)C- and (1)H-detection under fast MAS for the study of poorly available proteins: application to sub-milligram quantities of a 7 trans-membrane protein, J Biomol NMR, 62 (2015) 17-23.

[150] G.A. Morris, R. Freeman, Enhancement of Nuclear Magnetic-Resonance Signals by Polarization Transfer, Journal of the American Chemical Society, 101 (1979) 760-762.

[151] A.J. Shaka, P.B. Barker, R. Freeman, Computer-Optimized Decoupling Scheme for Wideband Applications and Low-Level Operation, Journal of Magnetic Resonance, 64 (1985) 547-552.

[152] M. Piotto, V. Saudek, V. Sklenar, Gradient-tailored excitation for single-quantum NMR spectroscopy of aqueous solutions, J Biomol NMR, 2 (1992) 661-665.

[153] G.S.V. Kuschert, A.J. Hoogewerf, A.E.I. Proudfoot, C.-w. Chung, R.M. Cooke, R.E. Hubbard, T.N.C. Wells, P.N. Sanderson, Identification of a Glycosaminoglycan Binding Surface on Human Interleukin-8, Biochemistry, 37 (1998) 1119311201.

[154] A. Nowacka, N.A. Bongartz, O.H. Ollila, T. Nylander, D. Topgaard, Signal intensities in (1)H-(1)(3)C CP and INEPT MAS NMR of liquid crystals, J Magn Reson, 230 (2013) 165-175.

[155] H.S. Lee, G. Spraggon, P.G. Schultz, F. Wang, Genetic incorporation of a metal-ion chelating amino acid into proteins as a biophysical probe, J Am Chem Soc, 131 (2009) 2481-2483.

[156] N.R. Latorraca, A.J. Venkatakrishnan, R.O. Dror, GPCR Dynamics: Structures in Motion, Chem Rev, 117 (2017) 139-155.

[157] J. Sarmiento, C. Shumate, K. Suetomi, A. Ravindran, L. Villegas, K. Rajarathnam, J. Navarro, Diverging mechanisms of activation of chemokine receptors revealed by novel chemokine agonists, PLoS One, 6 (2011) e27967.

[158] J.A. Goncalves, S. Ahuja, S. Erfani, M. Eilers, S.O. Smith, Structure and function of G protein-coupled receptors using NMR spectroscopy, Prog Nucl Magn Reson Spectrosc, 57 (2010) 159-180.

[159] S. Rajagopal, K. Rajagopal, R.J. Lefkowitz, Teaching old receptors new tricks: biasing seven-transmembrane receptors, Nat Rev Drug Discov, 9 (2010) 373-386.

[160] D.M. Rosenbaum, S.G. Rasmussen, B.K. Kobilka, The structure and function of G-protein-coupled receptors, Nature, 459 (2009) 356-363.

[161] V. Katritch, V. Cherezov, R.C. Stevens, Diversity and modularity of G protein-coupled receptor structures, Trends Pharmacol Sci, 33 (2012) 17-27.

[162] D.M. Rosenbaum, V. Cherezov, M.A. Hanson, S.G.F. Rasmussen, F.S. Thian, T.S. Kobilka, H.-J. Choi, X.-J. Yao, W.I. Weis, R.C. Stevens, B.K. Kobilka, GPCR Engineering Yields High-Resolution Structural Insights into β2;-Adrenergic Receptor Function, Science, 318 (2007) 1266.

[163] F. Sallusto, M. Baggiolini, Chemokines and leukocyte traffic, Nat Immunol, 9 (2008) 949-952.

[164] N.S. Gandhi, R.L. Mancera, Molecular dynamics simulations of CXCL-8 and its interactions with a receptor peptide, heparin fragments, and sulfated linked cyclitols, Journal of chemical information and modeling, 51 (2011) 335-358.

[165] M. Szpakowska, V. Fievez, K. Arumugan, N. van Nuland, J.-C. Schmit, A. Chevigné, Function, diversity and therapeutic potential of the N-terminal domain of human chemokine receptors, Biochemical pharmacology, 84 (2012) 1366-1380.

[166] S. Yan, C.L. Suiter, G. Hou, H. Zhang, T. Polenova, Probing structure and dynamics of protein assemblies by magic angle spinning NMR spectroscopy, Acc Chem Res, 46 (2013) 2047-2058.

[167] S.J. Opella, F.M. Marassi, Applications of NMR to membrane proteins, Arch Biochem Biophys, 628 (2017) 92-101.

[168] Y. Ding, Y. Yao, F.M. Marassi, Membrane protein structure determination in membrana, Accounts of chemical research, 46 (2013) 2182-2190.

[169] X. Ding, X. Zhao, A. Watts, G-protein-coupled receptor structure, ligand binding and activation as studied by solid-state NMR spectroscopy, The Biochemical journal, 450 (2013) 443-457.

[170] F.W. Studier, Protein production by auto-induction in high-density shaking cultures, Protein Expression and Purification, 41 (2005) 207-234.

[171] R.S. Thakur, N.D. Kurur, P.K. Madhu, Swept-frequency two-pulse phase modulation for heteronuclear dipolar decoupling in solid-state NMR, Chemical Physics Letters, 426 (2006) 459-463.

[172] R.S. Thakur, N.D. Kurur, P.K. Madhu, An experimental study of decoupling sequences for multiple-quantum and high-resolution MAS experiments in solid-state NMR, Magn Reson Chem, 46 (2008) 166-169.

[173] A. Pines, M.G. Gibby, J.S. Waugh, Proton‐Enhanced Nuclear Induction Spectroscopy. A Method for High Resolution NMR of Dilute Spins in Solids, The Journal of Chemical Physics, 56 (1972) 1776-1777.

[174] N.M. Szeverenyi, M.J. Sullivan, G.E. Maciel, Observation of spin exchange by two-dimensional fourier transform 13C cross polarization-magic-angle spinning, Journal of Magnetic Resonance (1969), 47 (1982) 462-475.

[175] M.H. Frey, S.J. Opella, Carbon-13 spin exchange in amino acids and peptides, Journal of the American Chemical Society, 106 (1984) 4942-4945.

[176] M. Baldus, A.T. Petkova, J. Herzfeld, R.G. Griffin, Cross polarization in the tilted frame: assignment and spectral simplification in heteronuclear spin systems, Mol Phys, 95 (1998) 1197-1207.

[177] J.S. Waugh, Uncoupling of local field spectra in nuclear magnetic resonance: determination of atomic positions in solids, Proceedings of the National Academy of Sciences, 73 (1976) 1394.

[178] X. Zhao, M. Edén, M.H. Levitt, Recoupling of heteronuclear dipolar interactions in solid-state NMR using symmetry-based pulse sequences, Chemical Physics Letters, 342 (2001) 353-361.

[179] R. Keller, The CARA/Lua Programmers Manual, DATONAL AG, (2003).

[180] J. Leppert, O. Ohlenschlager, M. Gorlach, R. Ramachandran, Adiabatic TOBSY in rotating solids, J Biomol NMR, 29 (2004) 167-173.

[181] A.J. Venkatakrishnan, X. Deupi, G. Lebon, F.M. Heydenreich, T. Flock, T. Miljus, S. Balaji, M. Bouvier, D.B. Veprintsev, C.G. Tate, G.F.X. Schertler, M.M. Babu, Diverse activation pathways in class A GPCRs converge near the G-protein-coupling region, Nature, 536 (2016) 484.

[182] M.F. Mesleh, S.J. Opella, Dipolar Waves as NMR maps of helices in proteins, Journal of magnetic resonance (San Diego, Calif. : 1997), 163 (2003) 288-299.

[183] A.C. Kruse, A.M. Ring, A. Manglik, J. Hu, K. Hu, K. Eitel, H. Hübner, E. Pardon, C. Valant, P.M. Sexton, A. Christopoulos, C.C. Felder, P. Gmeiner, J. Steyaert, W.I. Weis, K.C. Garcia, J. Wess, B.K. Kobilka, Activation and allosteric modulation of a muscarinic acetylcholine receptor, Nature, 504 (2013) 101-106.

[184] S.G.G. Rasmussen, B.T. DeVree, Y. Zou, A.C. Kruse, K.Y. Chung, T.S. Kobilka, F.S. Thian, P.S. Chae, E. Pardon, D. Calinski, J.M. Mathiesen, S.T. Shah, J.A. Lyons, M. Caffrey, S.H. Gellman, J. Steyaert, G. Skiniotis, W.I. Weis, R.K. Sunahara, B.K. Kobilka, Crystal structure of the β2 adrenergic receptor-Gs protein complex, Nature, 477 (2011) 549-555.

[185] H. Nomiyama, O. Yoshie, Functional roles of evolutionary conserved motifs and residues in vertebrate chemokine receptors, Journal of Leukocyte Biology, 97 (2015) 39-47.

[186] S.H. Park, F. Casagrande, M. Chu, K. Maier, H. Kiefer, S.J. Opella, Optimization of purification and refolding of the human chemokine receptor CXCR1 improves the stability of proteoliposomes for structure determination, Biochimica et biophysica acta, 1818 (2012) 584-591.

[187] C.V. Grant, C.H. Wu, S.J. Opella, Probes for high field solid-state NMR of lossy biological samples, Journal of magnetic resonance (San Diego, Calif. : 1997), 204 (2010) 180-188.

[188] C.V. Grant, Y. Yang, M. Glibowicka, C.H. Wu, S.H. Park, C.M. Deber, S.J. Opella, A Modified Alderman-Grant Coil makes possible an efficient cross-coil probe for high field solid-state NMR of lossy biological samples, Journal of magnetic resonance (San Diego, Calif. : 1997), 201 (2009) 87-92.

[189] N. Sinha, C.V. Grant, C.H. Wu, A.A. De Angelis, S.C. Howell, S.J. Opella, SPINAL modulated decoupling in high field double- and triple-resonance solid-state NMR experiments on stationary samples, Journal of magnetic resonance (San Diego, Calif. : 1997), 177 (2005) 197-202.

[190] M.H. Levitt, D. Suter, R.R. Ernst, Spin dynamics and thermodynamics in solid-state NMR cross polarization, The Journal of Chemical Physics, 84 (1986) 4243.

[191] A.A. Nevzorov, S.J. Opella, Structural fitting of PISEMA spectra of aligned proteins, Journal of magnetic resonance (San Diego, Calif. : 1997), 160 (2003) 33-39.

[192] S.H. Park, S.J. Opella, Triton X-100 as the "short-chain lipid" improves the magnetic alignment and stability of membrane proteins in phosphatidylcholine bilayers for oriented-sample solid-state NMR spectroscopy, Journal of the American Chemical Society, 132 (2010) 12552-12553.

[193] N. Sinha, C.V. Grant, S.H. Park, J.M. Brown, S.J. Opella, Triple resonance experiments for aligned sample solid-state NMR of (13)C and (15)N labeled

proteins, Journal of magnetic resonance (San Diego, Calif. : 1997), 186 (2007) 51-64.

[194] F.V. Filipp, N. Sinha, L. Jairam, J. Bradley, S.J. Opella, Labeling strategies for 13C-detected aligned-sample solid-state NMR of proteins, J Magn Reson, 201 (2009) 121-130.

[195] P. Lundström, K. Teilum, T. Carstensen, I. Bezsonova, S. Wiesner, D.F. Hansen, T.L. Religa, M. Akke, L.E. Kay, Fractional 13C enrichment of isolated carbons using [1-13C]- or [2- 13C]-glucose facilitates the accurate measurement of dynamics at backbone Calpha and side-chain methyl positions in proteins, Journal of biomolecular NMR, 38 (2007) 199-212.

[196] K. Nomura, M. Lintuluoto, K. Morigaki, Hydration and Temperature Dependence of13C and1H NMR Spectra of the DMPC Phospholipid Membrane and Complete Resonance Assignment of Its Crystalline State, The Journal of Physical Chemistry B, 115 (2011) 1499115001.

[197] M. Hong, K. Jakes, Selective and extensive 13C labeling of a membrane protein for solid-state NMR investigations, Journal of biomolecular NMR, (1999).

[198] S.V. Dvinskikh, H. Zimmermann, A. Maliniak, D. Sandström, Heteronuclear dipolar recoupling in solid-state nuclear magnetic resonance by amplitude-, phase-, and frequency-modulated Lee–Goldburg cross-polarization, The Journal of Chemical Physics, 122 (2005).

[199] W.K. Rhim, A. Pines, W.-J.S. B, Time-reversal experiments in dipolar-coupled spin systems, Physical Review B, (1971).

[200] E.C. Lin, S.J. Opella, 1H assisted 13C/15N heteronuclear correlation spectroscopy in oriented sample solid-state NMR of single crystal and magnetically aligned samples, J Magn Reson, 211 (2011) 37-44.

[201] J. Xu, P.E.S. Smith, R. Soong, A. Ramamoorthy, A Proton Spin Diffusion Based Solid-State NMR Approach for Structural Studies on Aligned Samples, The Journal of Physical Chemistry B, 115 (2011) 4863-4871.

[202] F.M. Marassi, A simple approach to membrane protein secondary structure and topology based on NMR spectroscopy, Biophys J, 80 (2001) 994-1003.

[203] S.H. Park, F.M. Marassi, D. Black, S.J. Opella, Structure and dynamics of the membrane-bound form of Pf1 coat protein: implications of structural rearrangement for virus assembly, Biophysical journal, 99 (2010) 1465-1474.

[204] C.H. Wu, A. Ramamoorthy, L.M. Gierasch, S.J. Opella, Simultaneous Characterization of the Amide 1H Chemical Shift, 1H-15N Dipolar, and 15N Chemical Shift Interaction Tensors in a Peptide Bond by Three-Dimensional Solid-State NMR Spectroscopy, Journal of the American Chemical Society, 117 (1995) 6148-6149.

[205] K. Yamamoto, R. Soong, A. Ramamoorthy, Comprehensive Analysis of Lipid Dynamics Variation with Lipid Composition and Hydration of Bicelles Using Nuclear Magnetic Resonance (NMR) Spectroscopy, Langmuir, 25 (2009) 7010-7018.

[206] S.H. Park, S. Berkamp, J. Radoicic, A.A. De Angelis, S.J. Opella, Interaction of Monomeric Interleukin-8 with CXCR1 Mapped by Proton-detected Fast MAS Solid-state NMR and Intermolecular Paramagnetic Relaxation Enhancement, (2017).

[207] G.A. Cook, S.J. Opella, Secondary structure, dynamics, and architecture of the p7 membrane protein from hepatitis C virus by NMR spectroscopy, Biochimica et biophysica acta, 1808 (2011) 1448-1453.

[208] K. Ding, A.M. Gronenborn, Sensitivity-enhanced 2D IPAP, TROSY-anti-TROSY, and E.COSY experiments: alternatives for measuring dipolar 15N-1HN couplings, J Magn Reson, 163 (2003) 208-214.

[209] C.V. Grant, S.L. Sit, D.A.A. Angelis, K.S. Khuong, C.H. Wu, L.A. Plesniak, S.J. Opella, An efficient 1H/31P double-resonance solid-state NMR probe that utilizes a scroll coil, Journal of Magnetic Resonance, 188 (2007) 279-284.

[210] J. Frank, M. Radermacher, P. Penczek, J. Zhu, Y. Li, M. Ladjadj, A. Leith, SPIDER and WEB: processing and visualization of images in 3D electron microscopy and related fields, J Struct Biol, 116 (1996) 190-199.

[211] C. Tanford, J.A. Reynolds, Characterization of membrane proteins in detergent solutions, Biochim Biophys Acta, 457 (1976) 133-170.

[212] T.A. Cross, S.J. Opella, Structural properties of fd coat protein in sodium dodecyl sulfate micelles, Biochem Biophys Res Commun, 92 (1980) 478-484.

[213] R.R. Vold, R.S. Prosser, A.J. Deese, Isotropic solutions of phospholipid bicelles: a new membrane mimetic for high-resolution NMR studies of polypeptides, J Biomol NMR, 9 (1997) 329-335.

[214] B.A. Lewis, G.S. Harbison, J. Herzfeld, R.G. Griffin, NMR structural analysis of a membrane protein: bacteriorhodopsin peptide backbone orientation and motion, Biochemistry, 24 (1985) 4671-4679.

[215] A.A. De Angelis, A.A. Nevzorov, S.H. Park, S.C. Howell, A.A. Mrse, S.J. Opella, High-resolution NMR spectroscopy of membrane proteins in aligned bicelles, Journal of the American Chemical Society, 126 (2004) 15340-15341.

[216] E.M. Landau, J.P. Rosenbusch, Lipidic cubic phases: a novel concept for the crystallization of membrane proteins, Proc Natl Acad Sci U S A, 93 (1996) 14532-14535.

[217] S. Faham, J.U. Bowie, Bicelle crystallization: a new method for crystallizing membrane proteins yields a monomeric bacteriorhodopsin structure, J Mol Biol, 316 (2002) 1-6.

[218] A. Nath, W.M. Atkins, S.G. Sligar, Applications of phospholipid bilayer nanodiscs in the study of membranes and membrane proteins, Biochemistry, 46 (2007) 2059-2069.

[219] E.N. Lyukmanova, Z.O. Shenkarev, A.S. Paramonov, A.G. Sobol, T.V. Ovchinnikova, V.V. Chupin, M.P. Kirpichnikov, M.J. Blommers, A.S. Arseniev, Lipid-protein nanoscale bilayers: a versatile medium for NMR investigations of membrane proteins and membrane-active peptides, J Am Chem Soc, 130 (2008) 2140-2141.

[220] T. Raschle, S. Hiller, T.-Y.Y. Yu, A.J. Rice, T. Walz, G. Wagner, Structural and functional characterization of the integral membrane protein VDAC-1 in lipid bilayer nanodiscs, Journal of the American Chemical Society, 131 (2009) 17777-17779.

[221] J.M. Glück, M. Wittlich, S. Feuerstein, S. Hoffmann, D. Willbold, B.W. Koenig, Integral membrane proteins in nanodiscs can be studied by solution NMR spectroscopy, Journal of the American Chemical Society, 131 (2009) 12060-12061.

[222] Z.O. Shenkarev, A.S. Paramonov, E.N. Lyukmanova, L.N. Shingarova, S.A. Yakimov, M.A. Dubinnyi, V.V. Chupin, M.P. Kirpichnikov, M.J.J. Blommers, A.S. Arseniev, NMR structural and dynamical investigation of the isolated voltage-sensing domain of the potassium channel KvAP: implications for voltage gating, Journal of the American Chemical Society, 132 (2010) 5630-5637.

[223] G.M. Anantharamaiah, J.L. Jones, C.G. Brouillette, C.F. Schmidt, B.H. Chung, T.A. Hughes, A.S. Bhown, J.P. Segrest, Studies of synthetic peptide analogs of the amphipathic helix. Structure of complexes with dimyristoyl phosphatidylcholine, J Biol Chem, 260 (1985) 10248-10255.

[224] I.G. Denisov, Y.V. Grinkova, A.A. Lazarides, S.G. Sligar, Directed self-assembly of monodisperse phospholipid bilayer Nanodiscs with controlled size, Journal of the American Chemical Society, 126 (2004) 3477-3487.

[225] S.R. Prosser, S.A. Hunt, J.A. DiNatale, R.R. Vold, Magnetically Aligned Membrane Model Systems with Positive Order Parameter: Switching the Sign of S z z with Paramagnetic Ions, Journal of the American Chemical Society, 118 (1996).

[226] A.Z. Kijac, Y. Li, S.G. Sligar, C.M. Rienstra, Magic-angle spinning solid-state NMR spectroscopy of nanodisc-embedded human CYP3A4, Biochemistry, 46 (2007) 13696-13703.

[227] Y. Li, A.Z. Kijac, S.G. Sligar, C.M. Rienstra, Structural analysis of nanoscale self-assembled discoidal lipid bilayers by solid-state NMR spectroscopy, Biophysical journal, 91 (2006) 3819-3828.

[228] P.A. McDonnell, K. Shon, Y. Kim, S.J. Opella, fd coat protein structure in membrane environments, J Mol Biol, 233 (1993) 447-463.

[229] G.A. Cook, S.J. Opella, NMR studies of membrane proteins, Methods in molecular biology (Clifton, N.J.), 637 (2010) 263-275.

[230] N. Tjandra, A. Bax, Direct measurement of distances and angles in biomolecules by NMR in a dilute liquid crystalline medium, Science, 278 (1997) 1111-1114.